Studies Toward an Optimized Synthesis of a Novel Imidazopyridinone DNA-PK Inhibitor

A thesis

submitted in partial fulfilment

of the requirements for the degree

of

Master of Science (Research) in Chemistry

at

The University of Waikato

by

Daniel A. Mora

THE UNIVERSITY OF
WAIKATO
Te Whare Wānanga o Waikato

2025

Abstract

Cancer is a disease of global significance, with cancer rates increasing year on year globally. A key challenge within the treatment of cancer is the cellular response to radiotherapy. When fractionated radiotherapy is targeted at cancerous cells DNA double strand breaks are promoted *via* free radical formation to induce cellular death. However, cellular responses activate the DNA double strand break repair mechanism to oppose these outcomes. Involved in this mechanism is the DNA-PK enzyme and the Auckland Cancer Society Research Centre (ACSRC) has developed an enzyme inhibitor SN39536 to inhibit the repair mechanism. Core aspects of the project surround the use and optimization of an alternative novel synthetic route to the drug as the original published route was developed allowing for structural diversity as opposed to efficiency.

There are three novel reactions at the beginning of the alternative route leading to a point of convergence with the ACSRC route at an imidazopyridinone intermediate; a nucleophilic aromatic substitution, a base-catalyzed hydrolysis and a Curtius rearrangement. Analogous reactions were originally reported by Astra Zeneca (AZ) with pyrimidine analogues however in this work they have been adapted and optimized for pyridine variants. Post optimization the highest yield achieved for the pyridine substrates were; 85.3% for the nucleophilic aromatic substitution, 89.9% for the base-catalyzed hydrolysis and 69.5% for the Curtius rearrangement. These are comparable to the AZ yields with their pyrimidine analogues however in each case the addition of heat and/or increased reaction times were consistently required to match the AZ yields – highlighting that the novel pyridine substrates are not as activated for these reactions.

The novel route generates the same imidazopyridinone intermediate as the ACSRC route in an overall yield of 53.3%. This is significantly lower than the 70.6% overall yield from the ACSRC route. Despite the novel route being viable for the synthesis of imidazopyridinones we propose it is currently an inferior alternative for the synthesis of SN39536.

A rearrangement of the novel route steps was then attempted to explore if the altered electronics of the substrates aid or diminish the synthetic yield of the novel reactions. We placed the final Buchwald-Hartwig amination of the original syntheses after the initial novel nucleophilic aromatic substitution however, we were unable to optimize this novel cross-coupling beyond a yield of 19.0%. Investigation into the reaction conditions were unable to discern why the cross-coupling was consistently unsuccessful. The limited information from our substrate studies suggests that the substrate for this reaction does not have the correct electronics to undergo the proposed cross-coupling. The 19.0% yield of this reaction currently renders the rearranged novel route an unviable alternative to both previous syntheses.

Acknowledgements

I would like to begin by thanking my academic supervisor Dr. Benjamin Dickson. Your mentorship and guidance across the last year and a half has been phenomenal and is greatly appreciated. You have been very approachable and were always more than happy to provide guidance when needed. My skills as a synthetic chemist, scientific writer and overall researcher have developed immensely under your supervision and I will carry them into my future ventures.

Special mention must be made to Dr. Michael Hay, Dr. Lydia Liew and rest of the team at the Auckland Cancer Society Research centre for further mentorship, the supply of specific reagents and other support. This project stems from the work you have done, and I am grateful to have had the opportunity to conduct research in a field I am passionate about. Your continued effort in the research of potential cancer treatment modalities is awe-inspiring.

I would also like to thank the University of Waikato chemistry staff for the ongoing support throughout the project with special mention to Jenny and Atiga for technical and NMR support. To everyone else who has worked in the C3.04 lab or who has had a role in the project or my journey I extend my thanks.

Finally, I would like to acknowledge everyone from my personal life who has been supportive of my academic journey and pursuit of higher education. From my friends to my family it is all very much appreciated. To my partner, your constant companionship, support and ongoing interest in the project has been invaluable. A final mention to my parents for the consistent unwavering support, without such I wouldn’t be in the position I am in today; for that I am extremely grateful.

Table of Contents

Abstract ..... **i**

Acknowledgements ..... **ii**

Table of Contents ..... **iii**

List of Figures ..... **vi**

List of Schemes ..... **viii**

List of Tables ..... **ix**

List of Acronyms and Abbreviations ..... **x**

1 Introduction **1**

1.1 Background 1

1.1.1 Cancer 1

1.1.2 Radiotherapy 1

1.1.3 Head & Neck Squamous Cell Carcinoma 2

1.1.4 Radiotherapy Induced DNA Damage Response Pathways 3

1.1.5 DNA-PK Inhibition 4

1.2 Synthetic Strategies 7

1.2.1 The Published ACSRC Synthetic Route to Inhibitor **2** 7

1.2.1.1 Brief Analysis of the ACSRC Route 7

1.2.1.2 Efficiency of the ACSRC Route 8

1.2.2 The Published AZ Synthetic Route to Inhibitor **3** 9

1.2.2.1 Brief Analysis of the AZ Route 9

1.2.3 A Novel Alternative Route to Inhibitor **2** 10

1.2.3.1 Proposed Synthetic Efficiency of the Novel Route 11

1.2.3.2 The Curtius Rearrangement to Form a Substituted 2-Imidazolidinone Ring 11

1.2.3.3 Rearranged Positioning of the Buchwald-Hartwig Coupling 12

1.3 Overview 14

2 Discussion **15**

2.1 Novel Synthesis of an Imidazopyridinone *via* a Curtius Rearrangement 15

2.1.1 Nucleophilic Aromatic Substitution 15
2.1.1.1 Characterization of Chloride **18** 18
2.1.2 Ester Hydrolysis 21
2.1.2.1 Characterization of Carboxylic Acid **19** 22
2.1.3 Curtius Rearrangement 23
2.1.4 *N*-Methylation 26
2.1.5 Buchwald-Hartwig Coupling 26
2.1.6 Comparison to the AZ Route 28
2.1.7 Comparison to the ACSRC Route 29
2.1.7.1 Phosphoryl Chloride Mediated Nucleophilic Aromatic Substitution 29
2.1.7.2 THP Installation 30
2.1.7.3 Hydrolysis vs Reduction 31
2.1.7.4 Formation of the THP-NH substituted 2-imidazolidinone ring 32
2.2 Rearrangement of the Novel Route 33
2.2.1 Initial Attempts at the Buchwald-Hartwig Coupling 33
2.2.1.1 Characterization of Aniline **20** 36
2.2.1.2 Crude Characterization of Dimer **21b** 39
2.2.2 Catalytic Optimization 40
2.2.3 Solvent and Base Investigations 43
2.2.4 Substrate Studies 46
2.2.4.1 Quantum Chemical Calculations 46
2.2.4.2 Model Study 47
2.2.4.2.1 Characterization of Aniline **23** 49
2.2.4.3 Protection of Aniline **11** 52
2.2.5 Reaction Feasibility 56
2.3 Evaluation 58
2.3.1 The Novel Route 58
2.3.2 Attempted Rearrangement of the Novel Route 59
2.3.3 Future Work 59

3 Experimental 61

3.1 General Details 61

3.2 Quantum Chemical Calculations 61

3.3 Catalytic Material 61

3.4 Synthetic Compounds 63

4 References 71

List of Figures

Figure 1: Contrast between the imidazo[4,5-*c*]quinoline core of the PIKK multi-kinase inhibitor 1 and the imidazo[4,5-*c*]pyridine-2-one core of imidazopyridinone **2** 5

Figure 2: The AZ DNA-PK inhibitor imidazopyrimidinone **3** 6

Figure 3: Comparison of the starting substrates between the ACSRC and novel route 11

Figure 4: Comparison of the S_NAr substrates for the novel route and the AZ route 16

Figure 5: Example intermediate structures of the S_NAr reaction; a key intermediate for the pyridine substrate **17** (**17i**); a key intermediate for the pyrimidine substrate **12** (**12i**) 16

Figure 6: Numbered structure of chloride **18** 18

Figure 7: Chair diagram of THP-R; example of expected geminal equivalency labelled; observed equivalent protons coloured 19

Figure 8: The 3H multiplet of chloride **18**; representative protons coloured 19

Figure 9: HSQC correlations of the 3H multiplet for chloride **18**; equivalent environments and correlations coloured 20

Figure 10: Possible dimerized structures **21a** and **21b**; R = ethyl ester 34

Figure 11: Numbered structure of aniline **20** 36

Figure 12: Aromatic ^{1}H coupling of the installed aniline on aniline **20** 37

Figure 13: HMBC correlations of H-6″ and 2″-Me to quaternary carbons on aniline **20** 38

Figure 14: HMBC correlation of O-CH_3 and 4″-C on aniline **20** 38

Figure 15: Aromatic ^{1}H region of dimer **21b** 39

Figure 16: Structural comparison of XPhos and BrettPhos 42

Figure 17: Electrostatic potential map of chloride **18** 46

Figure 18: Electrostatic potential map of chloride **10** 47

Figure 19: Proposed dimerization of pyridine **23** and aniline **11** 48

Figure 20: Alternative 2-chloropyridines that aniline **11** has been coupled to 49

Figure 21: Numbered structure of aniline **23** 50

Figure 22: Shared 1.9 Hz coupling between H-6 and H-4 on aniline **23**; example peak shifts accented red 50

Figure 23: Shared 0.9 Hz coupling between H-6 and H-3 on aniline **23**; example peak shifts accented red 51

Figure 24: HSQC of the H-4 signal on aniline **23** 51

Figure 25: HMBC revealing the shift of the final unassigned quaternary carbon on aniline **23** 52

Figure 26: Presence of two possible *N*-methylation sites within the rearranged novel route 53

Figure 27: Key functional difference between chloride **18** and chloride **10** 56

Figure 28: Overall yield of the novel route versus the ACSRC route to produce imidazopyridinone **9** 58

List of Schemes

Scheme 1: The ACSRC synthetic route to inhibitor **2** 7

Scheme 2: The AZ synthetic route to inhibitor **3** 9

Scheme 3: The AZ route with substrate adjustment to generate inhibitor **2** 10

Scheme 4: Traditional routes to generating acyl azides 12

Scheme 5: Proposed rearrangement of the novel route 13

Scheme 6: General catalytic cycle for Buchwald-Hartwig couplings 13

Scheme 7: S_NAr reaction mechanism on dichloride **17** 15

Scheme 8: Hydrolysis mechanism of ethyl ester **18** 21

Scheme 9: Conversion of carboxylic acid 19 to an acyl azide *via* DPPA and NEt_3 23

Scheme 10: Curtius rearrangement and ring formation generating imidazopyridinone **9** 23

Scheme 11: *N*-methylation mechanism on imidazopyridinone **9** 26

Scheme 12: Buchwald-Hartwig coupling reaction of chloride **10** and aniline **11** 26

Scheme 13: The ACSRC's chlorination of pyridinol **4** 29

Scheme 14: The ACSRC's S_NAr reaction on dichloride **5** 30

Scheme 15: The ACSRC's $SnCl_2$ reduction on nitropyridine **7** 31

Scheme 16: The ACSRC's CDI coupling on diamine **8** 32

Scheme 17: Novel Buchwald-Hartwig coupling of chloride **18** and aniline **11** 33

Scheme 18: Proposed formation of dimer **21b**; a) NH_2 of aniline **11** acting as the nucleophile; b) aniline NH of the coupling product **20** acting as the nucleophile 35

Scheme 19: Activation of the BrettPhos-PdG3 precatalyst; L = BrettPhos ligand 41

Scheme 20: Buchwald-Hartwig coupling of chloride **18** and aniline **11** using BrettPhos-PdG3 42

Scheme 21: Proposed generation of acid **19**'s carboxylate *via in situ* hydrolysis and deprotonation .. 44

Scheme 22: Proposed alternative mechanism for the formation of dimer **21b** 45

Scheme 23: Model Buchwald-Hartwig coupling on chloride **22** and aniline **11** 48

Scheme 24: Boc protection of aniline **11** 53

Scheme 25: Buchwald-Hartwig coupling of chloride **22** and carbamate **25** 54

Scheme 26: Buchwald-Hartwig coupling of chloride **18** and carbamate **25** 55

List of Tables

Table 1: Relevant IC_{50} data (nm) of compounds **1** and **2**, demonstrating PIKK selectivity..... 5

Table 2: Highest yield achieved (%) for the bases trialled in the novel S_NAr reaction 17

Table 3: Yield comparison (%) between the pyridine and pyrimidine analogues for equivalent reactions 28

Table 4: Price per gram of starting material (USD, ≥ 95 % purity) by chemical supplier 29

List of Acronyms and Abbreviations

$[M+H]^+$	Molecular ion plus proton
δ+	Partial positive charge
Δ	Heat
°C	Degrees Celsius
^{1}H-NMR	Proton nuclear magnetic resonance
^{13}C-APT	Carbon attached proton test
1D	One dimensional
2D	Two dimensional
ACSRC	Auckland Cancer Society Research Center
ATP	Adenosine triphosphate
AZ	Astra Zeneca
Boc	*tert*-Butoxycarbonyl
Boc_2O	Di-*tert*-butyl dicarbonate
br d	Broad doublet
br s	Broad singlet
BrettPhos	Dicyclohexyl-[3,6-dimethoxy-2-[2,4,6-tri(propan-2-yl)phenyl]phenyl]phosphane
BrettPhos-PdG3	Third generation BrettPhos-palladium precatalyst
CDI	Carbonyldiimidazole
d	Doublet
dba	Dibenzylideneacetone
DCM	Dichloromethane
dd	Doublet of doublets
ddd	Doublet of doublets of doublets
DEPT	Distortionless enhancement by polarization transfer
DFT	Density Functional Theory
DMA	Dimethylacetamide
DMF	Dimethylformamide
DNA	Deoxyribonucleic acid
DNA-PK	DNA-dependent protein kinase
DNA-PKcs	DNA-dependent protein kinase catalytic-subunit
DPPA	Diphenylphosphoryl azide

DSB	Double strand break
ESI	Electrospray ionisation
Et_3N	Triethylamine
EtOAc	Ethyl acetate
g	Grams
Gy	Gray
HMBC	Heteronuclear Multiple Bond Correlation
HNSCC	Head and neck squamous cell carcinoma
HRMS	High-resolution mass spectrometry
HSQC	Heteronuclear single quantum coherence
Hz	Hertz
IC_{50}	Half-maximal inhibitory concentration
*i*Pr	Isopropyl
iPr_2NEt	*N*,*N*-Diisopropylethylamine
J	Coupling constant
Jackiephos	2-{Bis[3,5-bis(trifluoromethyl)phenyl]phosphino}-3,6-dimethoxy -2′,4′,6′-triisopropyl-1,1′-biphenyl
Ku	Ku70-Ku80
LiHMDS	Lithium bis(trimethylsilyl)amide
lit.	Literature
L_nPd^0	Ligand-palladium(0) complex
m	Multiplet
M	Molar
m/z	Mass to charge ratio
MeCN	Acetonitrile
MeI	Iodomethane
MeOH	Methanol
meta	1,3 Substitution
MHz	Megahertz
mmol	Millimole
MS	Mass spectrometry
mTOR	Mammalian target of rapamycin
NHEJ	Non-homologous end joining
NMR	Nuclear magnetic resonance

OAc	Acetate
ortho	1,2 Substitution
PI3K	Phosphatidylinositol-3 kinase
para	1,4 Substitution
PCy_2	Dicyclohexylphosphine
pH	Potential of hydrogen
PIKK	Phosphoinositide-3-kinase-related kinase
pKa	Negative logarithm of the acid dissociation constant
ppm	Parts per million
q	Quartet
quant.	Quantitative
s	Singlet
S_NAr	Nucleophilic aromatic substitution
SSB	Single strand break
t	Triplet
THF	Tetrahydrofuran
THP	Tetrahydropyran
TLC	Thin layer chromatography
TOF	Time of flight
tt	Triplet of triplets
XPhos	Dicyclohexyl[2′,4′,6′-tris(propan-2-yl)[1,1′-biphenyl]-2-yl]phosphane

1 Introduction

1.1 Background

1.1.1 Cancer

The human genome is a complex and finely tuned collection of nucleic acid sequences that comprises the biological information relevant to maintaining life on a cellular level. However, instability and dynamic alterations within the genome encoding for the various cellular growth and repair mechanisms can lead to the development of unregulated, abnormal and invasive cellular growth; cancer.[1]

Cancer results in a mass of abnormal cells that grow uncontrollably, possess the ability to avoid programmed cell death (apoptosis)[1] and have the potential to spread locally and/or to distant sites in the body *via* the bloodstream or lymphatic system; in oncology this is known as a malignant tumour.[2]

If left untreated the malignant tumour will invariably disrupt local and/or distant functioning normal cells within tissues and organ systems posing various deleterious health effects to the organism and an increased likelihood of death as the disease progresses with time.[3]

In the year 2021, the governing healthcare body of New Zealand, Te Whatu Ora, reported 27,869 registrations of individuals newly diagnosed with cancer and 10,488 registered deaths resulting from cancer.[4] These are significant statistics when under the consideration that New Zealand is a country that has a population of approximately 5.3 million. Cancer remains as of today a disease of large focus within the medical field with primary themes surrounding the advancement of existing treatments and the development of novel treatments.

1.1.2 Radiotherapy

Radiotherapy is currently one of the main tools utilized in the treatment of cancer. Radiotherapy involves the use of radioactive compounds or sources of high energy ionising radiation to induce cellular damage at targeted tumour sites in order to irreparably damage the tumour cells and prevent further cellular growth and division. There are two main categories of radiation that can be administered depending on the type of cancer, anatomical location and treatment required; electromagnetic radiation or particulate radiation. The former refers to high-energy photon rays (i.e. X-rays or Gamma-rays) and the latter refers to high-energy particle beams (i.e. proton, electron and neutron beams). However, regardless of which radiation modality is chosen, the irreparable damage to the tumour cells is achieved

via direct damage to cellular DNA or indirect cellular damage sustained by the production of free radicals as a consequence of the high energy radiation administered.[5]

As a treatment radiotherapy is generally considered non-selective due to the lack of absolute discrimination between cancerous cells and healthy cells (resulting in unavoidable side-effects), however, technological advancements allow for administration of radiotherapy into regions of cancerous cells to be done with relatively high precision, allowing for radiotherapy to be efficacious in the treatment of localized squamous cell carcinomas.[5] The efficacy and commonality of radiotherapy treatment is reflected by the 50% proportion of cancer patients whom receive it throughout the course of the illness, with it contributing towards 40% of curative treatment.[6]

1.1.3 Head & Neck Squamous Cell Carcinoma

HNSCCs are a set of squamous cell carcinomas that form within squamous cells that comprise epithelial tissue located on and within the head and neck.[7] In New Zealand approximately 500-550 new cases of head and neck cancers are diagnosed each year[8], with 90% of those comprising of squamous cell carcinomas. The 5-year survival rate for this carcinoma type across all age-ranges and anatomical sites was calculated to be 66% during the period of 2002 to 2006 (increasing from 55% between 1992 to 1996).[9]

Radiotherapy for the treatment of HNSCCs is considered to be the primary treatment modality due to the localized nature of the tumour which allows for the precise administration of the radiation into the tumour site.[10] However despite the efficacy of radiotherapy in the treatment of these carcinomas, DNA damage response mechanisms are a vital line of defence for the irradiated and damaged cells promoting two outcomes: cellular survival and the maintenance of the genome.[11] Thus providing a means for the cancer cells to survive the damage induced by the radiotherapy.

Additionally, it is well documented that solid tumours including HNSCCs are typically less oxygenated than regular tissue, and this hypoxic environment presents a complementary limitation toward radiotherapy treatment in where the hypoxic environment and oxygen depleting effects of radiotherapy hinder the damage fixation of free-radical induced DNA damage by oxygen.[12]

These limitations result in radiotherapy not being as effective as it has the potential to be. The latter limitation has been partially addressed by the introduction of fractionated dosages of radiotherapy, either hyperfractionated which consists of several small doses delivered frequently (e.g. 60 × 1.2 Gy doses over 5 weeks) or hypofractionated which is a smaller number of larger doses delivered less frequently (e.g. 12 × 4 Gy doses over 4 weeks). Hyperfractionation aims to reduce toxicity toward normal tissue by allowing greater time for repair processes to take place between fractions. This also allows for reoxygenation of hypoxic tumour regions, improving the efficacy of the next fraction. In

contrast, hypofractionation takes advantage of newer technologies to deliver higher doses more accurately, sparing normal tissues while being more lethal to tumour tissues and making the repair processes less critical (as normal tissue within the radiation field will die). Both modalities receive clinical application however due to the accelerated hypoxia-mediated radioresistance characteristic of HNSCCs, modern accelerated-hyperfractionated dosage schemes are employed allowing for greater reoxygenation of irradiated tissue (compared to hypofractionation or other dosage schemes), thus discouraging the aggressive formation of the hypoxic environment that these tumours typically reside in.[13] Despite this, the limitations mediated by DNA damage response mechanisms remain a significant challenge in promoting effective radiotherapy outcomes with efforts to overcome this through the development of inhibitors targeting various proteins.

1.1.4 Radiotherapy Induced DNA Damage Response Pathways

The ionizing radiation administered to cancerous tissue during radiotherapy is capable of inducing DNA SSBs and DNA DSBs. These strand breaks result in disruption to the base ordering, structural integrity of the double helical shape and the encoded genomic information of the DNA. Both types of these strand breaks are damaging to the genome of the cell, however with specific regards to radiotherapy, inducing DSBs is one of the primary mechanisms that cancerous cell damage and subsequent cancerous cell death is achieved.[14]

This is the result of DSBs being one of the most severe types of DNA damage that can be sustained due to the potential loss of large chromosomal regions which can cause cellular death. The DSB in contrast to the SSB possesses a greater potential for cellular lethality. There are classically two well-established pathways for the repair of DNA DSBs; homologous recombination and NHEJ.[15]

Homologous recombination is a multi-step repair pathway that involves recombination between sister chromatids during the S-phase of the cell cycle to repair the broken strands, however specific conditions are required for this mechanism to occur including matching sequence identities, alignment in space, physical compatibility and the presence of a sister chromatid.[15] This results in the regeneration of the original DNA sequence.[16]

This is contrasted to NHEJ which acts upon the broken DNA strands and ligates them together, resulting in the generation of an altered DNA sequence lacking homology and containing insertions or deletions.[16] The NHEJ repair pathway begins with the DSB being recognized by the Ku heterodimer, which is then bound by the DNA-PKcs forming the DNA-PK enzyme complex. This DNA-PK complex then allows for the canonical binding of further enzymes and proteins to enact the process of NHEJ. The initial Ku-DNA-PKcs complex is critical regarding this DNA damage repair pathway, and without it NHEJ does not occur.[17] Currently, there is extensive ongoing research into developing compounds to inhibit this

repair mechanism most of which is aimed at inhibiting the functionality of the DNA-PKcs and hence the Ku-DNA-PKcs halting the NHEJ process at a critical early step.

Hence, the NHEJ DSB repair pathway which includes the DNA-PK enzyme actively works against the desired outcome of the radiotherapy; to induce cellular damage to the cancerous cells for the purpose of promoting complete cell death. This provides critical insight into a key DNA damage response mechanism that poses a significant challenge in promoting effective radiotherapy outcomes for the treatment of HNSCCs.

1.1.5 DNA-PK Inhibition

Inhibition of the DNA-PK enzyme serves as a means to radiosensitize cancerous cells through interruption of NHEJ mediated repair and promote the desired outcomes from radiotherapy *via* cellular sensitization to DNA DSBs.[18]

The DNA-PK enzyme is classified as a nuclear serine/threonine protein kinase that serves as a signalling enzyme within the NHEJ pathway *via* functionality alterations made to the NHEJ machinery through autophosphorylation and phosphorylation of serine and threonine residues.[14] DNA-PK belongs to the PIKK family.[19] The PIKKs are related to the PI3Ks which in humans consists of five other members; ataxia-telangiectasia mutated, ataxia- and Rad3-related protein, suppressor of morphogenesis in genitalia, transformation/transcription domain-associated protein and mTOR. Until recently, there was a lack of high-resolution data regarding the exact structure of DNA-PK; other members of the PIKK family provided valuable structural insights and were used as proxies for the structure of DNA-PK.[20]

Although not all members within the PIKK family share functionality, there are common structural motifs between them leading to a range of potential inhibition strategies however most relevant in the case of DNA-PK is the ATP binding region which is highly conserved across members of the PIKK family (and kinases generally). Generally, the ATP binding region of kinases consists of two independent lobes; a smaller N-lobe which is comprised of a five-stranded β sheet that facilitates nucleotide binding and a larger highly conserved αC helix which includes the catalytic residues and the substrate-binding site. ATP binding connects the two lobes allowing for successful phosphorylation of the catalytic substrate. Competitive inhibition of this ATP binding site leads to a blocking and disruption of the catalytic activity of the enzyme. These principles have been applied to DNA-PK.[21]

The ACSRC employed the use of mTOR as a scaffold and studied the binding interactions of the known PI3K and PIKK multi-kinase inhibitor **1** (Dactolisib)[22] (Figure 1), which exhibits inhibitory action *via* the aforementioned ATP-competitive inhibition of the ATP binding site.[23] Both the DNA-PK and mTOR kinases are within the same PIKK kinase family and share structurally related ATP binding regions and motifs hence this methodology was used to adapt the imidazo[4,5-*c*]quinoline of inhibitor **1** into the

relatively unexplored imidazo[4,5-*c*]pyridine-2-one core. The latter core has since been explored and optimized through structure-activity relationship studies resulting in the development of the lead compound imidazopyridinone **2** (SN39536)[22] (Figure 1).

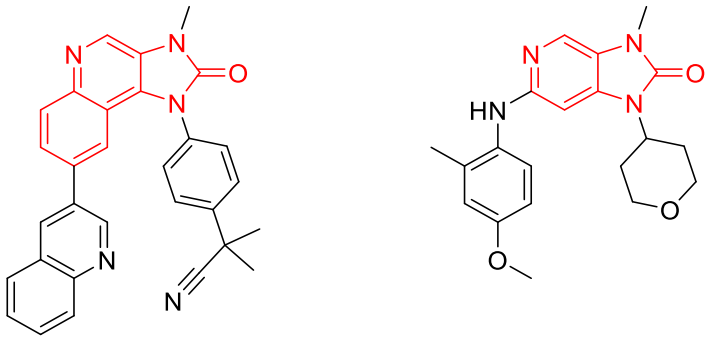

1 **2**

Figure 1: Contrast between the imidazo[4,5-*c*]quinoline core of the PIKK multi-kinase inhibitor 1 and the imidazo[4,5-*c*]pyridine-2-one core of imidazopyridinone 2

Table 1: Relevant IC_{50} data (nm) of compounds 1 and 2, demonstrating PIKK selectivity[22–24]

Compound	DNA-PK	PI3Kα	PI3Kβ	PI3Kγ	PI3Kδ	mTOR
1	7.5	4	75	5	7	20.7
2	7.95	1840	8830	10700	6820	31300

Compound **2** demonstrates potent inhibition of DNA-PK and acceptable selectivity when screened against mTOR and members of the related PI3K family (Table 1). Additionally, inhibitor **2** has been shown to be an effective radiosensitizer of human tumour cells *in vitro*, achieving effective tumour drug concentrations for a minimum of 3 hours post administration providing further evidence that compound **2** is a great inhibitor choice.[22] When contrasted to compound **1**, a lack of selectivity is apparent despite similar levels of DNA-PK inhibition (Table 1). This lack of selectivity would provide a significant level of off target activity rendering it a poor compound to progress with.

In parallel to the ACSRC's development of inhibitor **2**, AZ developed and validated the DNA-PK inhibitor imidazopyrimidinone **3** (AZD7648)[25] (Figure 2).

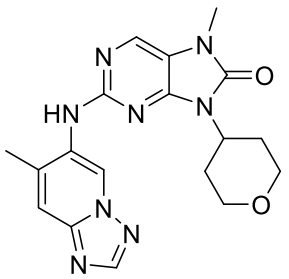

3

Figure 2: The AZ DNA-PK inhibitor imidazopyrimidinone 3

Inhibitor **3** was developed utilizing an alternative methodology to inhibitor **2** *via* a high throughput screen of the AZ library to search for compounds that showed inhibition toward a selection of kinases. These were then further optimized with the goal of enhancing the DNA-PK inhibition, selectivity and potency, leading to compound **3**.[25] Inhibitors **2** and **3** are markedly similar structures aside from two explicit differences; variation in the nitrogenous heterocycle on the core skeleton and the different aniline substituents. Information gathered regarding the substitutions and binding modes of both inhibitors are hence partially complementary.

Comparing the investigations of inhibitors **2** and **3**, there is agreement that the best substituents for the imidazo-nitrogens are a methyl group and THP ring. The ACSRC identified the THP substitution to be critical in retaining potency as any substitution other than a five- or six membered hetero- or carbo-cycle resulted in a loss of potency and selectivity, indicating that this substituent plays a specific binding role within DNA-PK contrasted to other PIKK members.[22] AZ did not investigate this substitution within the same context however they established that when compared to 1,4 substituted cyclohexanes, biochemical potency remains unchanged however cell potency increases suggesting a positive influence upon cell permeability.[25] The *N*-methyl group was determined by the ACSRC to be the largest tolerated substituent with anything larger providing too great of a steric burden resulting in a loss of potency.[22] As for the aniline substitution the ACSRC determined by screening multiple aniline derivatives that compounds containing the 2-Me and 4-H bond acceptor motif showed a 40-364 fold sensitivity increase against PI3Kα and a 270-3440 fold sensitivity increase against mTOR. The informally dubbed aniline "magic-methyl" group has been deduced to promote potency and activity by increasing lipophilic bonding interactions and potentially creating an induced rotation of the ring system compared to the core.[22] This is also hypothesized by AZ who suggested that the methyl group increases potency by promoting lipophilic interactions within the hydrophobic pocket consisting of Tyr3791, Leu3806 and Ile3940.[25] However, the choice of 4-methoxy is contested. AZ's investigations begun with the exact aniline substructure of inhibitor **2** however there was concern that this labile methoxy group poses a potential reactive metabolite liability, so investigations were focused on deriving a group to mimic the

methoxy which they predicted with their DNA-PK homology model to bind near multiple polar groups within hydrogen bonding distance. They deduced the triazole moiety to be an appropriate substitution for the methoxy group.[25]

1.2 Synthetic Strategies

1.2.1 The Published ACSRC Synthetic Route to Inhibitor 2

The procedure utilized by the ACSRC to synthesize inhibitor **2** is a six-step synthetic route.[22]

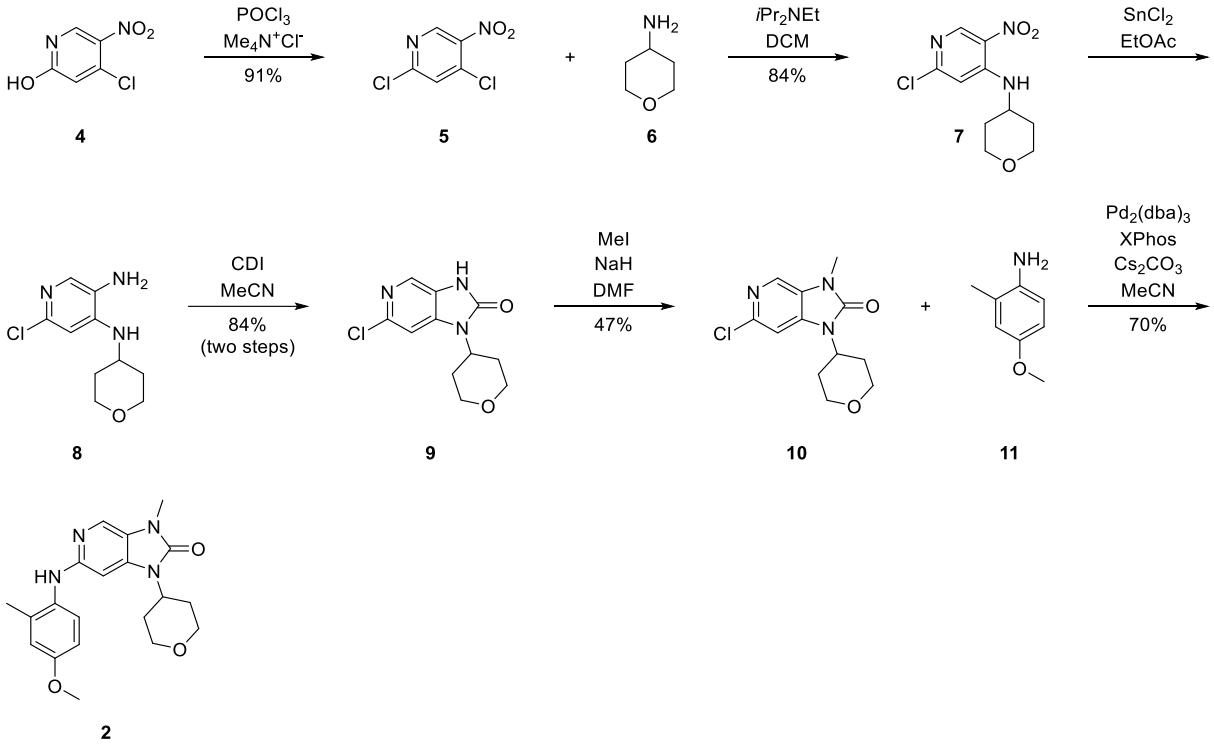

Scheme 1: The ACSRC synthetic route to inhibitor 2[22]

1.2.1.1 Brief Analysis of the ACSRC Route

To begin commercially available pyridinol **4** (Scheme 1) is treated with $POCl_3$ and $Me_4N^+Cl^-$ at 120 °C. This undergoes chlorination *via* substitution of an aryl phosphate ester intermediate by Cl^- yielding dichloride **5** (Scheme 1). with a reported yield of 91%. Despite the high yield of this reaction, this is a relatively harsh process to begin the synthesis with, requiring the use of $POCl_3$ which is toxic and corrosive alongside high temperature; this may prove challenging and hazardous at an industrial scale.

Following isolation of dichloride **5** an S_NAr reaction is performed to regioselectively install the THP-NH side chain at the 4-position using amine **6** (Scheme 1) and a molar excess of *i*Pr_2NEt in DCM, producing chloride **7** (Scheme 1) in an 84% yield. The electronics of the ring structure are tailored to favour selectivity toward the 4-position chloride with the electron withdrawing pyridine nitrogen and the nitro group residing *ortho* and *para* respective to the leaving group giving a more stable *Meisenheimer complex* versus if substitution happened at the 2-chloride position. This results in the critical regioselectivity of the reaction. This reaction is run under relatively standard conditions for an S_NAr reaction and should not have any major issues on an increased scale.

Subsequent treatment of nitropyridine **7** with an excess of $SnCl_2$ in EtOAc at 50 °C provides diamine **8** (Scheme 1). The use of $SnCl_2$ as a reductant provides a notable advantage over other reduction mechanisms in that the 2-chloride is preserved. The use of catalytic hydrogenation with a platinum group catalyst such as Pd/C carries the risk of chloride reduction alongside the nitro group and in the final step of the route the halide is a necessary handle for sidechain installation.

To form the substituted 2-imidazolidinone ring, diamine **8** is treated with a molar equivalent amount of CDI in MeCN at 20 °C. Initial nucleophilic acyl substitution occurs between the primary aniline group and the CDI, then subsequent attack by the secondary aniline ejects the remaining imidazole forming imidazopyridinone **9** (Scheme 1) in an 84% yield (across two steps including the $SnCl_2$ reduction). The utilization of CDI and the reaction conditions that are employed allows for a one-pot synthesis of the bicyclic compound as opposed to having to undertake separate reactions, this provides great utility in shortening the route and improving efficiency.

N-methylation is then carried out on imidazopyridinone **9** utilizing an excess of NaH as the base and MeI as the alkylating agent. This produced intermediate **10** (Scheme 1) with a reported yield of 47%. This is a relatively standard methylation procedure employing commonly used reagents however there remains notable safety concerns with regards to the hazards imposed by NaH and MeI.

The final step within the synthetic procedure involves performing a Buchwald-Hartwig cross-coupling reaction between chloride **10** and an appropriate aniline. Amination within this reaction occurs *via* a palladium mediated catalytic cycle. Chloride **10** was treated with a slight molar excess of aniline **11** (Scheme 1), $Pd_2(dba)_3$, XPhos and Cs_2CO_3 in MeCN at 120 °C, forming inhibitor **2** in a 70% yield.

1.2.1.2 Efficiency of the ACSRC Route

This synthetic route (Scheme 1) is designed to allow for structural diversity as this was the route employed to produce the analogues that led to the discovery of inhibitor **2**. The route introduces two of the three critical *N*-substituted components in the final steps of the route allowing for differing moieties to be installed. However, this is contrasted to the early THP-NH installation which requires entirely new

scaffolds to alter the substitution of this position. The overall yield is 21%, and this leaves ample opportunity to explore alternative synthetic strategies in order to improve the efficiency or substitute the reactions to increase the overall synthetic yield.

1.2.2 The Published AZ Synthetic Route to Inhibitor 3

In looking critically at the reported synthesis of AZ's inhibitor **3**, there is similarity but the key differences provide insight into an alternative approach towards the synthesis of the ACSRC's inhibitor **2**.

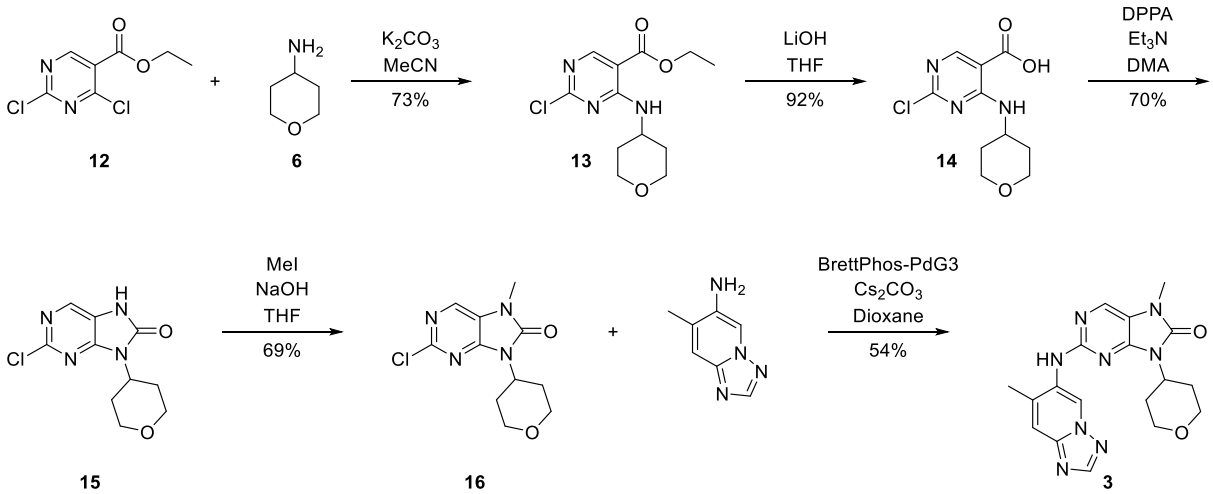

Scheme 2: The AZ synthetic route to inhibitor 3[25]

1.2.2.1 Brief Analysis of the AZ Route

Analogous to the second step within the ASCRC route, this route begins with the substitution of the chloride *ortho* to the ester group on dichloride **12** (Scheme 2) with amine **6** *via* the S_NAr reaction mechanism, producing chloride **13** (Scheme 2) in a 73% yield.

Ethyl ester **13** in the subsequent step is treated with a molar excess of LiOH in an H_2O/THF mixture. This facilitates the base-catalyzed hydrolysis of the ester producing a carboxylate. This is then acidified with aqueous 2M HCl, precipitating out the product as carboxylic acid **14** (Scheme 2) with a 92% yield.

In contrast to the ACSRC route, the THP-NH substituted 2-imidazolidinone ring is generated *via* intramolecular nucleophilic attack following a Curtius rearrangement of an intermediary acyl azide. The acyl azide is produced by the addition of DPPA to carboxylic acid **14** in the presence of NEt_3. After stirring at room temperature for 1 hour the acyl azide is thermally decomposed to an isocyanate with the introduction of heating (120 °C). This allows for the intramolecular rearrangement *via* nucleophilic

attack from the NH group on the isocyanate, forming imidazopyrimidinone **15** (Scheme 2) at a yield of 70%.

From this point onwards there is a convergence with the ACSRC route, with the final two steps being identical in reaction mechanism to the ACSRC route only differing by the conditions and substrates; an *N*-methylation is conducted on imidazopyrimidinone **15** generating intermediate **16** (Scheme 2) followed by a subsequent Buchwald-Hartwig amination producing inhibitor **3** (Scheme 2). It is through the structural similarities between inhibitors **2** and **3** that there is a potential to apply the AZ synthetic strategy the synthesis of inhibitor **2**.

1.2.3 A Novel Alternative Route to Inhibitor 2

The synthetic route published by AZ to synthesize inhibitor **3** has been adjusted to generate inhibitor **2** to explore if the route is viable and any potential differences in synthetic efficiency contrasted to the ACSRC route. The first key difference from the ASCRC route lies within the substitution of the first three reactions with the described AZ reactions (Scheme 3). Of note this alternative route converges with the ACSRC route at reaction four (*N*-methylation).

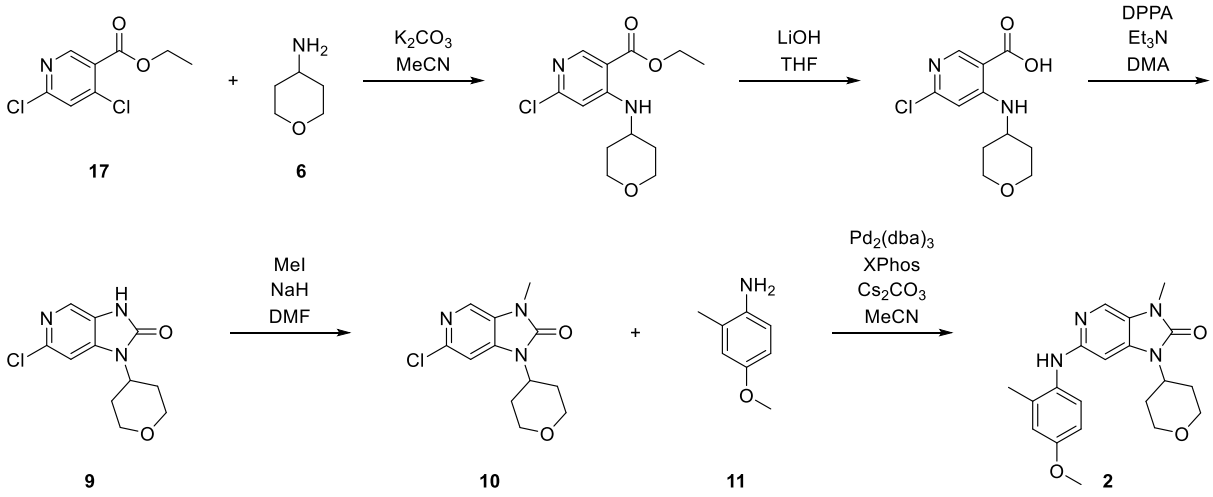

Scheme 3: The AZ route with substrate adjustment to generate inhibitor 2

The second key difference is the starting material alteration from nitropyridine **4** to ethyl nicotinate **17** (Scheme 3, Figure 3) to allow for these reactions (Scheme 3).

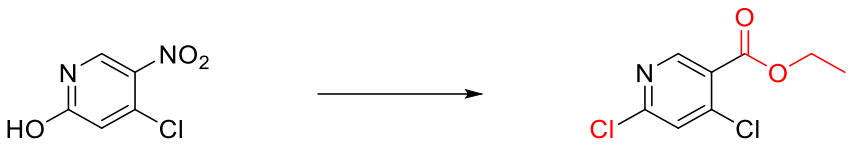

4

ACSRC Starting Substrate

17

Adjusted Starting Substrate

Figure 3: Comparison of the starting substrates between the ACSRC and novel route

1.2.3.1 Proposed Synthetic Efficiency of the Novel Route

The proposed route is exploratory in nature to determine primarily if the different electronics of the pyridine core can be accommodated (contrasted to AZ's pyrimidine core) across a number of steps. These altered reactions may provide an advantage over the ACSRC route in terms of synthetic efficiency and simplicity. Additionally, this feasibility study may be useful in providing options for scale up syntheses in the future. From the perspective of efficiency, the dichloride motif on ethyl nicotinate **17** bypasses the need for the initial $POCl_3$ reaction in the ACSRC route shortening the proposed route and avoiding the use of hazardous reagents. Another synthetic advantage within the proposed route is that the final two reaction substrates and conditions (that is the methylation and Buchwald-Hartwig amination) are identical to those used by the ACSRC which have already been explored and optimized.

1.2.3.2 The Curtius Rearrangement to Form a Substituted 2-Imidazolidinone Ring

This reaction provides an alternative mechanism to the ACSRC's CDI coupling to form the substituted 2-imidazolidinone ring. This is allowed by the presence and transformations of the ester group throughout the novel route. The transformations begin with an ester hydrolysis which is advantageous as it avoids the requirement of the $SnCl_2$ reduction, replacing it with a typically high yielding reaction while simultaneously minimizing exposure of the substrate to carcinogenic inorganic material. This minimization provides an advantage as it lessens any potential inorganic residue contamination of the drug, which if sufficient could hinder the advancement of the drug with potential toxicity and safety concerns.[26] Additionally the replacement of the nitro-group with the ethyl ester alleviates safety concerns from a synthesis standpoint as the mutagenicity and genotoxicity of nitroaromatic compounds is well documented[27] and the reactions in the novel route avoid the presence of this functional group entirely.

Post hydrolysis, the resultant carboxylic acid is converted to an acyl azide with DPPA, followed by the heat induced Curtius Rearrangement of the acyl azide to an isocyanate. Subsequent intramolecular rearrangement then forms the substituted 2-imidazolidinone ring. The rearrangement discovered by

Theodore Curtius[28,29] has always been of mainstream significance due to the versatility of the isocyanate group. However, traditional acyl azide synthesis has always been of a laborious nature (Scheme 4).

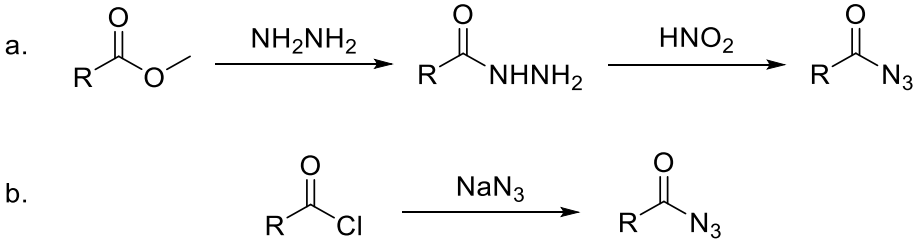

Scheme 4: Traditional routes to generating acyl azides[30]

Traditional routes involve the use of extremely hazardous reagents[30] (Scheme 4), with notable mentions of NH_2NH_2 and NaN_3 both of which are acutely toxic[31,32] and explosive.[32,33] This changed when Shioiri *et al* published a paper disclosing the use of DPPA in the streamlined conversion of a carboxylic acid to an acyl azide.[34] This holds great importance in organic synthesis as it allows for the more accessible generation of isocyanates through the Curtius rearrangement. This is how the isocyanate intermediate is generated on the way to the substituted 2-imidazolidinone ring. This isocyanate then goes on to react with the amine of the installed THP-NH group forming the urea bond giving the substituted 2-imidazolidinone ring. The reaction proceeding from the carboxylic acid to the 2-imidazolidinone ring has been demonstrated as a feasible one-pot procedure by AZ. It is proposed that this reaction alongside the ester hydrolysis may be synthetically more efficient and scalable than the ACSRC's reduction and CDI coupling regarding the synthesis of inhibitor **2**.

1.2.3.3 Rearranged Positioning of the Buchwald-Hartwig Coupling

The final key advantage of the proposed route is the opportunity to overhaul the route by adjusting the sequence of reactions, we propose placing the Buchwald-Hartwig amination toward the beginning of the route at the second step (Scheme 5), where it is expected to alter the electronics of the synthetic intermediates. This allows for investigation as to whether these altered electronics aid or diminish the synthetic yields.

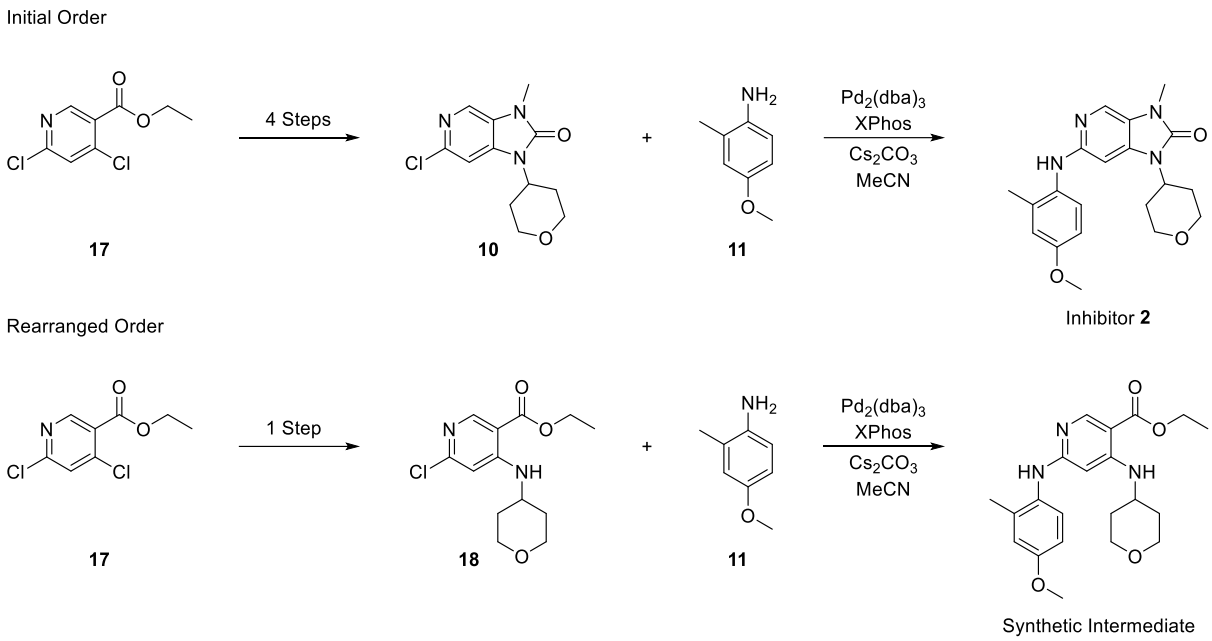

Scheme 5: Proposed rearrangement of the novel route

This was predicted not to be a viable option in the ACSRC route due to the perception that the nitro group on nitropyridine **7** would deactivate the chloride. The ester group of the proposed substrate ethyl nicotinate **17** should not be as deactivating and we anticipated this could make cross-coupling more facile. There is also advantage in putting the palladium mediated step early to minimize potential palladium residue in the end product (more purifications post exposure). Similarly to the removal of the $SnCl_2$ reduction this provides advantages from the perspective of minimizing inorganic contamination of the drug which could hinder its clinical progression.[26] However due to this cross-coupling occurring through a sensitive palladium mediated cycle (Scheme 6) substrate functionality and overall compatibilities needs to be considered.

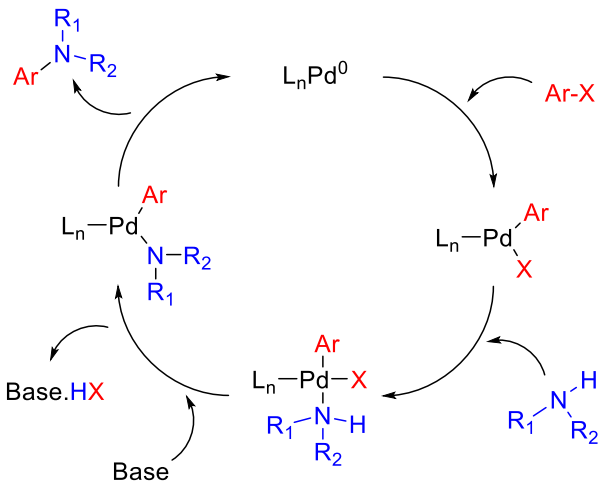

Scheme 6: General catalytic cycle for Buchwald-Hartwig couplings[35]

There are a variety of confounding variables to consider when investigating optimal Buchwald-Hartwig amination conditions notably including but not limited to the choice of phosphine ligand, palladium source, base and solvent. All factors need to be compatible with the nature and functional groups of the substrate. However, if sufficiently optimized a high yielding reaction can be achieved.

1.3 Overview

Radiotherapy is a critical component for the treatment of various forms of cancer, including HNSCC. As DNA-PK is a significant component in regulating the NHEJ DNA damage response mechanism, inhibition of this enzyme serves as a means to radiosensitize cancerous cells. Inhibitor **2** has been developed as a preclinical compound to radiosensitize HNSCC cells. This thesis will examine a novel route to synthesize this compound to determine whether the proposed route (Scheme 3) is viable and provides any advantages to synthetic efficiency over the published ACSRC route (Scheme 1). The optimizations of each reaction and the underpinning rationale behind them will be examined alongside comparisons to the analogous AZ and ACSRC reactions. Our attempted rearrangement of the proposed novel route will then be explored (Scheme 5) in order to determine whether any synthetic advantage can be derived over the initial arrangement. Performance of a novel Buchwald-Hartwig cross-coupling is anticipated to be a key factor in the investigation of the rearrangement.

2 Discussion

2.1 Novel Synthesis of an Imidazopyridinone *via* a Curtius Rearrangement

2.1.1 Nucleophilic Aromatic Substitution

The first reaction attempted was a substitution reaction combining dichloride **17** and amine **6** (Scheme 7). This reaction proceeds through the S_NAr mechanism where an electron-deficient aromatic ring is attacked by a base-activated nucleophile displacing the halide resulting in the substituted product.

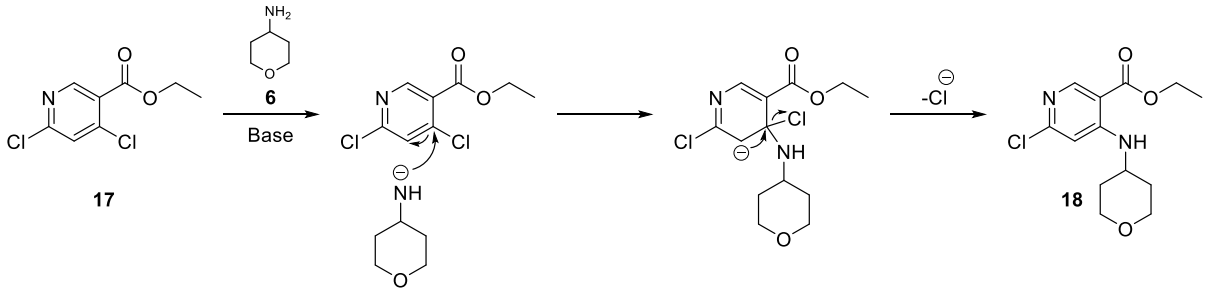

Scheme 7: S_NAr reaction mechanism on dichloride 17

The initial attempt established a baseline yield following the AZ conditions (1:1:2.5 molar ratio of **17**:**6**: K_2CO_3). The reaction was initially run at room temperature for 16 hours however TLC analysis of the reaction mixture indicated significant portions of unreacted dichloride **17**, so the reaction was left for an additional 24 hours. TLC analysis after the additional time indicated that the majority of dichloride **17** had been consumed. The precipitate from the reaction was discarded and without further workup the organic layer was dried under reduced pressure. The crude product was purified by column chromatography producing chloride **18** (Scheme 7) in a 67.4% yield. This was comparable to the AZ yield of 73.0% using the pyrimidine equivalent **12** (Scheme 2). While the yields were similar between these processes it is notable that the reaction with dichloride **17** required 24 additional hours revealing a significant disadvantage.

The extended reaction time indicated lower susceptibility of the pyridine starting material to substitution compared to the pyrimidine equivalent. In light of this, we attempted to reduce the reaction time by increasing the temperature of the reaction. The reaction was heated at 75 °C for 16 hours, then worked-up in an identical manner generating chloride **18** in a 55.9% yield. This yield indicated that heating the

reaction for 16 hours provides some improvement over the 16-hour room temperature conditions (which only gave a small amount of product). Despite this, the yield remained substantially lower than the 40-hour reaction. Considering these points, we anticipated that benefit could be derived from heating for 40 hours. The reaction was hence heated at 75 °C for 40 hours producing chloride **18** in a 70.4% yield, this represented a modest improvement over the room-temperature reaction while matching the AZ equivalent albeit with a longer reaction time. These were adopted as our standard conditions, as at a larger scale even a modest improvement is significant.

Due to the reaction requiring 40 hours alongside the addition of heat in order to match the AZ yield inferences can be made regarding the differing electronics of the starting materials;

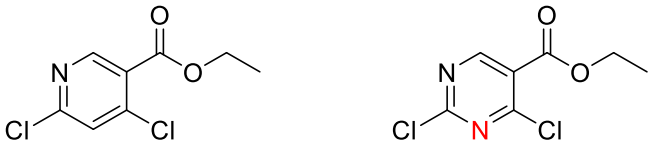

17 **12**

Figure 4: Comparison of the S_NAr substrates for the novel route and the AZ route

By inspection of the starting materials, it would be reasonable to speculate that they are electronically quite similar (Figure 4), however based on the findings of these reactions, the pyridine ring of dichloride **17** is less suited towards accommodating the S_NAr mechanism compared to the pyrimidine of dichloride **12**. We can rationalize this by observing the ring of dichloride **17** containing one less nitrogen compared to dichloride **12** resulting in a decreased ring electrophilicity making the carbon less susceptible to nucleophilic attack. Further evidence towards our findings can be found when the predicted stabilities of the *Meisenheimer complexes* are compared (Figure 5).

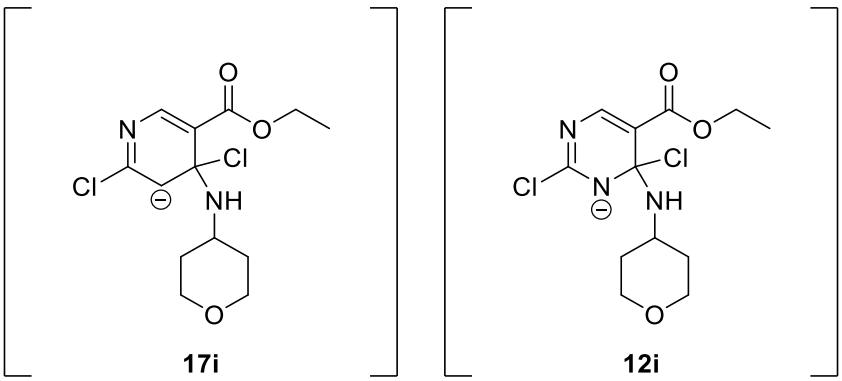

17i **12i**

Figure 5: Example intermediate structures of the S_NAr reaction; a key intermediate for the pyridine substrate 17 (17i); a key intermediate for the pyrimidine substrate 12 (12i)

The resonance structures of the intermediates suggests that the extra pyrimidine nitrogen on the intermediate **12i** (Figure 5) should provide additional stabilisation of the carbanion intermediate when compared to the pyridine equivalent **17i** (Figure 5). We propose the discussed factors lead to a less favoured S_NAr reaction.

The final change was the screening of differing bases. The base is involved in the critical step of nucleophile generation (in this case deprotonation of the amine) so the potential for alternative bases to promote the reaction and further increase the yield was investigated. Using our standardized conditions we employed NEt_3 as the base. After the general work-up, chloride **18** was generated in a yield of 63.0%. The next base to be trialled was *i*Pr_2NEt which produced chloride **18** in a 65.8% yield. The diminished yields provided by the amine bases suggests they deprotonate amine **6** less efficiently than the carbonate bases despite the relative increased pKa of the tertiary amine bases (10.75 for NEt_3 and 10.98 for *i*Pr_2NEt) over carbonates (10.25 for K_2CO_3). This was investigated further by trialling a final base of Cs_2CO_3. Improved yields with Cs_2CO_3 as opposed to K_2CO_3 despite identical reaction conditions is a well observed phenomenon in organic synthesis in reactions where anionic nucleophiles are generated *in situ*. This is due to the much less pronounced ion-pairing of Cs^{2+} to CO_3^{2-} when contrasted to the ion pairing of K_2CO_3. This results in more efficient release CO_3^{2-}. This effect is pronounced by the relatively large dielectric constant of the reaction solvent; MeCN.[36] Until this point a recurring theme throughout all reactions was the lingering presence of unreacted dichloride **17** and the absence of unreacted amine **6**. So, alongside the trialling of Cs_2CO_3, the amount of amine **6** was increased to a molar ratio of 1.5 in an attempt to push the reaction further to completion. These two adjustments produced the greatest yield of chloride **18** at 85.3% (Table 2). The increased quantity of amine **6** somewhat confounds interpretation of this result, but nonetheless the combination of these changes provided improved reaction conditions. These were the only bases screened as we were conscious of a need to balance basicity to prevent ester hydrolysis.

Table 2: Highest yield achieved (%) for the bases trialled in the novel S_NAr reaction

Base	Highest Yield Achieved
K_2CO_3	70.4
NEt_3	63.0
iPr_2NEt	65.8
Cs_2CO_3*	85.3

* This yield includes the adjustment of the THP to a molar ratio of 1.5

2.1.1.1 Characterization of Chloride 18

Initial identification of the compound was achieved with MS, observing an $[M+H]^+$ peak at 285.1 *m/z*. The ^{1}H-NMR and the ^{13}C-APT spectra were then acquired to support the proposed structure. The ^{13}C-APT experiment was chosen as it provides additional information alongside the peak shifts regarding the nature of the carbon peak; with CH_2/C being phased inversely to CH_3/CH. This gives the information of the three standard DEPT (45, 90 and 135) variants in one experiment with only a minor penalty to sensitivity.

A quartet at 4.33 ppm and a triplet at 1.38 ppm indicated the presence of the retained ethyl ester consistent with the structure of the starting material dichloride **17**. In addition, there were two well resolved aromatic protons aligning with the two aromatic protons expected on chloride **18**. The APT experiment revealed that the structure contained one non-aromatic quaternary, three aromatic quaternaries, three CH_2 environments and four CH/CH_3 environments which aligned with the structure of chloride **18** (Figure 6).

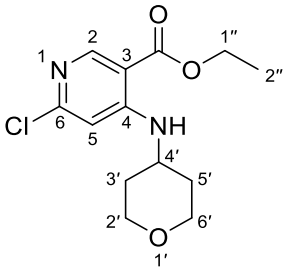

18

Figure 6: Numbered structure of chloride 18

As installation of the THP sidechain was the key structural change in this reaction sequence, the observation of nine protons through integration in the aliphatic region was encouraging. Regarding the THP methylene protons we anticipated to observe distinct chemical shifts for the geminal protons forming each methylene unit at 2′/6′-CH_2 and 3′/5′-CH_2 alongside the lone 4′-CH proton giving three unique proton environments (Ha and Hb at 6′-CH_2 labelled for illustration in Figure 7). Aligning with this would be only three distinct carbon environments representing the symmetry in the ring. The experimental carbon signals matched this expectation, however the ^{1}H-NMR data showed four proton environments; three 2H multiplets and one 3H multiplet. Additionally, HSQC revealed that differing 2H multiplets correlated to identical carbons. These observations suggested diasterotopicity of the geminal protons giving the equivalencies coloured in Figure 7.

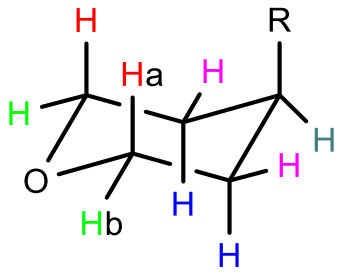

Figure 7: Chair diagram of THP-R; example of expected geminal equivalency labelled; observed equivalent protons coloured

Through analysis of the peak shapes evident despite the overlap, we were able to assign the downfield area of the 3H multiplet as corresponding to the methine signal and the upfield portion corresponding to a pair of diasterotopic protons (Figure 8).

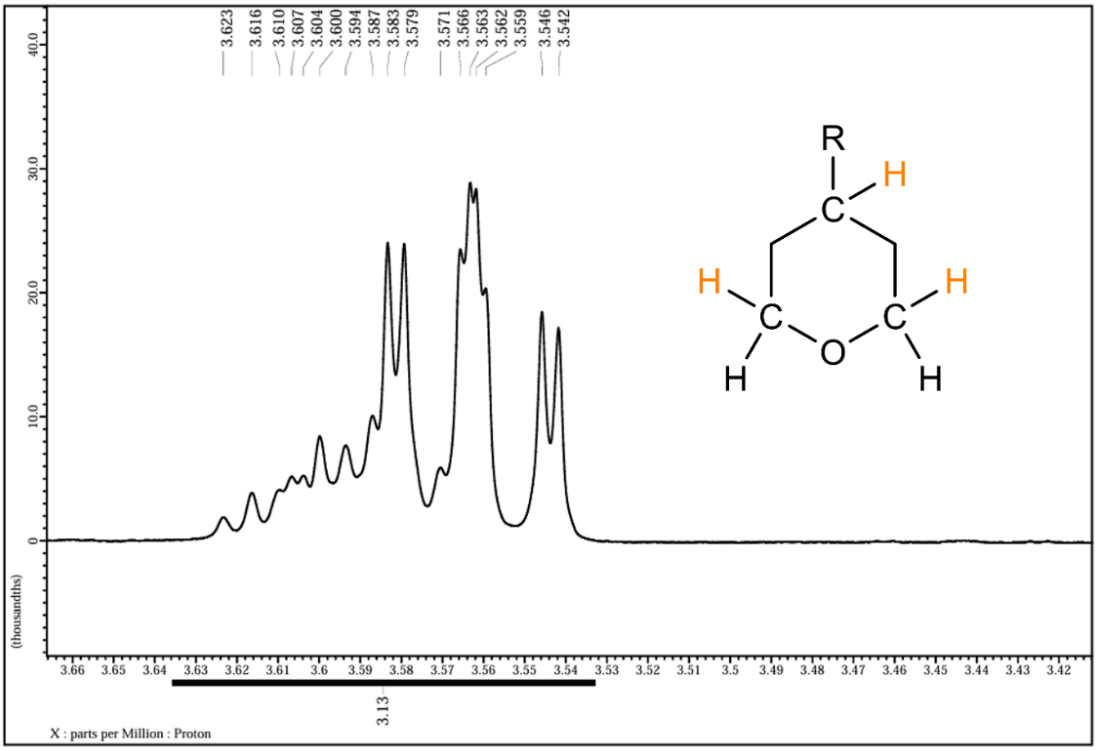

Figure 8: The 3H multiplet of chloride 18; representative protons coloured

HSQC provided further evidence of this overlap where the multiplet correlated to two different carbons (Figure 9) contrasted to the expected one if the peak did not include the methine proton.

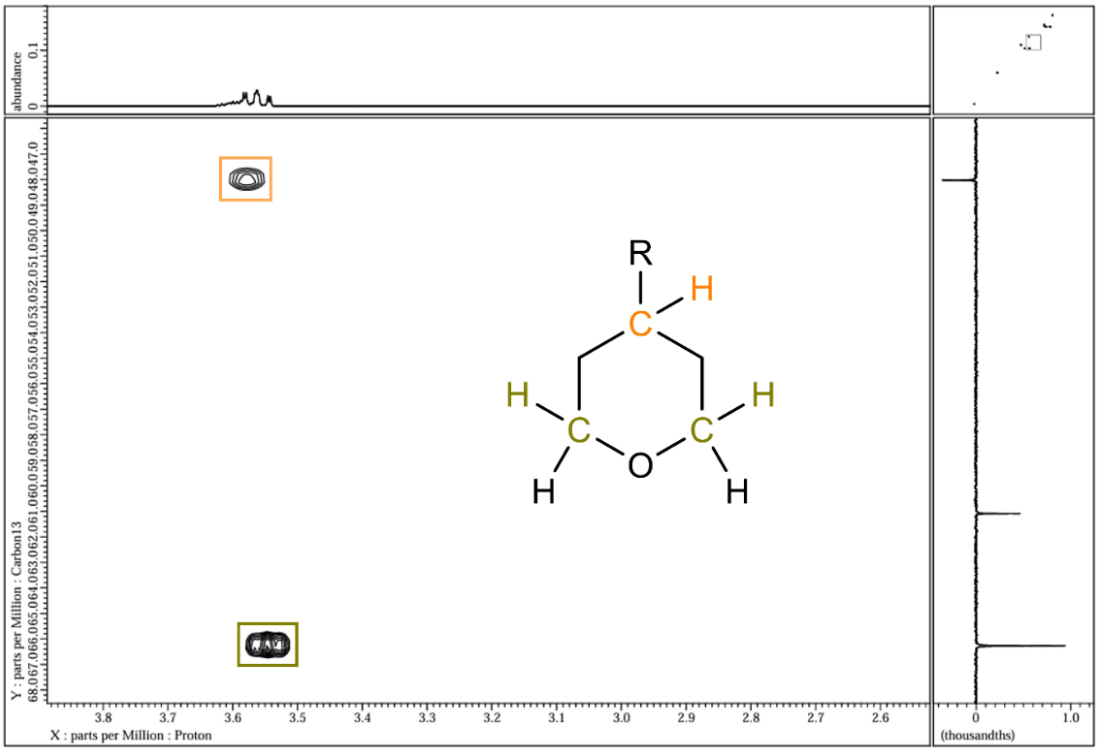

Figure 9: HSQC correlations of the 3H multiplet for chloride 18; equivalent environments and correlations coloured

The two farthest downfield of the THP protons were assigned to be the H-6′ and H-2′ protons due to the deshielding effect of the neighbouring oxygen within the ring. One of these signals was also the 3H multiplet (Figure 8) hence this signal was also assigned to be the methine proton H-4′. The remaining two 2H multiplets were assigned to the remaining THP protons; H-5′ and H-3′. Post proton assignment, HSQC and the APT allowed for the assignments of the related carbons.

The aromatic protons were identified by the proton integration values of two singlets within the aromatic shift region of the ^{1}H-NMR spectrum. HSQC and the APT revealed that these peaks at 8.67 ppm and 6.54 ppm both correlated to CH carbons which confirmed their identity. The positioning of either aromatic proton and associated carbon was indistinguishable with standard 1D and 2D experiments due to the proton deficiency of the ring which rendered HMBC ineffective for this purpose. However, the aromatic protons had distinctive shifts with one being notably further upfield than the other (6.54 ppm vs 8.67 ppm) which was consistent with the literature and the ACSRC's characterisation of structurally similar compounds.[37] Hence, they were assigned based upon this literature with H-5 being the upfield of the two leaving H-2 being the downfield alternative. Non-standard NMR experiments would be required to decipher these experimentally and this was deemed unnecessary in light of the other evidence allowing assignment.

The remaining positions to be assigned were the quaternary carbons of the ring and the carbonyl which aligned with the remaining signals of the APT. HMBC analysis was ineffective due to both aromatic protons showing long range coupling to every quaternary carbon despite adjustment of the long-range *J* value. Out of the remaining four carbons signals the one notably downfield to the rest (167.8 vs 155.9, 154.9 and 107.1 ppm) was assigned to be the carbonyl quaternary due to its extremely deshielding environment, and presence in the characteristic range for ester carbonyl signals.

Of the remaining three peaks, the signal at 107.1 ppm was noticeably upfield to the rest. Inspection of the ring revealed that two carbons (3-C, 5-CH) were distinct from the remainder as they did not have any direct bonding to ring or exocyclic nitrogens which would be expected to cause a downfield shift. A carbon of this type had been assigned (5-CH) and hence by this reasoning and the similarity in shift values (107.1 ppm vs 104.8 ppm) 107.1 ppm was likely 3-C. Additionally, this reasoning was supported by the similarity in the shift values of the remaining quaternaries (155.9 and 154.9 ppm) to 2-CH (153.5 ppm); all of which were adjacent to a ring or exocyclic nitrogen. These final two quaternaries were unable to be distinguished so they were not specifically assigned. Advanced NMR methodology such as the 1,1 ADEQUATE experiment[38] could allow for the assignment of these however the NMR instrument was not configured to this, and this study would have been outside the scope of the project.

2.1.2 Ester Hydrolysis

In the next step of the novel route, the base-catalyzed hydrolysis of ethyl ester **18** was carried out (Scheme 8).

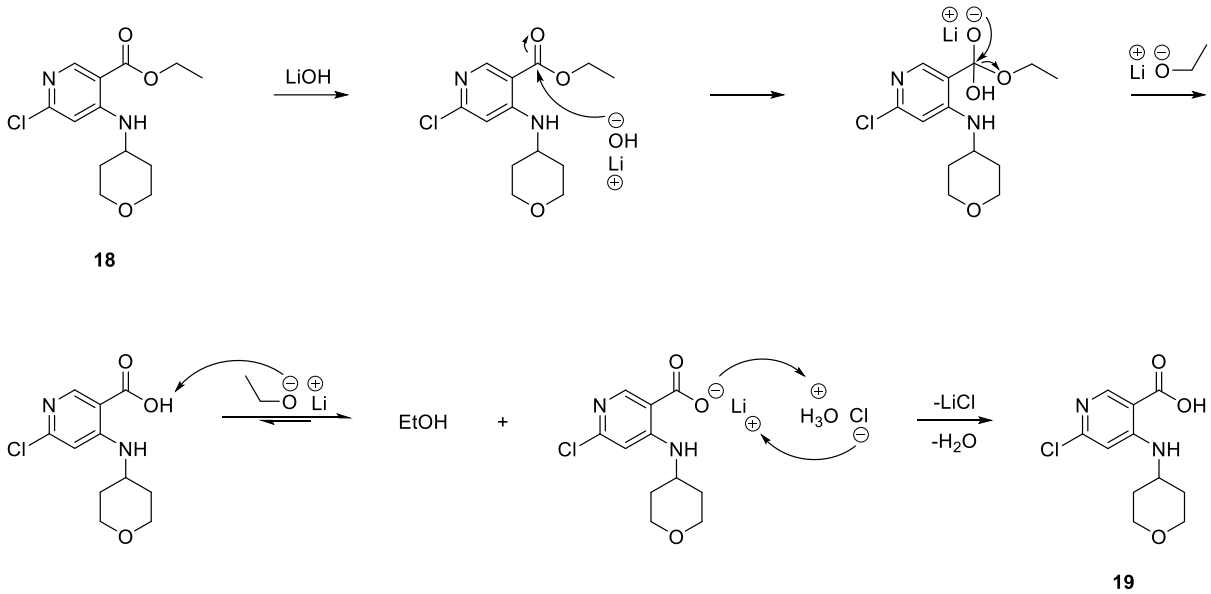

Scheme 8: Hydrolysis mechanism of ethyl ester 18

As with the previous step, our initial conditions were chosen to match the AZ work. This involved stirring ethyl ester **18** and LiOH at a molar ratio of 1:2 at room temperature for 3 hours in THF/H_2O. Subsequent removal of THF *in vacuo*, followed by acidification with 2M HCl produced the crude product as a precipitate. Isolation of the precipitate by filtration furnished carboxylic acid **19** (Scheme 8) in an 81.5% yield. This was lower than the yield AZ achieved of 92.0% with their pyrimidine analogue **13** (Scheme 2). The reaction was reattempted under identical conditions, but with more careful assessment of reaction progression with TLC analysis. After 3 hours, it was evident that an amount of ethyl ester **18** remained, so the reaction was then left for a further 16 hours at which point ethyl ester **18** was no longer detected by TLC. Following work-up, carboxylic acid **19** was isolated in a yield of 89.9% which marked a slight increase and highlighted that the additional reaction time was required to drive the reaction forward. The slightly diminished yield compared to AZ alongside the longer reaction time is consistent with the findings of the S_NAr reaction where an exact replication of the AZ conditions with a pyridine analogue produces a less efficient reaction. For this reaction it is expected that the pyridine of ethyl ester **18** be less electron withdrawing than the pyrimidine of ethyl ester **13**, resulting in a less δ+ carbonyl carbon that is less susceptible to hydrolysis.

2.1.2.1 Characterization of Carboxylic Acid 19

MS initially identified the compound ($[M+H]^+$ of 257.1 *m/z*) and standard 1D and 2D NMR experiments were employed to characterize carboxylic acid **19**. Regarding the NMR, retention of the THP group was suggested by the presence of three 2H multipets and a 3H multiplet. Additionally, the ^{1}H-NMR and HSQC experiments confirmed the diasterotopic nature of these protons. The retention of the carbonyl was indicated by a downfield quaternary carbon with a near identical shift to what was seen in the characterization of ethyl ester **18** (169.0 ppm vs 167.8 ppm). This evidence was consistent with the structure of the starting material **18** which verified the presence of the THP group and carbonyl.

The key transformation of this reaction was the hydrolysis of ethyl ester **18**. The well-resolved triplet and quartet signal that defined the ethyl ester in the starting material **18** being absent in the ^{1}H-NMR spectrum confirmed its hydrolysis. The remaining assignments were the two aromatic protons and the three quaternary carbons of the ring. The magnitudes of these remaining shifts matched the pattern present in ethyl ester **18** and were hence assigned with the same reasoning. This gives H-5 as the most upfield aromatic signal and 3-C as the most upfield of the remaining quaternary signals. The quaternaries 4-C and 6-C remained indistinguishable.

2.1.3 Curtius Rearrangement

To form the substituted 2-imidazolidinone ring we used a one-pot procedure telescoping two reactions. The first step of this process converts the carboxylic acid into an acyl azide using DPPA and NEt_3 (Scheme 9).

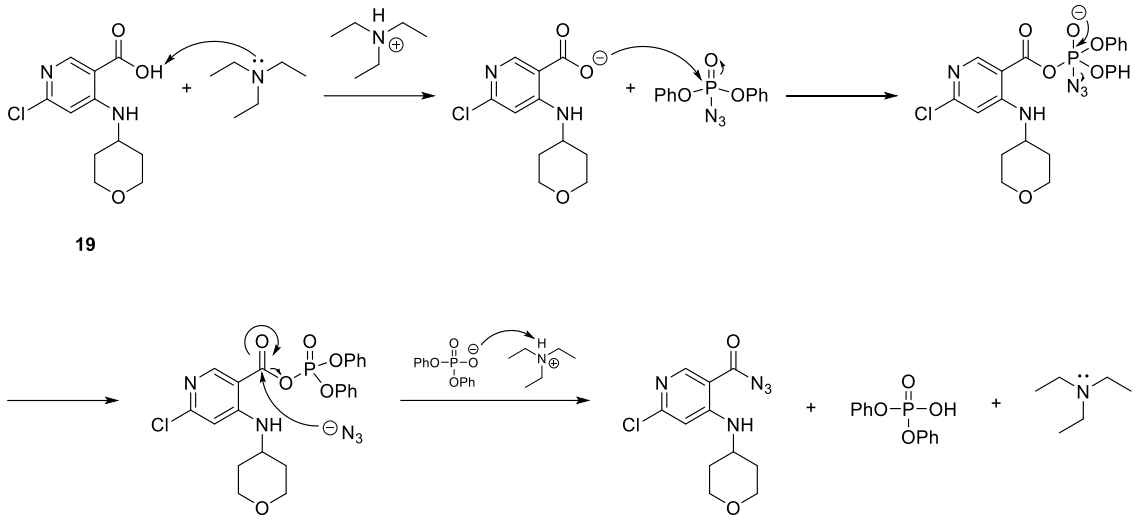

Scheme 9: Conversion of carboxylic acid 19 to an acyl azide *via* DPPA and NEt_3

In the second step heat promotes a Curtius rearrangement converting the newly formed acyl azide group into an isocyanate. Subsequent intramolecular nucleophilic attack by the amine onto the carbonyl with concurrent proton transfer generates the new ring system forming imidazopyridinone **9** (Scheme 10).

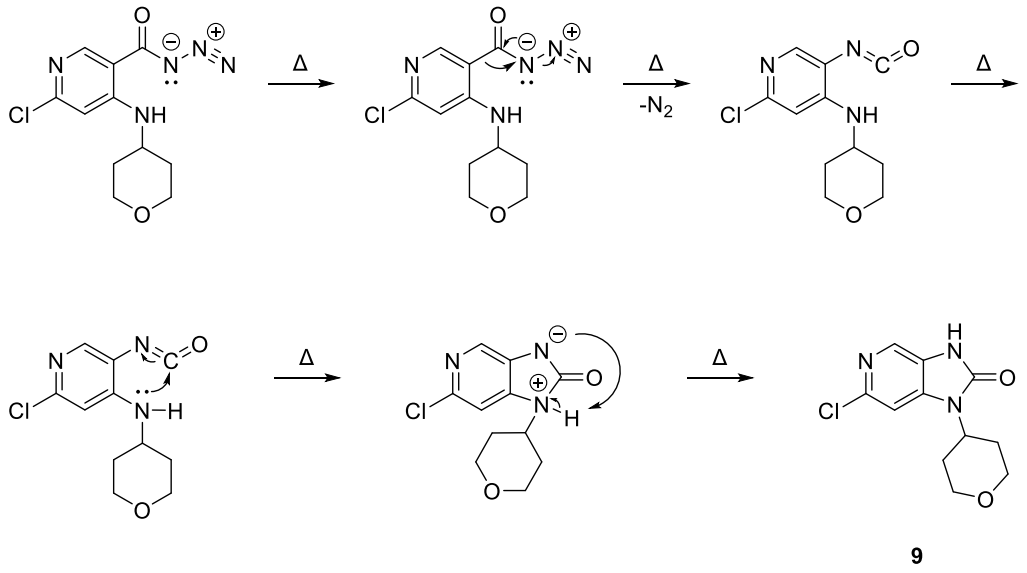

Scheme 10: Curtius rearrangement and ring formation generating imidazopyridinone 9

As with previous steps, the initial conditions trialled followed the AZ procedure. Due to this procedure utilizing DPPA and generating an intermediate structure containing a highly energetic and reactive azide moiety we had concern regarding the safety profile of this reaction as introducing this group onto an organic compound can introduce explosive properties.[32] The reaction set-up was aimed to mitigate any potential explosive hazard by using a blast shield, precise temperature control alongside reagent amounts and ensuring reaction-ware was free from any contamination pre and post reaction (rigorous $NaHCO_3$ and H_2O washing for everything exposed to any aspect of the reaction).

In the first attempt carboxylic acid **19**, DPPA and NEt_3 (molar ratio of 1:1:1) in DMA was stirred at room temperature for 1 hour, then heated at 120 °C for 16 hours. The reaction was quenched by pouring onto ice and isolation of the product was attempted by filtration of the precipitate. This was dried *in vacuo* giving imidazopyridinone **9** in a 18.3% yield.

Confirming the structure of the product produced from this reaction and the following attempts was achieved by analysis of the melting point and ^{1}H-NMR. The melting point (278-281 °C) was found to sufficiently match the reported literature value (281-283 °C).[22] The ^{1}H-NMR spectrum for the product also matched the literature reporting on imidazopyridinone **9** by the ACSRC.[22] Analysis of the ^{1}H-NMR spectrum was straightforward as between compounds **19** and **9**, the number of protons in each environment and the general nature of those environments remained unchanged. The chemical shifts values of the respective peaks however did change, notably with one aromatic peak experiencing an upfield shift and the other a downfield shift which was likely caused by the altered electronics of the pyridine ring due to the formation of the adjacent substituted 2-imidazolidinone ring.

This initial yield was significantly lower than the reported AZ yield of 70.0% with their pyrimidine equivalent **14** (Scheme 2). While the previous steps indicated that we should expect a different reactivity from the pyridine system of carboxylic acid **19**, such a significant difference seemed unlikely. TLC analysis of the remaining post-work up aqueous residues indicated the presence of product that had been left behind. Further imidazopyridinone **9** was extracted from this phase with EtOAc, followed by judicious backwashing with H_2O to remove DMA whilst retaining the recovered product. This yielded an additional 12.9% of imidazopyridinone **9** giving an overall yield of 31.4%. This was still well-below the AZ yield. In addition to the low yield, NMR analysis indicated lingering DMA contamination despite multiple H_2O washes of the organic phase and heating under strong vacuum; so the already low yield was an over-estimate.

In the next attempt, the reaction conditions were repeated as prior but the work-up was modified proceeding directly to the liquid-liquid extraction post ice quench. This was then purified by column chromatography giving imidazopyridinone **9** in a 62.8% yield, however, despite the altered purification procedure NMR analysis revealed a lingering quantity of DMA. Regardless, this was a notable increase in yield over the previous attempt indicating that a significant cause for the low yield was an ineffective

isolation procedure. This required difference in isolation is likely due to the solubility differences between AZ's imidazopyrimidinone **15** and imidazopyridinone **9** where the pyridine ring of **9** provides more Lewis basicity allowing for more pronounced hydrogen bonding. The greater polarity of imidazopyridinone **9** over imidazopyrimidinone **15** would lead to an increased predicted solubility in H_2O.

Due to TLC analysis of previous attempts revealing an amount of unreacted carboxylic acid **19** and the acyl azide formation being the limiting factor preceding the Curtius rearrangement, the next variation investigated whether the initial conversion of the carboxylic acid to the acyl azide was given enough time to take place sufficiently hence the acyl azide formation was increased to 6 hours. Additionally, since we had noted the impact the electronic difference of the pyridine compared to the pyrimidine had on the other reactions this seemed like a sensible adjustment. In all other regards, the procedure was kept the same. After isolation and purification, the product was triturated with an EtOAc/hexanes mixture (1:1) in an attempt to remove residual DMA, furnishing imidazopyridinone **9** in a 69.5% yield, marking significant improvement to our prior results and giving a comparable result to the AZ process albeit after an increased reaction time. While NMR analysis still indicated DMA contamination, this was minor indicating that the trituration is effective in removing residual DMA from the product. We deemed these conditions suitable and did not further optimize the reaction as AZ had already published an extensive investigation of this reaction on their pyrimidine substrate **14**, employing a continuous flow set-up which we could not match. Additionally, these investigations discovered the generation of potentially explosive azide impurities and byproducts when the optimizations were scaled.[39] These two factors rendered further optimization of the reaction outside the scope of the project.

Nonetheless, we did consider what changes could be feasibly made. Due to the one-pot nature of the reaction the conditions must accommodate both the acyl azide generation and the Curtius rearrangement. Alterations to reaction solvent would have proven advantageous in a purification context however the choices are limited due to the solubility challenges associated with the carboxylic acid substrate and the 120 °C temperature requirement for the Curtius rearrangement. Additionally, base choice is limited for the reaction where a non-nucleophilic base is required due to the presence of the cleavable phosphate ester bond during the acyl azide generation (Scheme 9) and the electrophilic isocyanate carbonyl being susceptible to nucleophilic attack. As for investigation into the quantity of reagents these quantities should remain unchanged from the AZ reaction due to the mentioned safety concerns.

2.1.4 *N*-Methylation

The penultimate reaction was the *N*-methylation of imidazopyridinone **9** forming intermediate **10** (Scheme 11).

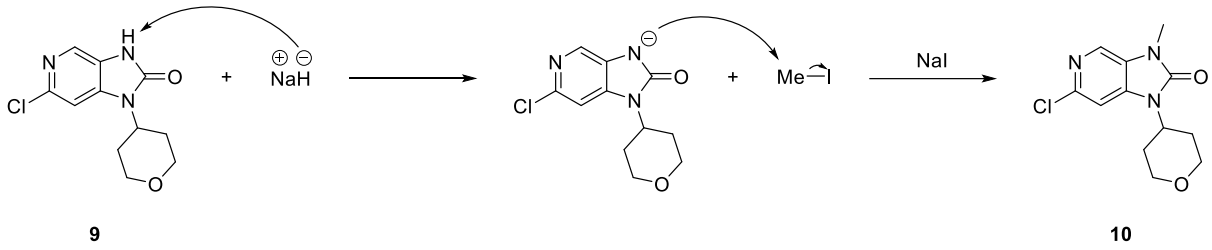

9 **10**

Scheme 11: *N*-methylation mechanism on imidazopyridinone 9

This is the point in the route where it converges with the optimized ACSRC route and hence we chose reagents and conditions to mirror the ACSRC procedure with DMF, NaH and MeI rather than the AZ procedure. The best yield achieved for this reaction was 66.4% which is a significant increase over the reported ACSRC yield of 47% (Scheme 1). In comparison to the equivalent *N*-methylation of the AZ pyrimidine equivalent **15**, differing conditions were used for the methylation procedure however the yield is directly comparable to the 69% AZ achieved (Scheme 2). The observed melting point (190-192 °C) alongside the ^{1}H-NMR analysis of the produced product matched the ACSRC's literature reporting of chloride **10**.[22] Due to the methylation resulting in the addition of three equivalent protons the critical ^{1}H-NMR observation to be made when the synthesized compound was assessed was the added methyl signal in the spectrum as a clear 3H singlet.

2.1.5 Buchwald-Hartwig Coupling

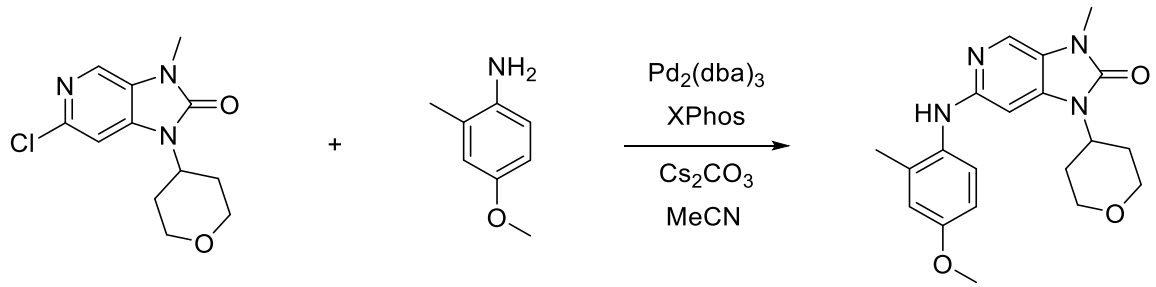

10 **11** **2**

Scheme 12: Buchwald-Hartwig coupling reaction of chloride 10 and aniline 11

The cross-coupling was well interrogated by the ACSRC team, as evident in the large number of analogues made.[37] They reported coupling aniline **11** to chloride **10** (Scheme 12) achieving a yield of 70% (Scheme 1). In our attempts at this coupling we substituted the use of dioxane with MeCN following advice from Dr Lydia Liew (ACSRC) as it had been proven to be a suitable alternative with easier processing due to the lower boiling point. The initial attempt at this reaction in a sealed pressure vessel (due to the reaction temperature exceeding the boiling point of MeCN) generated inhibitor **2** in a 27.8% yield, indicating an issue with either our reagent or substrate quality, or reaction set-up. However, as we had succeeded in producing inhibitor **2**, putting effort into re-optimizing a known reaction was not a priority.

During subsequent novel Buchwald-Hartwig couplings, we became suspicious of the quality of the $Pd_2(dba)_3$ in use and attempts to recrystallize the existing catalyst had poor returns. This prompted synthesis of fresh $Pd_2(dba)_3$ following the procedure outlined by Ananikov *et al*. $Pd(OAc)_2$, NaOAc and dba (molar ratio of 1:10:2) were stirred in MeOH at 40 °C for 3 hours. The solid was then collected *via* vacuum filtration and washed (MeOH and H_2O). The solid was dissolved in $CHCl_3$ and dried *in vacuo*. The crude product was recrystallized from minimal $CHCl_3$ in an excess of acetone overnight under refrigeration.[40] Post isolation, $Pd_2(dba)_3 \cdot CHCl_3$ was afforded in a 41.7% yield. An attempted purity investigation was undertaken using the ^{1}H-NMR methodology outlined in the same paper. This method utilizes integration in the assessment of free dba in solution as a proxy measurement for complex purity, however, insufficient resolution of the required peaks in our spectrum did not allow for an empirical assessment of the purity. While the purity of the catalyst couldn't be determined by this method, successful catalysis of a Buchwald-Hartwig coupling provides a pragmatic solution to this question, so the Buchwald-Hartwig coupling between chloride **10** and aniline **11** was reattempted. The reaction conditions and work-up were kept the same as prior however the newly synthesized catalyst was used. This attempt yielded inhibitor **2** in a greatly increased 86.4% yield confirming the newly synthesized catalyst was sufficiently active while also verifying the poor catalytic quality of the one used prior. This highlights the significance of catalyst quality which will be covered in *Section 2.2.2*.

Structural confirmation of these Buchwald products was achieved by ^{1}H-NMR and analysis of the melting point. The ^{1}H-NMR data was found to match the ACSRC's literature data for inhibitor **2**.[22] Critical to this was the new addition of three aromatic signals from the aniline with distinct splitting patterns (two doublets and a doublet of doublets) and the addition of two new 3H singlets. The ^{1}H-NMR signal pattern of the attached aniline is discussed in further detail in *Section 2.2.1.1*. However, it is noteworthy that the observed melting point at 169-171 °C did not completely align with the reported literature value (176-178 °C).[22] We suspect that this was due to a slight contamination of the product not seen on TLC nor NMR analysis. This would be consistent with the brown colouring of the compound compared to the cream colouring reported by the ACSRC.[22]

2.1.6 Comparison to the AZ Route

The individual reaction outcomes from the novel route have already been compared to the equivalent steps in the AZ route however in terms of a route comparison; the overall yield of the optimized novel route up to imidazopyridinone **9** is 53.3% directly comparing to the 47.0% overall yield that AZ achieved with their pyrimidine substrate to generate imidazopyrimidinone **15** (Table 3).

Table 3: Yield comparison (%) between the pyridine and pyrimidine analogues for equivalent reactions

Reactions	Novel Pyridine Substrates	AZ's Pyrimidine Substrates[25]
S_NAr	85.3	73.0
Hydrolysis	89.9	92.0
Curtius Rearrangement	69.5	70.0
Overall	53.3	47.0

The recurring requirements of either an extended reaction time or the addition of heat when a pyridine analogue is deployed highlights that pyridine isn't as activated for these reactions. However, alternative reaction conditions have been found that provide equivalent efficiency (Table 3) to the pyrimidine analogues, exemplifying that this route is viable for the synthesis of imidazopyridinones.

From a safety perspective both routes employ similar reagents and generate identical substrates aside from the pyridine vs pyrimidine motif and can be considered to have equivalent safety profiles. Considering the safety of the individual reactions the S_NAr and hydrolysis reactions are relatively benign procedures with unremarkable conditions and reagents. However, the acyl azide generation and Curtius rearrangement procedure employs the use of DPPA and generates an acyl azide intermediate, both of which introduce new hazards that need to be managed with additional lab safety procedures.

2.1.7 Comparison to the ACSRC Route

Although the route has been shown to be a viable alternative for synthesis of imidazopyridines, another key purpose of this study was to determine the viability compared to the established ACSRC route for the synthesis of inhibitor **2**.

2.1.7.1 Phosphoryl Chloride Mediated Nucleophilic Aromatic Substitution

The ACSRC route begins with a chlorination reaction to prepare the substrate for THP installation on the next step.

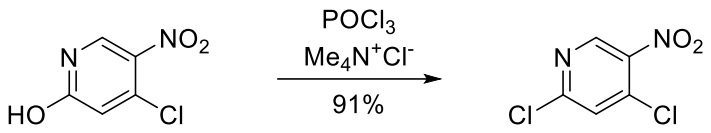

4 **5**

Scheme 13: The ACSRC's chlorination of pyridinol 4

The pyridinol group is substituted for a chloride yielding dichloride **5** (Scheme 1, Scheme 13). This step has no direct comparison in the novel route which already begins with a dichloride substrate; dichloride **17**. Despite the chlorination generating dichloride **5** in a 91% yield (Scheme 1, Scheme 13), having a shortened route is advantageous regarding synthetic efficiency. Additionally, to see if there was any cost-benefit difference we sought prices for the relevant starting materials from suppliers used by the groups at the ACSRC and/or the University of Waikato.

Table 4: Price per gram of starting material (USD, ≥ 95 % purity) by chemical supplier*

Suppliers**	Dichloride 17	Pyridinol 4	Dichloride 5***
BLDPharm	$0.95	$10.00	$6.24
Fluorochem	$1.31	$9.98	$8.43
AK Scientific	$1.25	$10.88	$6.30
Combiblocks	$0.95	$7.50	$6.24

* Calculated from the largest amount of compound offered to account for bulk-buying discounts

** bldpharm.com, fluorochem.co.uk, aksci.com, combi-blocks.com

*** This would be the ACSRC's starting material if they omitted the chlorination and started from an equivalent point to the novel route (pre-THP installation)

It is evident that the novel route possesses the cheaper starting material (Table 4) and hence has a significant advantage from this perspective. It is also observable that based on pricing there is little justification for the ACSRC route to start from pyridinol **4**, however there must have been alternative justification for starting with this compound.

From the standpoint of safety, the absence of this reaction enhances the overall safety profile of the novel route by eliminating the use of $POCl_3$ and $Me_4N^+Cl^-$ (which serves as a counter-ion) both of which are corrosive and toxic.

2.1.7.2 THP Installation

In both routes installation of the THP is done using comparable conditions. The ACSRC report a yield of 84% using *i*Pr_2NEt and DCM as the solvent to produce chloride **7** (Scheme 1, Scheme 14).

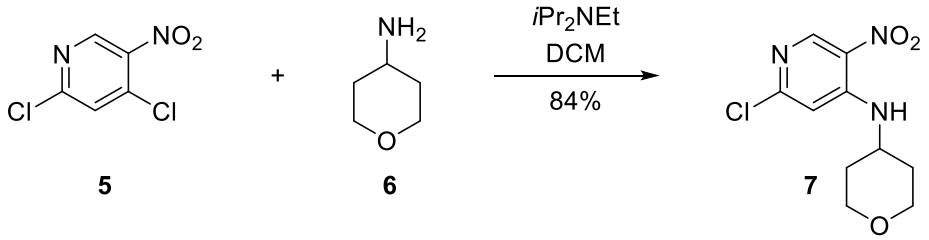

Scheme 14: The ACSRC's S_NAr reaction on dichloride 5

This is compared to the 85.3% yield achieved in the novel route equivalent on dichloride **17** using Cs_2CO_3 and MeCN for the solvent. Initially the reactions seem equivalent with regards to synthetic efficiency however the novel route requires an additional 24 hours and heating indicating that the reaction is not as efficient. This is expected if you evaluate the substituents of the two starting materials with the ethyl ester of dichloride **17** having an inferior electron withdrawing effect compared to the nitro group on the ACSRC's dichloride **5**, leading to dichloride **17** being less activated for S_NAr compared to dichloride **5**. From a product isolation perspective, the use of Cs_2CO_3 in the novel procedure allows for easy removal of the base from the mother liquor by filtration. This is due to the poor solubility of Cs_2CO_3 in MeCN. This is contrasted to the miscibility of *i*Pr_2NEt in DCM leaving it solvated in the organic fraction during the work-up.

In terms of safety both bases have similar safety profiles. However, the nitro group on the ACSRC's substrates does pose an additional safety concern when compared to the relatively unreactive ethyl ester equivalent on the novel route's substrates. This is due to the toxic, unstable and reactive nature of aromatic nitro compounds if handled incorrectly.[41] Despite the reactions being of the same kind and possessing similar product isolation procedures, the nitro group present on both the ACSRC's substrate

(**5**) and product (**7**) implies that in a scale-up context the reactions will need to be handled differently to the novel route equivalent. This is primarily due to the runaway reaction hazards associated with scaling and processing organic nitro compounds. This additional hazard results from potential processing contaminants decreasing the expected thermal stability of the compound.[41]

2.1.7.3 Hydrolysis vs Reduction

The hydrolysis of the novel route and the reduction of the ACSRC route (Scheme 15) are preparatory conversions for the formation of the 2-imidazolidinone ring.

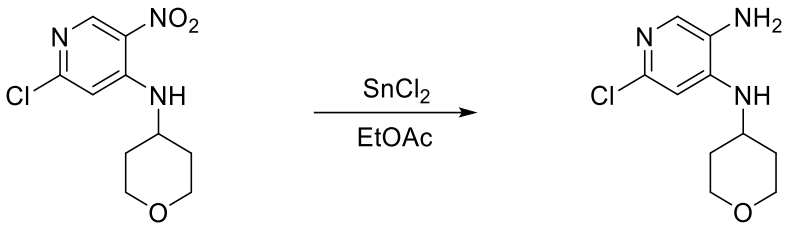

7 **8**

Scheme 15: The ACSRC's $SnCl_2$ reduction on nitropyridine 7

The highest achieved yield for the hydrolysis reaction is 89.9% however the yield for the ACSRC's reduction was reported across two steps (Scheme 1), so a direct comparison of synthetic efficiencies is only fair if the hydrolysis yield is considered along with the following Curtius rearrangement yield. Despite this, other aspects of the reactions can be analysed. Both reactions require the use of corrosive and toxic substances however the hydrolysis possesses the advantage of minimizing exposure of the substrate to inorganic material while achieving the same purpose of the ASCRC reduction; preparing the substrate for cyclisation.

From a safety and reaction processing point of view the hydrolysis poses much less hazard when compared to the reduction. This is due to the already mentioned risks associated in scaling reactions involving organic nitro compounds.[41] Additionally, these risks are amplified by the precise temperature requirement of the reaction (held between 50 °C and 60 °C) where processing contaminants may reduce the thermal stability of nitropyridine **7**.

2.1.7.4 Formation of the THP-NH substituted 2-imidazolidinone ring

For the formation of the THP-NH substituted 2-imidazolidinone ring the ACSRC employed the use of the peptide coupling reagent CDI (Scheme 16).

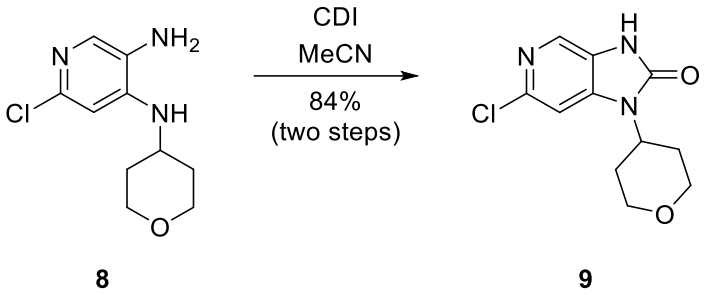

8 **9**

Scheme 16: The ACSRC's CDI coupling on diamine 8

The resultant product, imidazopyridinone **9**, marks where the routes converge, however the reactions to form this product differ. The ACSRC's $SnCl_2$ reduction and CDI coupling generates imidazopyridinone **9** in an 84% yield (Scheme 1, Scheme 16) compared to the novel route's hydrolysis and Curtius rearrangement which produces **9** in a 62.5% yield. The CDI reaction requires minimal reagents only requiring MeCN, CDI and the substrate in comparison to the novel equivalent requiring NEt_3, DPPA, DMA and the substrate. From a reaction efficiency and atom economy perspective the CDI coupling is the superior reaction. This is also the case from a safety perspective where DPPA is acutely toxic, NEt_3 is corrosive and the acyl azide intermediate poses explosive risks which is enhanced by the 120 °C temperature requirement, although the one-pot nature of this reaction does attempt to minimize this (due to isolation of the azide not being required). From a reaction processing perspective, the large amount of safety concerns associated with this reaction would likely make it an extremely difficult reaction to scale compared to the relatively benign nature of the CDI coupling. These reasonings indicate that the CDI reaction is superior in most aspects however the one significant disadvantage of this reaction is the 96-hour time requirement. This is notably longer than the optimized DPPA reaction where two of these reactions can be completed and worked up in the time of one CDI coupling. Whether the higher throughput reaction is worth the trade-off for safety, poorer atom economy and greater waste generation is a matter of preference. The comparison of the overall yields between the ACSRC route and the novel route will be discussed in *Section 2.3.1*.

2.2 Rearrangement of the Novel Route

To investigate whether rearranging the steps of the novel route provided any synthetic advantage, the Buchwald-Hartwig coupling to install aniline **11** was pursued as the second reaction in the route after installation of the THP-NH (Scheme 5).

2.2.1 Initial Attempts at the Buchwald-Hartwig Coupling

The same conditions as the prior Buchwald-Hartwig coupling were trialled initially (Scheme 17).

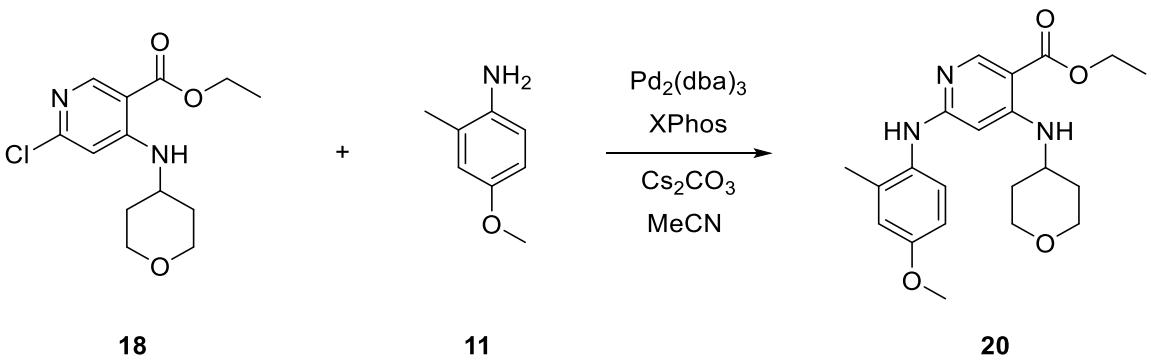

18 **11** **20**

Scheme 17: Novel Buchwald-Hartwig coupling of chloride 18 and aniline 11

This involved stirring chloride **18**, aniline **11**, Cs_2CO_3, XPhos and $Pd_2(dba)_3$ in a degassed solution of MeCN at 120 °C overnight. The molar ratio of components was 1 mol of substrate:1.2 mol of aniline:2.2 mol of base:0.2 mol of XPhos and 5 mol% of $Pd_2(dba)_3$. These reaction conditions and ratios were adopted as the standard Buchwald-Hartwig conditions for all couplings with $Pd_2(dba)_3$. Post reaction, the mixture was cooled to room temperature, filtered through diatomaceous earth and concentrated *in vacuo*. TLC analysis of this concentrate revealed a crowded TLC plate suggesting more compounds than expected. Column chromatography was employed for purification however the TLC plate mobile phase did not translate well to the silica column giving significant coelution. Despite this, analysis of the eluents by MS revealed the presence of two distinctive ions at 386.2 *m/z* and 634.3 *m/z*. The peak at 386.2 *m/z* was consistent with the expected $[M+H]^+$ of the desired coupling product aniline **20** (Scheme 17) however the peak at 634.3 *m/z* was unexpected. This initial attempt afforded no appreciable amount of clean material hence the reaction was reattempted.

The conditions above were repeated albeit with a more careful column procedure. This produced aniline **20** in a 10.2% yield. This was a very low yield with little synthetic viability however this aspect was ignored as this reaction was still in the early stages of optimization. The spot representing the 634.3 *m/z*

peak was tentatively assigned to be a dimerised structure as it aligned with the expected $[M+H]^+$ of such. However, the presence of two amine groups on the starting substrate gave us the possibility of two constitutional isomers **21a** and **21b** (Figure 10).

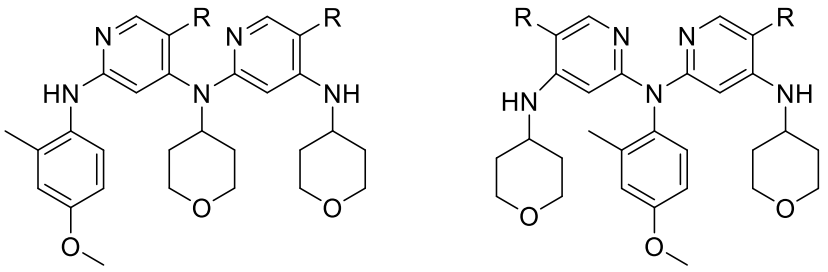

21a

$C_{34}H_{43}N_5O_7$

633.3 amu

21b

$C_{34}H_{43}N_5O_7$

633.3 amu

Figure 10: Possible dimerized structures 21a and 21b; R = ethyl ester

A pure sample of this structure was unable to be isolated however analysis of the crude ^{1}H-NMR spectrum of the semi-pure fraction suggested it be the dimerized structure **21b** (see *Section 2.2.1.2*).

Due to the exceptionally low yields and the lack of any appreciable side-products contributing to the expected mass balance we considered whether any product or related structures were being lost during the isolation procedure. The diatomaceous earth used for filtering was washed further with solvents of increasing polarity; TLC analysis of these extracts revealed nothing of significance. Additionally, the column was flushed with solvents of increasing polarity up to 10% MeOH:DCM, to confirm there was nothing notable trapped on the silica. This was of concern due to the likely palladium content of the loaded mixture which may have been coordinating itself to the product or related structures trapping it on the silica. TLC and MS analysis of the flushed extract returned no indication of this. This confirmed nothing was recoverable from the work-up and isolation procedures and it was estimated that approximately (due to the impure nature of the eluent) 0.08 mmol of dimer **21b** was generated. When compared to the small quantity of aniline **20** afforded, the higher quantity of dimer (0.08 mmol vs 0.07 mmol) suggested it to be the main product of the reaction.

In order to generate the dimerized structure a total of two new C-N bonds need to be successfully formed which implies that the dimer had gone through the catalytic cycle twice; once to generate the desired product aniline **20** (with the NH_2 of aniline **11** acting as the nucleophile) then again to form dimer **21b** (with the aniline NH of the product **20** acting as the nucleophile) (Scheme 18).

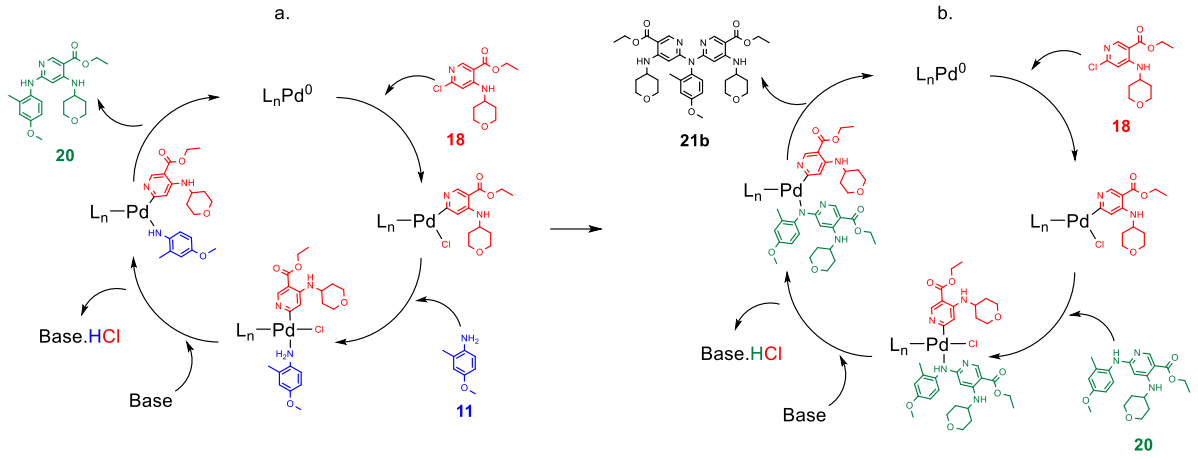

Scheme 18: Proposed formation of dimer 21b; a) NH_2 of aniline 11 acting as the nucleophile; b) aniline NH of the coupling product 20 acting as the nucleophile

Given the results of this reaction suggesting that a greater amount of dimer **21b** is generated compared to aniline **20**, inferences were made regarding the nucleophilicity of the NH_2 on aniline **11** compared to the aniline NH of the expected coupling product **20**. The initial logic suggested that surprisingly the aniline NH of the desired product **20** must be a better nucleophile compared to the primary amine of aniline **11** to allow the product **20** to enter the catalytic cycle again. However, both this coupling and the ASCRC's coupling are with aryl chlorides and the same aniline (**11**) hence this conclusion did not align with the 70% product yield of the ACSRC's Buchwald-Hartwig coupling, as the mono-aryl aniline is the predominant compound produced (Scheme 1).

This disagreement led to the decision to repeat the reaction with a lower temperature to the standard conditions. The 120 °C temperature that had been used is considered a typical temperature to run a Buchwald-Hartwig coupling at when an inorganic carbonate base is used and the substrate is moderately complex. The higher temperature is meant to allow the catalyst to be sufficiently active in the presence of potentially coordinating functional groups (with pyridine's nitrogen being a relevant example).[35] However, it was thought that the 120 °C temperature may be allowing the aniline NH on aniline **20** to function as a more effective nucleophile leading to the generation of dimer **21b**. If this is the case, it's implied that aniline **20** is the kinetically favoured product and dimer **21b** is the thermodynamically favoured product.

The adjusted reaction was stirred at 90 °C as opposed to 120 °C. After the standard work-up, aniline **20** was isolated in a 17.1% yield (0.1 mmol) alongside a crude 0.03 mmol of dimer **21b**. The ratio of dimer **21b** produced to the desired coupling product **20** had decreased with the drop in temperature as was proposed. Although this was a success, the yield of aniline **20** is still not suitable for a viable synthesis suggesting that the temperature was not the issue and a deeper mechanistic issue with the reaction is present.

Further evidence toward this was present when an investigation into the mass balance of this reaction was undertaken concerning the amount of starting material consumed. The ratio of chloride **18** consumed to aniline **20** formed is 1:1. Only 0.1 mmol of aniline **20** was afforded accounting for 0.1 mmol of the chloride **18**. Considering dimer **21b** the ratio of starting material consumed to dimer produced is increased to 2:1 and since 0.06 mmol of dimer **21b** was estimated to have formed this accounts for a further 0.12 mmol of chloride **18**. The formation of aniline **20** and dimer **21b** equates to only 0.22 mmol of starting material represented in the products, in contrast to the 0.7 mmol input. These were the only two compounds identified and since aniline coupling partners do not allow for β-hydride elimination (which is the competing pathway at the reductive elimination step of the catalytic cycle)[35] this suggests that either the majority of chloride **18** (0.48 mmol out of the input 0.7 mmol) does not engage with the catalytic cycle at all or that the mechanism is inhibited at a certain point preventing further reaction. The low yields from these initial attempts at the novel cross-coupling were considered insufficient to continue with the rearranged synthesis, so our attention was placed into optimizing this this reaction.

2.2.1.1 Characterization of Aniline 20

Standard ^{1}H and ^{13}C NMR experiments were employed to confirm the structure of aniline **20**. The existence of the ethyl ester was confirmed by the presence of a well-resolved quartet (4.29 ppm) and a triplet (1.37 ppm). Additionally, retention of the THP-NH group was suggested by five aliphatic multiplets; four 2H multiplets and a single 1H multiplet. HSQC correlations from these signals confirmed the diastereotopicity of the protons which aligned with the stereochemistry of the THP ring. Furthermore, the presence of two well-resolved aromatic singlets with one being notably upfield to the other (5.39 ppm vs 8.61 ppm) implied the correct substitution pattern of the pyridine ring. This set of evidence suggested the retention of the desired starting material substituents from chloride **18**. The structural change that defined the reaction was the coupling of aniline **11** to C-6 (Figure 11).

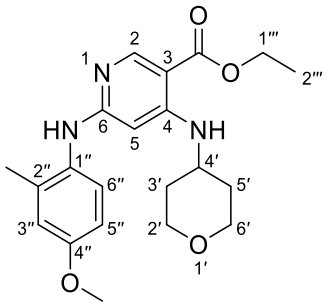

20

Figure 11: Numbered structure of aniline 20

This change was indicated by the additional signals within the aromatic region of the ^{1}H-NMR spectrum and two 3H singlets when compared to the proton spectrum of chloride **18**. The non-aromatic singlets represented the two methyl groups, with the downfield (3.82 ppm) of the two being assigned as O-CH_3 due to the deshielding of the oxygen which left 2.24 ppm with the CCH_3-2″ assignment. The aromatic signals displayed distinct splitting patterns due to the π system of the aromatic ring promoting the transmission of spin information. All three of the aromatic signals integrated to 1H however two of them were doublets (7.20, 6.83 ppm) whereas the other was a doublet of doublets (6.77 ppm). Upon examining the *J* values (all coupling constants presented throughout this thesis have been calculated from the 8.d.p chemical shift measurements) of the 6.77 ppm signal, two constants of differing magnitudes were revealed; 8.6 and 2.9 Hz. In aromatic systems 8.6 Hz is consistent with an *ortho* coupling (~ 7-9 Hz) and 2.9 Hz aligns as a *meta* coupling (~ 2-3 Hz).[42] Based on this coupling pattern the peak at 6.77 ppm was assigned as H-5″. The doublet at 7.20 ppm possessed the same *ortho J* value allowing its assignment as H-6″, and the doublet at 6.83 ppm displayed the *meta J* value and was assigned as H-3″ (Figure 12). HSQC correlations enabled assignment of the associated carbons.

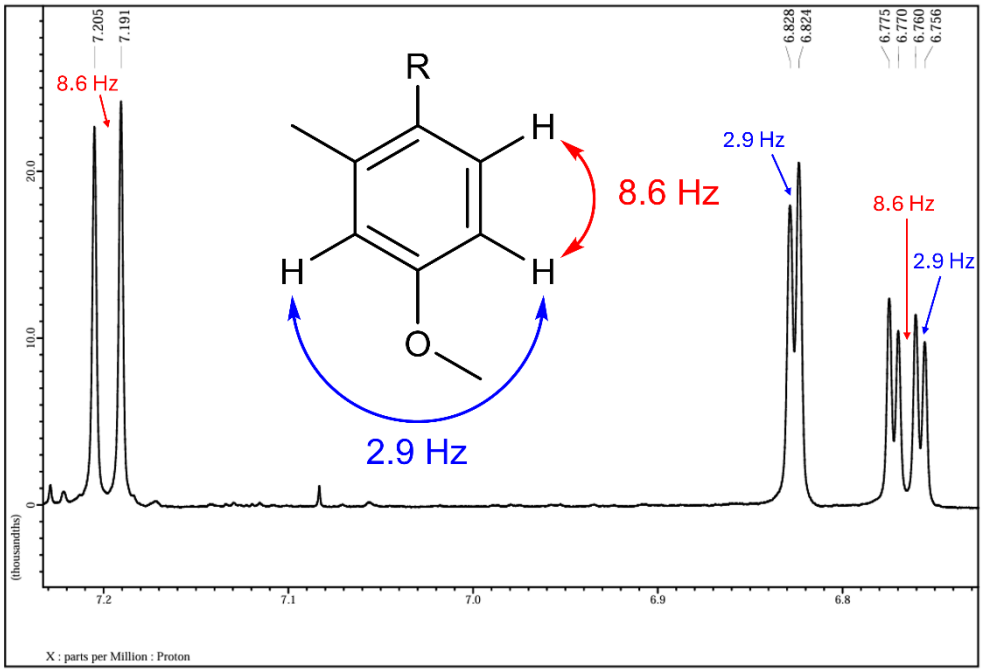

Figure 12: Aromatic ^{1}H coupling of the installed aniline on aniline 20

Interrogation of the HMBC experiment allowed for the assignment of the aniline quaternary signals with the 2″-CCH_3 protons showing correlations to two unassigned carbon signals at 136.0 ppm and 130.4 ppm which suggested that these represent 1″-C and 2″-C (green/red colouring in Figure 13). H-6″ displayed correlations to the mentioned carbon signal at 136.0 ppm and an additional unassigned signal at 157.9 ppm. This provided evidence that the 136.0 ppm signal was likely 1″-C (blue/red colouring in Figure 13).

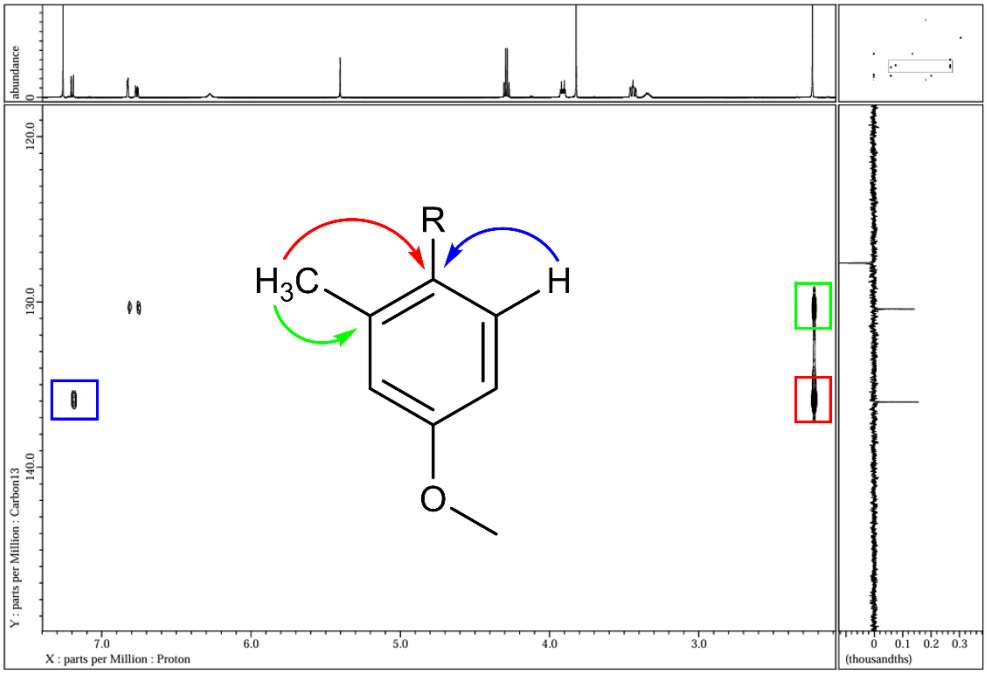

Figure 13: HMBC correlations of H-6″ and 2″-Me to quaternary carbons on aniline 20

This left 130.4 ppm the assignment as 2″-C (green colouring in Figure 13) and the remaining 157.9 ppm signal as the final quaternary 4″-C. Assignment of the 4″-C signal was supported by a singular HMBC correlation between the O-CH_3 protons and the 157.9 ppm signal (Figure 14).

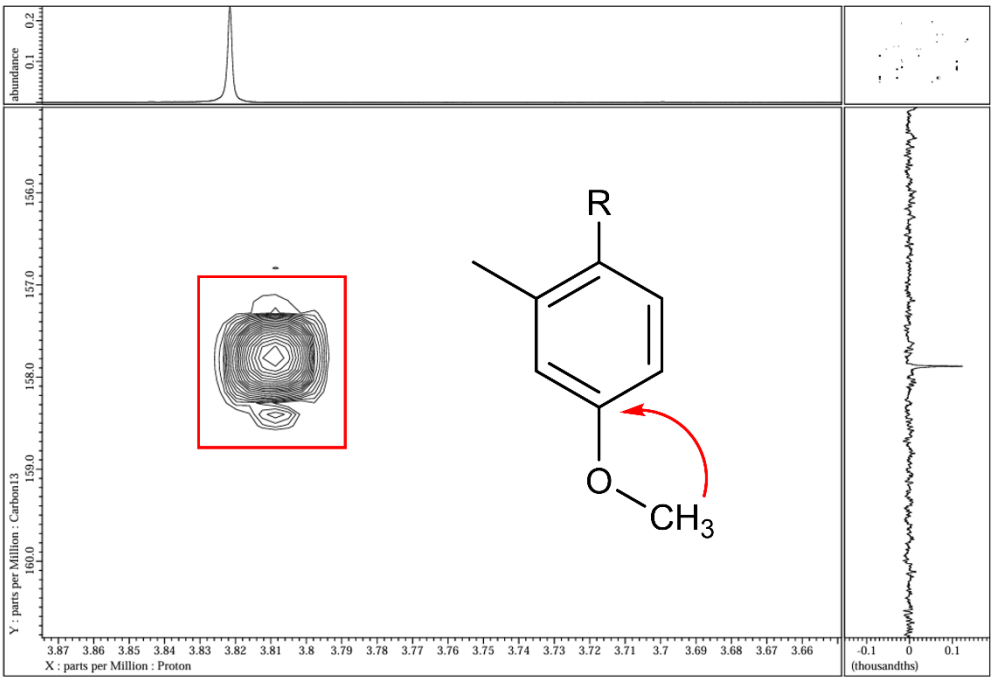

Figure 14: HMBC correlation of O-CH_3 and 4″-C on aniline 20

The remaining three quaternary signals displayed the same shift pattern as the quaternaries for the analogous 3,4,6-trisubstituted pyridine structures. As such these were assigned by the logic presented during the characterisation of chloride **18**. This gave the two downfield signals (160.8 ppm, 155.0 ppm) as 4-C and 6-C (indistinguishable) and the notably upfield signal (101.2 ppm) as 3-C.

2.2.1.2 Crude Characterization of Dimer 21b

Analysis of the ^{1}H-NMR of the crude isolate was used to distinguish which of the isomers (Figure 10) our dimer was. All the present peaks were consistent with the findings of aniline **20** however when the integrations were normalized (to the O-CH_3 signal of 3H as that is a consistency between the isomers) it was confirmed that the integrations for all the proton signals had doubled except for the signals that we knew to be from the aniline (Figure 15).

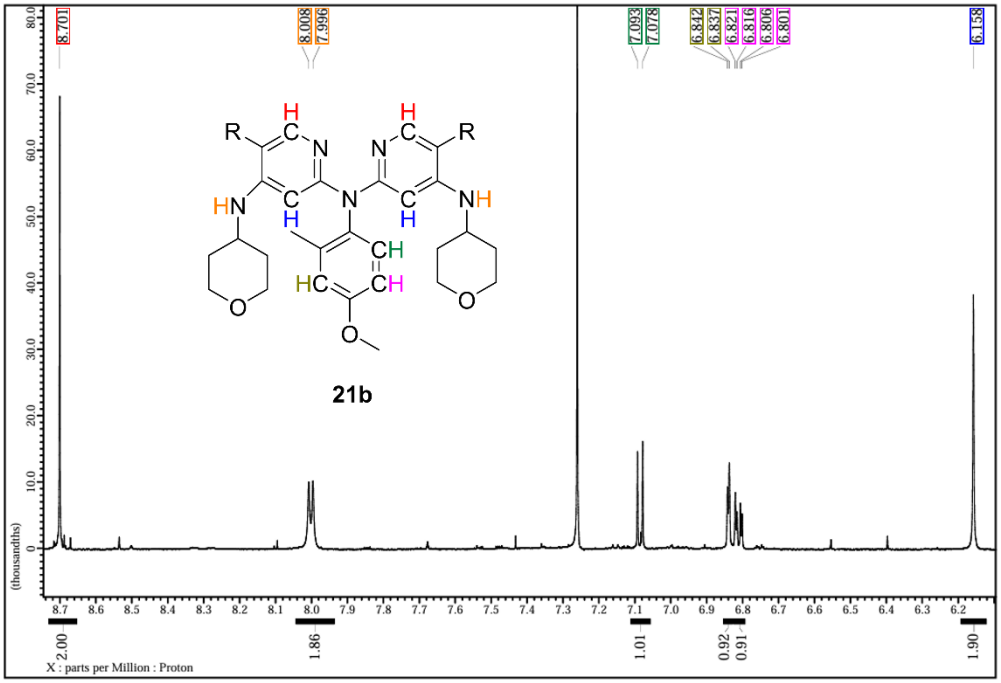

Figure 15: Aromatic ^{1}H region of dimer 21b

This was evidence that the structure of our dimer was isomer **21b**. If it were hypothetically isomer **21a** there would be more signals than what was observed due to the asymmetry of this isomer. Throughout our studies we were unable to gather a pure enough sample (with the aromatic region being the most resolved of the acquired ^{1}H-NMR data) to fully characterize this compound however our knowledge of the catalytic cycle, the notably distinct ion mass and the crude ^{1}H-NMR analysis made it highly likely that the dimer was isomer **21b**.

2.2.2 Catalytic Optimization

The ACSRC's optimized coupling system shows that aniline **11** is a suitable coupling partner and nucleophile. The key difference lies in the pyridine substrate, so we thought there was a possibility that the problem lay with palladium insertion into chloride **18** which is the first step of the cycle (Scheme 18). It is often the case in many palladium mediated cross-coupling reactions that the oxidative addition of the substrate onto the metal center is the rate limiting step, and historically with the early generation ligands, palladium sources and in unoptimized systems the aryl chlorides posed the greatest challenge due to the strength of the C-Cl bond.[43] The substrate **18** is an aryl chloride that is seemingly not-engaging with the catalytic cycle; aligning with what has historically been encountered for the Buchwald-Hartwig coupling of aryl chlorides. These challenges have for the most part been overcome by the discovery of new palladium(0) sources, highly optimized phosphine ligands, and a better mechanistic insight into how the catalytic cycle operates.[44]

Key to the cycle is the palladium(0)-phosphine ligand complex which is contingent upon a sufficiently pure catalyst with the capability of forming the active palladium(0) species in solution; so an investigation into the catalytic quality of the $Pd_2(dba)_3$ in use was undertaken. $Pd_2(dba)_3$ is a commonly employed palladium source in cross-coupling reactions due to the efficient exchange of the dba ligand with phosphine ligands in solution generating the active palladium(0) complex, however it is known to begin noticeable decomposition after a period of about six months into elemental palladium and dba.[40] The exact age and storage history of the $Pd_2(dba)_3$ in use was unknown so the repurification procedure outlined in Ananikov *et al* was done as this has been shown to produce a refurnished $Pd_2(dba)_3.CHCl_3$ of high purity.[40] $Pd_2(dba)_3$ (0.5 g) was dissolved in the minimum amount of $CHCl_3$ required precipitating out a visually significant amount elemental palladium. This was filtered out and the $CHCl_3$ extract was dried *in vacuo*. This was redissolved with a minimum amount of $CHCl_3$ and an excess of acetone was added. This was left overnight under refrigeration. The crystals were collected, washed (cold acetone) and dried *in vacuo*. This gave $Pd_2(dba)_3 \cdot CHCl_3$ in a 34.7% yield (0.198 g). Confirmation of purity was unable to empirically assessed by the method given by Ananikov *et al* due to insufficient resolution of the required ^{1}H-NMR peaks to be analysed. However, at the minimum an increased purity was assumed due to the precipitated removal of elemental palladium during the procedure. The significant loss of mass due to the removal of the elemental palladium demonstrates that the $Pd_2(dba)_3$ in use was of a poor quality and was likely forming significant amounts of inactive elemental palladium *in situ* opposed to the active palladium(0) species. This likely would have been resulting in a significant underdosing of catalyst within the reactions; giving a potential reason as to why a significant amount of material in the prior reactions was not engaging in the catalytic cycle.

After repurification of the catalyst, the coupling of aniline **11** to chloride **18** was reattempted twice with the defined standard conditions. Despite expecting some increase in yield due to using a catalyst of

higher purity the reattempts generated aniline **20** in diminished yields of 8.6% and 5.6%. The previous findings of the reactions suggested that the formation of dimer **21b** is produced in a similar magnitude to the product hence the dimer was not specifically isolated although TLC and MS analysis suggested its presence. The poor yields of these reactions despite the assumed increase in catalytic purity signified that there is an alternative or additional factor within the catalytic cycle that needs to be adjusted.

The investigation into catalytic adjustment was concluded by the trialling of a newly purchased BrettPhos-PdG3 precatalyst. BrettPhos-PdG3 is comprised of a pre-configured palladium-BrettPhos complex and are designed to autoactivate to the active L_nPd^0 complex *in situ* in the presence of the reaction base *via* deprotonation and reductive elimination of a carbazole (Scheme 19).[35]

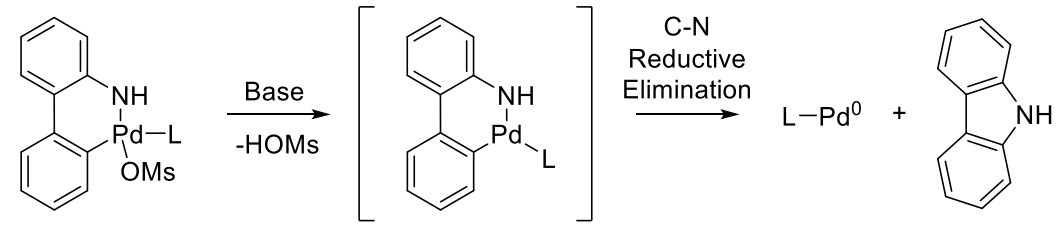

BrettPhos-PdG3

Scheme 19: Activation of the BrettPhos-PdG3 precatalyst; L = BrettPhos ligand[35]

This avoids the need for traditional catalyst pre-activation before entrance into the catalytic cycle of the reaction as many common sources of palladium such as $Pd(OAc)_2$ exist in the +2 oxidation state as opposed to the required 0. This is not a specific advantage when compared to the use of $Pd_2(dba)_3$ as this exists as a palladium(0) complex and the simple exchange of dba ligands for the phosphine retains the 0 oxidation state.[45] However, this is a double edged sword as there exists conditions where the equilibrium of this ligand exchange can be unfavourable leading to a lack of dba dissociation or possible dba reassociation and hence suboptimal concentrations of the active L_nPd^0 complex.[46] Hence a distinct advantage the precatalyst has over the $Pd_2(dba)_3$/XPhos catalyst is the absence of the potentially problematic dba. Additionally, the precatalyst would ensure the quality of catalyst *in situ* was of high purity, allowing for proper dosing while also providing a different phosphine ligand to trial.

The vast array of potential amine coupling partners is unlimited and the correct choice of phosphine ligand can determine the success or failure of a reaction in some circumstances. A commonly adopted type of phosphine ligand for this type of coupling is the biaryl monophosphine ligand. Differing ligand architectures of this type influence the reactivity of the catalyst.[35] Until this point the only phosphine ligand that had been trialled was XPhos as this was the ligand employed by the ACSRC for the coupling of aniline **11**. However they have also demonstrated the viability of the BrettPhos ligand (through the use of BrettPhos-PdG3) for the coupling of alternative anilines to varying imidazopyridinones.[37] Both

BrettPhos and XPhos are commonly employed ligands of the biaryl monophosphine type and differ only by substituents present on the 'top ring' (Figure 16).

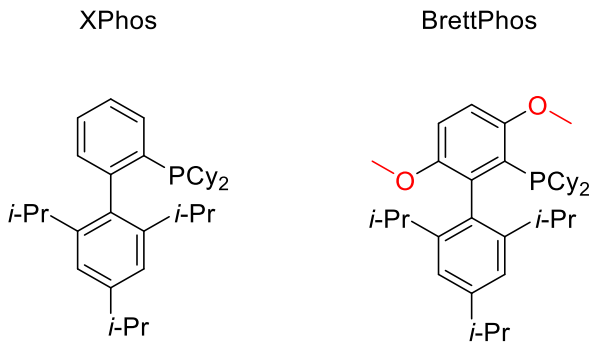

Figure 16: Structural comparison of XPhos and BrettPhos

The substituents on the top ring are typically selected to fix the conformation of the bound ligand in order to enhance the rate of reductive elimination of the product as the catalytic complex aims to relieve the heavy steric strain.[35] The addition of the methoxy on the top ring of BrettPhos (Figure 16) typically results in an enhanced rate of reductive elimination over unsubstituted alternatives such as XPhos.[35] Additionally, the methoxy substituents allow for an alternative palladium binding mode that increases both the reactivity and stability of the resultant L_nPd^0 complex.[47] Furthermore, BrettPhos has been demonstrated within the literature to be a viable option for the coupling of primary anilines and aryl chlorides with a selectivity for monoarylation[47] which was relevant to our coupling due to the recurring formation of dimer **21b**. We expected to observe an increase in the yield of aniline **20** if the catalytic system used prior was not reactive enough or did not sufficiently encourage the reductive elimination of the product.

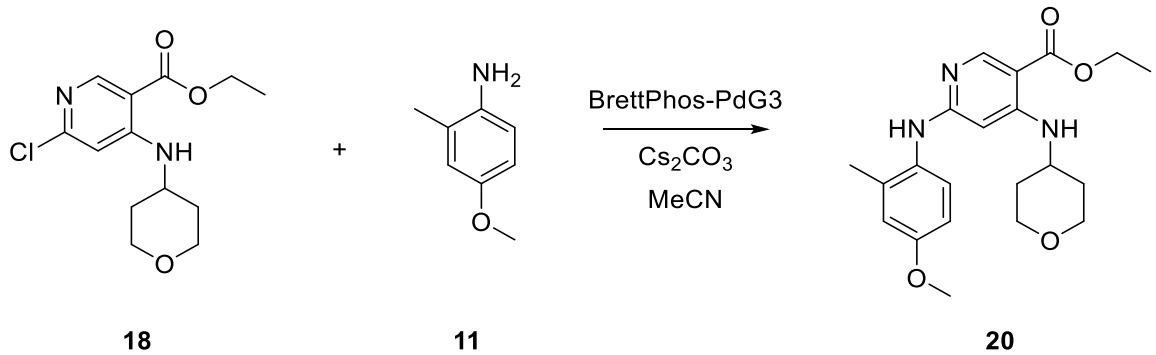

Scheme 20: Buchwald-Hartwig coupling of chloride 18 and aniline 11 using BrettPhos-PdG3

The reaction was reattempted with the standard conditions however with the BrettPhos-PdG3 catalyst (5 mol%) (Scheme 20). After the standard work-up aniline **20** was given in an 11.4% yield. Similar to the prior reaction, MS and TLC indicated the formation of dimer **21b** within the reaction. Additionally, due to the ejected carbazole as a biproduct from the precatalyst activation (Scheme 19) it was critical to consider whether this was acting as a possible nucleophile within the catalytic cycle as resultant reaction poisonings *via* aryl halide depletion have been reported in the literature.[48] However, MS analysis provided assurance that this was not occurring. The result of this reaction and those post recrystallisation of the $Pd_2(dba)_3$ suggested that both the source of palladium and the phosphine ligand were not the reasons behind a lack of chloride **18** engaging with the catalytic cycle. At this point in the optimization, we were confident that the catalytic adjustments could be concluded for the time being allowing for other factors of the reaction to be investigated.

2.2.3 Solvent and Base Investigations

Within the Buchwald-Hartwig coupling the reaction solvent can have a critical influence on the rate and selectivity of the reaction due to factors such as coordination capability, polarity and whether the active catalyst species is stable. MeCN was the solvent of choice in the standard conditions for the couplings attempted due to its inert nature and solvation capability of the reactants and reagents excluding Cs_2CO_3. Additionally, due to the moderate dielectric constant of the solvent it should be expected to provide extra stability to any charged intermediates and structures present during the reaction.[49] However, this added stability comes at the cost of the MeCN being known to coordinate to palladium as a ligand. It is critical to recognize that the active catalytic complex, L_nPd^0, is an under ligated palladium center with a deficient coordination number (allowing oxidative addition of the substrate).[49] Thus it remained a possibility that MeCN was acting as a coordinating ligand disrupting the active catalytic complex which may have been hindering the oxidative addition of the substrate.[50]

The ACSRC originally employed the use of dioxane as their reaction solvent hence it seemed logical to investigate whether this alteration could provide utility to our reaction. The standard conditions were mirrored from the trial with the BrettPhos-PdG3 precatalyst except dioxane was used as the solvent. An increased amount of degassing by nitrogen sparging with a needle was employed during this trial to further promote catalytic stability as the L_nPd^0 complex is air-sensitive and is prone to degradation by atmospheric oxygen.[35] After the standard work-up aniline **20** was afforded in a markedly low 5.6% yield. This confirmed that the choice of solvent likely wasn't the factor giving the exceedingly low reaction yields.

The only remaining component outside of the coupling partners within the reaction to investigate was the implications of base choice and whether competing side-reactions facilitated by the base were

occurring. If competing reactions were taking place this would result in the consumption of reaction feedstock and altered electronics of the substrate; changing the fundamental conditions of the desired reaction. The first side-reaction considered was the base-catalyzed hydrolysis of the ethyl ester on chloride **18**. The findings of the THP installation of the novel route show that the use of Cs_2CO_3 preserves the ester functionality in those conditions. However, there was concern that the 120 °C temperature of the Buchwald-Hartwig coupling was facilitating a possible hydrolysis. Additionally, despite alkali carbonates not being typical bases employed for the hydrolysis of esters there are some literature examples documenting that is a possibility to be considered.[51] This was of concern due to the basic reaction medium allowing the carboxylate of the acid **19** to be in solution which are known to be highly coordinating towards palladium centers. They have great importance as palladium catalysis ligands used for selective C-H bond activations.[52] Thus an *in situ* hydrolysis provides opportunity for coordinative deactivation of the palladium(0)-phosphine ligand complex (Scheme 21).

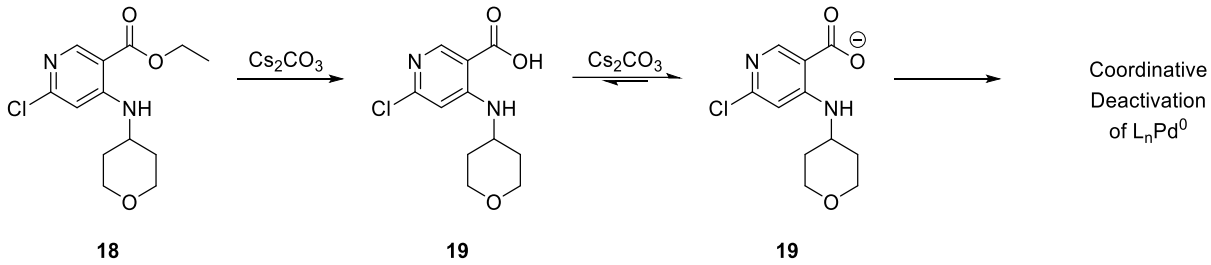

Scheme 21: Proposed generation of acid 19's carboxylate *via in situ* hydrolysis and deprotonation

The second side-reaction to be considered was whether an S_NAr was occurring. We considered this due to the continued presence of electron withdrawing substituents on the ring and the presence of another C-Cl group. The electronics of the C-Cl bond is a critical determinant in whether an S_NAr is possible, and it was thought that the ester and NH may possess enough electron withdrawing ability to activate the bond. We speculated the possibility of this reaction to be contingent upon whether aniline **11** was a strong enough nucleophile as the attached aromatic ring would reduce the nucleophilicity of the amine (due to resonance delocalisation of the nitrogen's lone pair of electrons) when compared to amine **6**. If an S_NAr reaction were to be occurring *in situ* this provides an alternative mechanism for the formation of the dimer **21b** in where aniline **20** is generated through an S_NAr which then proceeds to act as the nucleophile in the catalytic cycle generating the dimerized structure **21b** (Scheme 22).

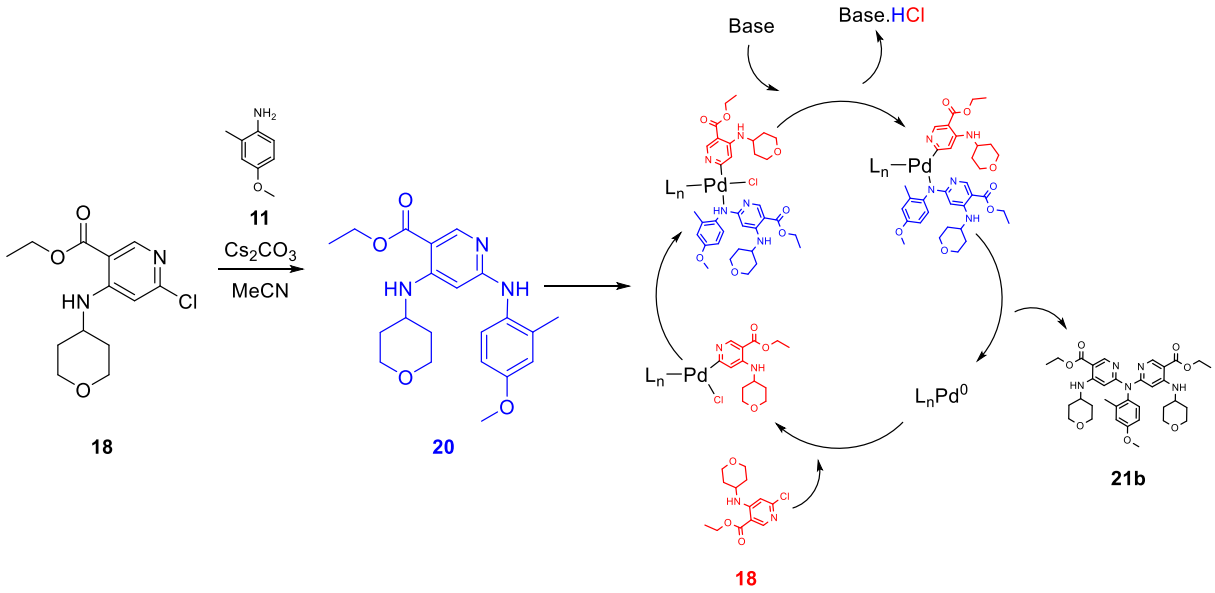

Scheme 22: Proposed alternative mechanism for the formation of dimer 21b

The possibility of these two reactions was investigated by testing with conditions mirroring the coupling however without the presence of palladium or phosphine ligand. Initially chloride **18** was stirred in a degassed mixture of MeCN and Cs_2CO_3 at 120 °C overnight. TLC and MS analysis revealed no polarity or mass change consistent with hydrolysis to carboxylic acid **19** indicating that the substrate is stable under these conditions. Aniline **11** was added to reaction mixture and stirred at 120 °C for an additional 16 hours to investigate whether an S_NAr reaction would take place. Further TLC and MS analysis showed no polarity or mass change consistent with the transformation to aniline **20**, confirming that neither of the proposed reactions were occurring. These studies into the base and solvent implied that it was unlikely to be these components rendering an unsuccessful cross-coupling reaction. The conclusion of these studies marked the end of investigation into the easily altered conditions of the coupling; this suggested that the unsuccessful reaction was due to the nature and structure of the substrates.

2.2.4 Substrate Studies

2.2.4.1 Quantum Chemical Calculations

Due to the experimental investigations not providing any clear indication as to why the reaction was consistently unsuccessful, we sought to explore computationally the seemingly stark difference in reactivity between our novel substrate chloride **18** and the ACSRC's substrate chloride **10**. The electronic structures of chlorides **18** and **10** were hence investigated by theoretical DFT calculations using Q-Chem 6.0.[53] To begin, an optimized model of the molecular geometries was generated by the iterative determination and optimization of stationary points. That is the minima and transition states on the potential energy surfaces of the molecules. The geometrical models were iteratively optimized until true energy minima were reached by repeated refinement cycling each time an imaginary frequency was calculated. Once only real frequencies were present the single point energies were calculated giving the solutions to the electronic Schrödinger equation for the fixed nuclear positions of the molecules. The resulting wave functions were analysed using the open-source program 'Multiwfn 3.8'; where the electron density and electrostatic potential were mapped across the volume of the molecule. A surface analysis was carried out to determine the electronic maxima and minima of the 0.01 isosurface (i.e. the surface of a volume representing 99% of the electron density).[54–57] The 'Visual Molecular Dynamics'[58] software was used to visualize these results; extrema are marked and colour scales are matched to facilitate visual comparison on Figures 17 and 18. Calculations and figure generation were carried out by Dr. Ben Dickson (project supervisor), interpretation of data was conducted by the author.

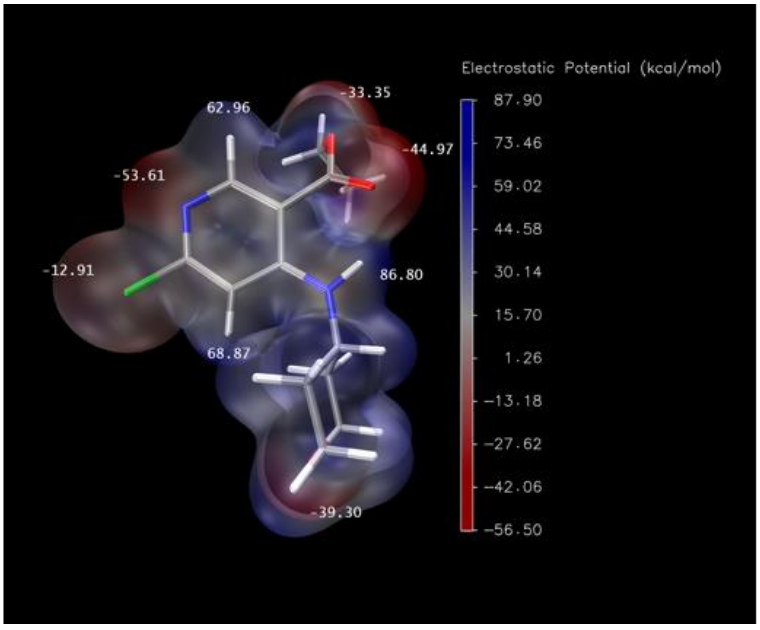

Figure 17: Electrostatic potential map of chloride 18

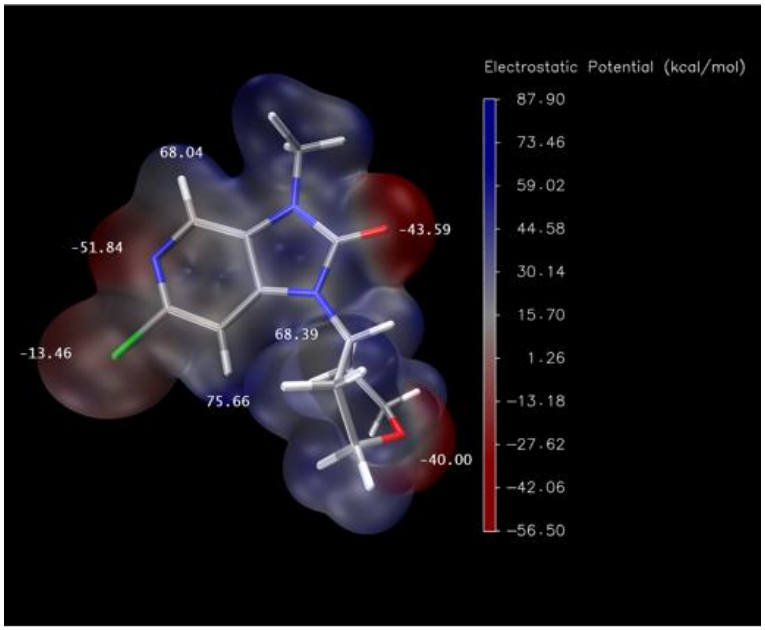

Figure 18: Electrostatic potential map of chloride 10

On comparison of the electrostatic potential maps for chlorides **18** (Figure 17) and **10** (Figure 18) we observed a lack of significant difference in the electron density of the aromatic rings. The electronics of this region would determine the activation of the C-Cl bond for oxidative addition to the L_nPd^0 complex and these calculations suggested the electronics of these bonds are more similar than the reactivity of chloride **18** led us to believe. We had anticipated there may be a notable difference between the electronics of chlorides **18** and **10**, however there were no obvious features of their electronic structures that explain the difference in reactivities we had observed. It is critical to maintain we considered our analysis of these calculations with caution. Although there did not appear to be any obvious difference in electronics, we were hesitant to over-interpret the calculations due to the team's lack of specific expertise in interpreting DFT calculations.

2.2.4.2 Model Study

Due to the uncertainty associated with our computational analysis of the electronics of chloride **18**, we decided to experimentally explore whether there was a relationship between its substituents and our poor coupling yields. This was undertaken by attempting the coupling of aniline **11** to an unfunctionalized substrate; chloride **22** (Scheme 23). This mimics the 2-chloropyridine functionality of chloride **18** without any further substituent effects.

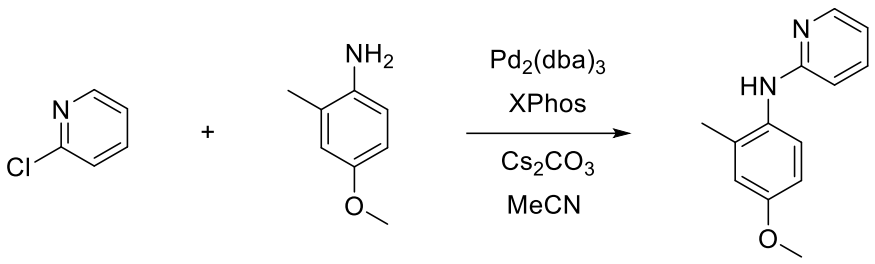

22 **11** **23**

Scheme 23: Model Buchwald-Hartwig coupling on chloride 22 and aniline 11

The standard Buchwald-Hartwig conditions ($Pd_2(dba)_3 \cdot CHCl_3$/XPhos) were employed for this coupling (Scheme 23). This was chosen over BrettPhos-PdG3 as this combination provided the highest yields across all other coupling attempts. Initial MS analysis of the crude reaction mixture indicated distinct ions at 215.1 *m/z* and 292.3 *m/z*. 215.1 *m/z* aligns with the expected $[M+H]^+$ of aniline **23** (Scheme 23). However, 292.3 *m/z* would be the approximate expected $[M+H]^+$ for the dimerized structure **24** (Figure 19). This structure was not successfully isolated due to significant co-elution during the attempted purification of the crude material.

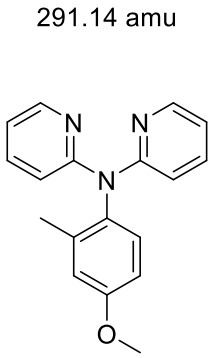

24

Figure 19: Proposed dimerization of pyridine 23 and aniline 11

Post purification, aniline **23** was isolated as a brown viscous gum in a 1.1% yield. This was suspected to be slightly contaminated, so a melting point was not sought however an NMR and MS characterisation was accomplished. Even considering that the yield is an overrepresentation, this is the lowest yield achieved throughout all cross-couplings attempted. The poor yields of this model reaction and the other couplings implied that there is an issue when coupling aniline **11** to 2-chloropyridines (the common functionality between chlorides **10**, **18** and **22**) that are not also imidazopyridinones (additional functionality of the ACSRC's chloride **10**). However, the literature contradicted this as there is a

precedent for the Buchwald-Hartwig coupling of aniline **11** to 2-chloropyridines that are not imidazopyridinones (Figure 20).[59,60]

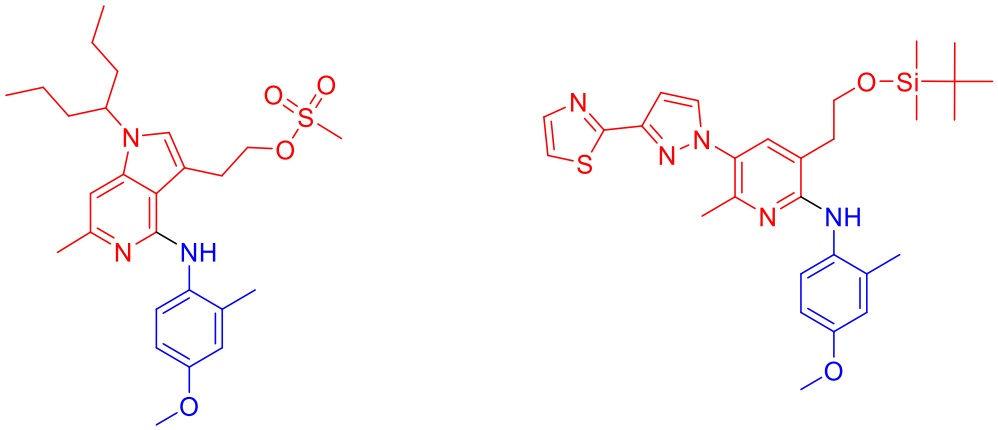

Ref. 59

88% yield

Ref. 60

Yield not reported

Figure 20: Alternative 2-chloropyridines that aniline 11 has been coupled to[59,60]

The ACSRC's successful coupling of aniline **11** to chloride **10** and our issue in coupling aniline **11** to 2-chloropyridines disagreeing with the literature precedent suggested that there is a balance to the functionality required when coupling aniline **11** to 2-chloropyridines (i.e. a balance to the contribution of functional groups to electronic and steric effects). We were unable to discern this from our computational work, however the unsuccessful couplings with our novel substrate chloride **18** implied that this balance is seemingly absent from its structure. This potentially implicates it as being the problematic reaction component within our coupling.

2.2.4.2.1 Characterization of Aniline 23

Due to the identical substructure of the aniline component to the novel Buchwald-Hartwig coupling product **20** this area of the molecule was assigned first. As with aniline **20** the protons H-3′, H-5′ and H-6′ (Figure 11) were assigned based on the distinct splitting (a doublet, doublet of doublets and a doublet respectively) and coupling constants of the ^{1}H-NMR aromatic peaks (2.9 Hz, 8.6 + 2.9 Hz and 8.6 Hz respectively). The O-CH_3 and methyl components of the ring were confirmed by the presence of two 3H singlets with the O-CH_3 assignment being distinctly downfield to the other. Analogous HMBC evidence to the assignment of the quaternary carbons for aniline **20** was present and hence the equivalent system for this compound was assigned with this reasoning. The coupling constants and magnitudes of the chemical shifts were consistent with what was assigned for aniline **20** confirming the

installation of aniline **11** onto chloride **22**. The remaining protons to be assigned were the aromatic protons on the pyridine ring (Figure 21).

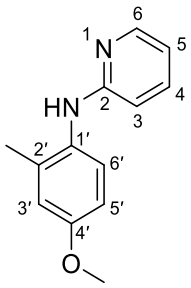

23

Figure 21: Numbered structure of aniline 23

These assignments presented a unique challenge due to the higher order splitting across the ring. The higher order splitting made the exact peak shapes difficult to discern. Key assignments were hence made with chemical reasoning and the few coupling constants that were resolved. H-6 was assigned to the most downfield of the aromatic signals (8.13 ppm) due to the expected deshielding effect of the adjacent nitrogen. A coupling constant of 1.9 Hz was resolved from this peak and matched to the signal at 7.37-7.42 ppm. This was near the typical constant range for a *meta* coupling (~ 2-3 Hz)[42], this would typically be too large for a *para* coupling and too small for an *ortho* coupling so it was assigned as H-4 (Figure 22).

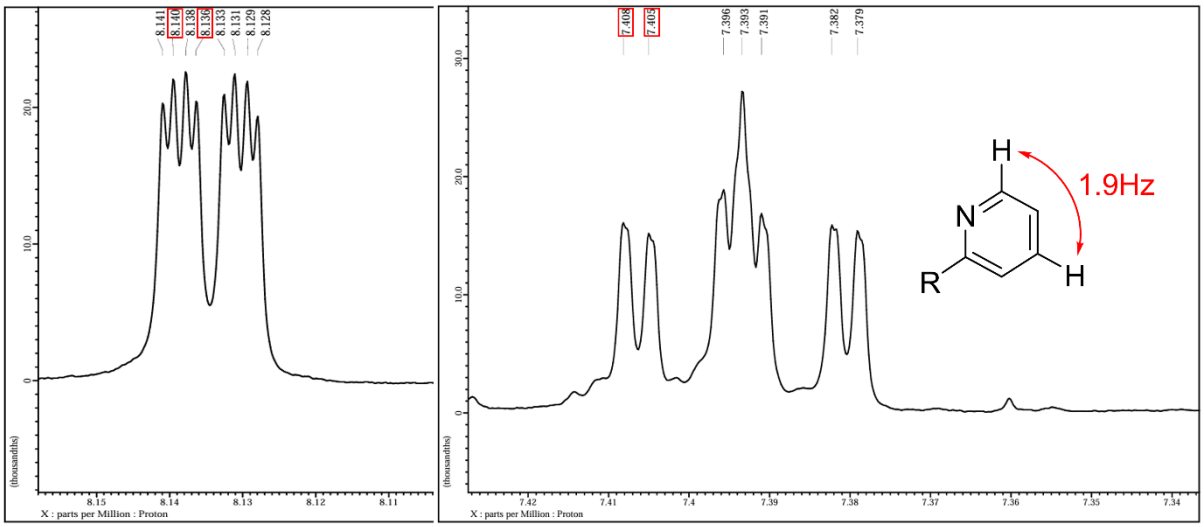

Figure 22: Shared 1.9 Hz coupling between H-6 and H-4 on aniline 23; example peak shifts accented red

Another coupling constant from the 8.13 ppm signal that was identified was 0.9 Hz. This constant was consistent with a *para* coupling, which are typically not visible or are at values lower than 1 Hz.[42] This was matched to the signal at 6.36-6.39 ppm, giving it the assignment of H-3 (Figure 23).

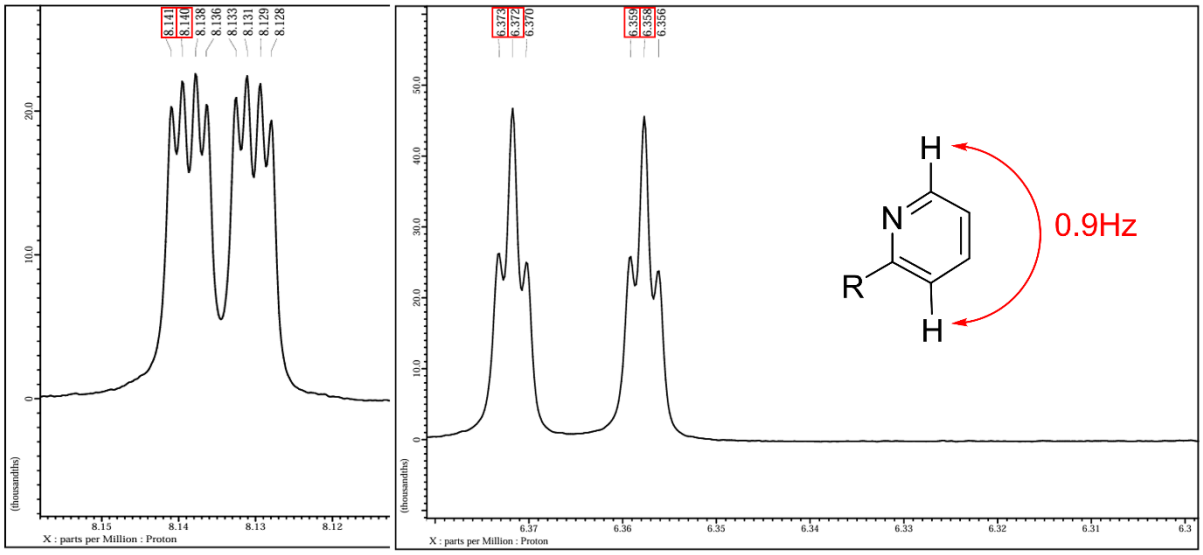

Figure 23: Shared 0.9 Hz coupling between H-6 and H-3 on aniline 23; example peak shifts accented red

This left the remaining aromatic proton signal at 6.64 ppm with the assignment H-5. The associated carbons were assigned with HSQC. However, the H-4 signal showed correlations to two distinct carbons (Figure 24).

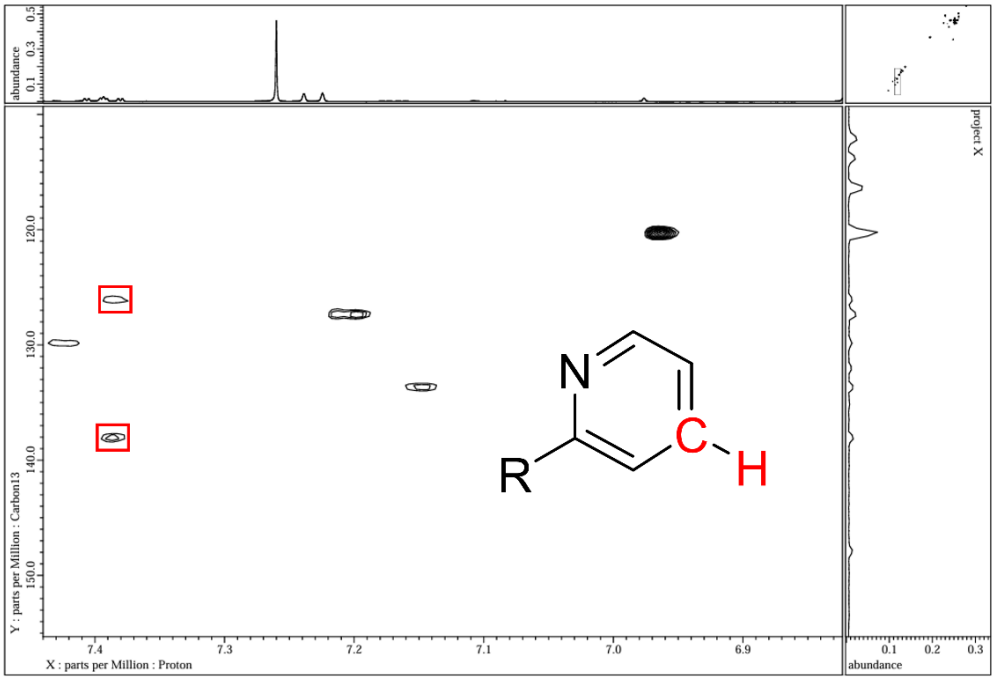

Figure 24: HSQC of the H-4 signal on aniline 23

Due to a low signal-noise ratio observed in the APT experiment the position of this peak was inferred from the HMBC where it was revealed that the upfield correlation (top correlation on Figure 24) of the two correlated to what was perceived as slight contamination. This left the assignment of 138.0 ppm (bottom correlation on Figure 24) as 4-CH.

The last assignment to be made was the pyridine quaternary carbon. Again, due to a low signal-noise ratio on the APT this was investigated through HMBC. A long-range *J* of 8 Hz on the HMBC pyridine spin system showed distinct ^{3}J C-H correlations. This gave a correlation between 7.38-7.42 ppm and the final unassigned carbon signal at 158.0 ppm which was assigned as the pyridine quaternary signal 2-C (Figure 25).

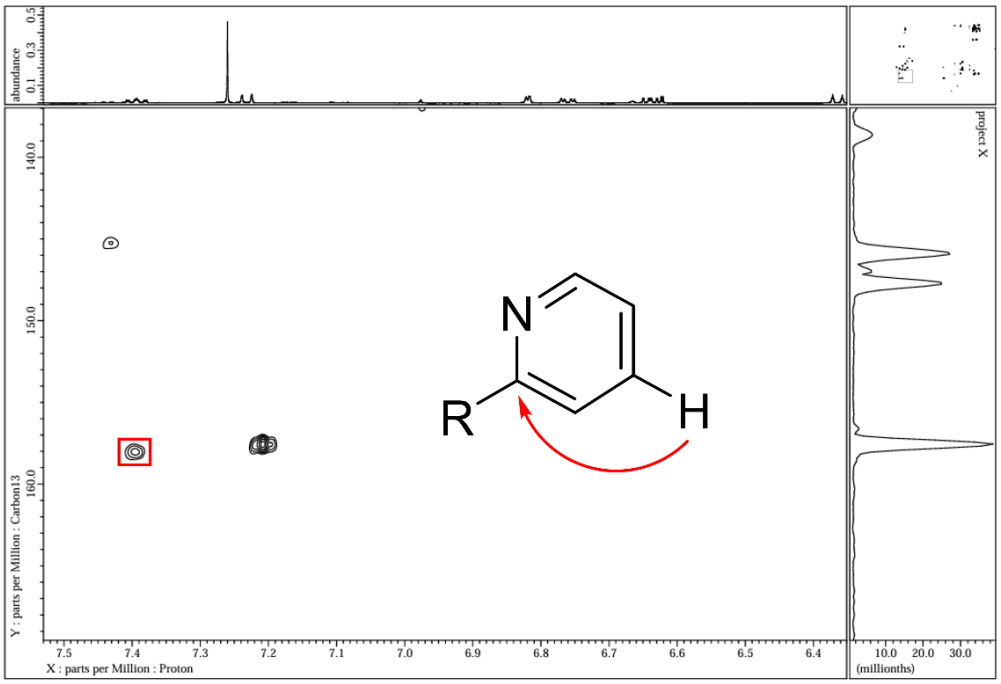

Figure 25: HMBC revealing the shift of the final unassigned quaternary carbon on aniline 23

This was the most downfield of the assigned carbons aligning with the expected electronics of the pyridine system where this carbon was in the most deshielded environment of this compound; between both nitrogens.

2.2.4.3 Protection of Aniline 11

Another piece of experimental evidence we possessed, consistent with a malfunctioning reaction, was the recurrent observation of byproducts consistent with dimer formation. We decided to prevent their formation *via* protection of the aniline, in order to establish if this improved the yield of the expected coupling product. The protecting group when incorporated into the product should hinder the amine

from being a nucleophile in subsequent catalytic cycles. Additionally, protection of the aniline NH would have been a requirement of the rearranged route eventually to prevent the presence of two possible *N*-methylation sites (Figure 26) hence this provided opportunity to investigate whether protection of the aniline NH pre-installation was viable. Protection was proposed by installation of a Boc group onto aniline **11** (Scheme 24).

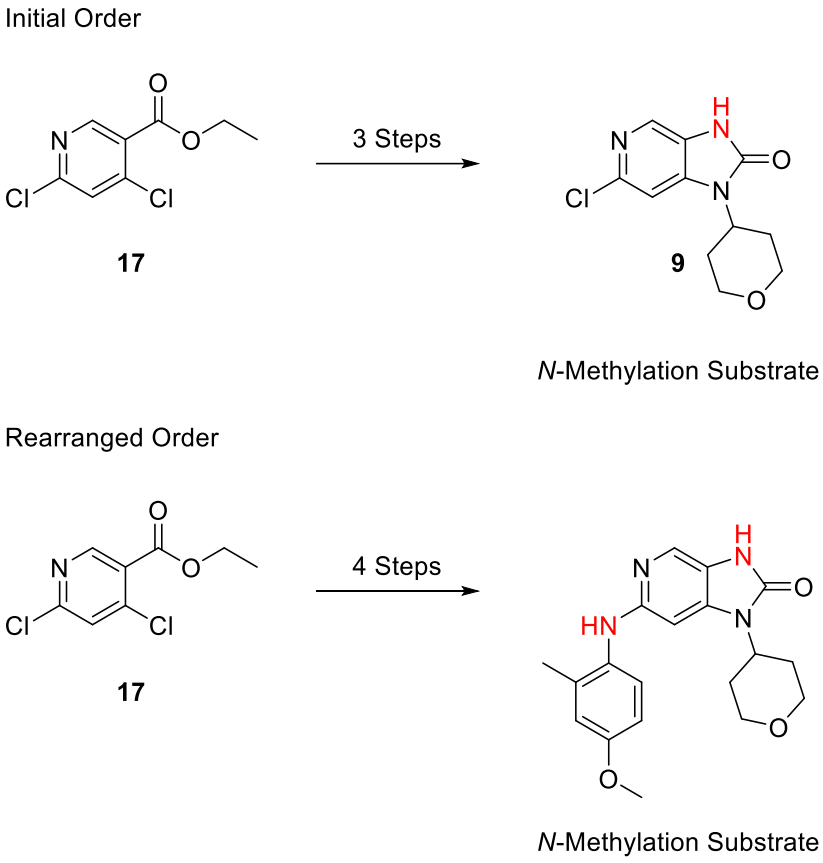

Figure 26: Presence of two possible *N*-methylation sites within the rearranged novel route

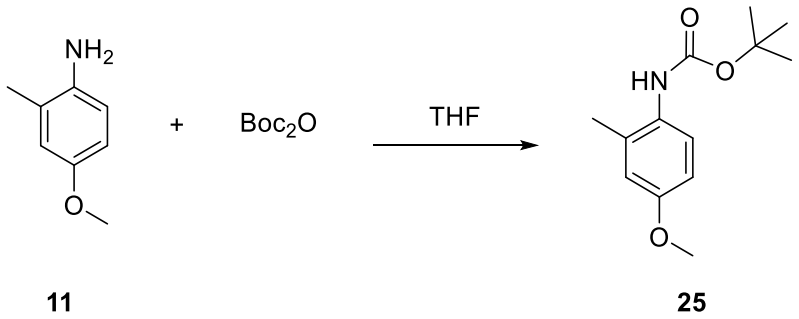

Scheme 24: Boc protection of aniline 11

Protection of aniline **11** was attempted by stirring with Boc_2O in THF at reflux for 2 hours following literature precedent.[61] The reaction was cooled to room temperature and the solvent was removed *in vacuo*. Carbamate **25** (Scheme 24) was isolated with column chromatography in a 6.6% yield. Confirmation of the structural identity was done by MS and ^{1}H-NMR where the two 3H methyl singlets of the ring and the 9H Boc group singlet were strong indicators of the successful synthesis of carbamate **25**. Additionally, the ^{1}H-NMR data matched the literature values.[61] In the next attempt the reaction was stirred at reflux overnight in an attempt to improve the yield. The same work-up procedure was used after cooling the reaction and carbamate **25** was isolated in a quantitative yield.

The coupling of the carbamate **25** was first attempted on the model substrate chloride **22** to provide a simple coupling partner, establish the competence of carbamate **25** to participate in a Buchwald-Hartwig coupling and to determine if it improved the outcome.

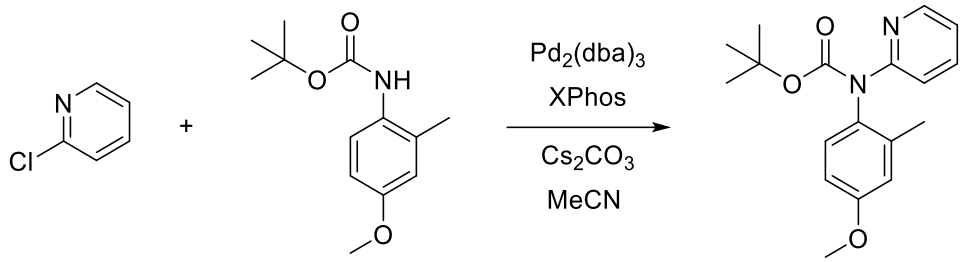

22 **25** **26**

Scheme 25: Buchwald-Hartwig coupling of chloride 22 and carbamate 25

The standard conditions were employed with chloride **22**, carbamate **25** and $Pd_2(dba)_3 \cdot CHCl_3$/XPhos (Scheme 25). During the standard work-up, MS analysis of the reaction after filtration through diatomaceous earth revealed a distinctive ion at 215.1 *m/z* aligning with what was expected to be the product mass minus the Boc group due to its facile cleavage during ionization. The standard work-up was attempted however carbamate **26** (Scheme 25) was unable to be isolated despite multiple attempts with column chromatography. What appeared to be clean fractions by TLC were revealed to be impure by MS and NMR (where nothing was distinguishable within the ^{1}H-NMR spectrum). Analysis of the fraction expected to contain carbamate **26** reported both the expected ion of **26** and an intense ion at 493.3 *m/z*. The exact structure of the 493.3 *m/z* peak remained a mystery however the only distinguishable feature was that the peak showed a complex abundance pattern that was not consistent with the typical organic elements. This was plausibly derived from palladium contamination as that was the only possible source of inorganic material. This would be consistent with the uninterpretable ^{1}H-NMR spectrum where coordination of the palladium contamination to the organic components would be expected to drastically alter the expected environments present, however this was not investigated further. We considered if the inability to isolate anything was due to a lack of appreciable product and

whether this could be due to an incorrect choice of phosphine ligand as the nucleophile identity should typically relate to the choice of ligand. Hence the reaction was reattempted with the only other phosphine available; BrettPhos (through the use of the PdG3 catalyst). This gave identical isolation issues and no appreciable amount of clean product despite MS implying its presence. The literature suggested that a specialized ligand such as JackiePhos would be required for a coupling of this nature due to the steric hinderance of the carbamate[62] group on **25** however this was unavailable to us. Despite these unsuccessful couplings the reaction was attempted with the intended substrate chloride **18** (Scheme 26).

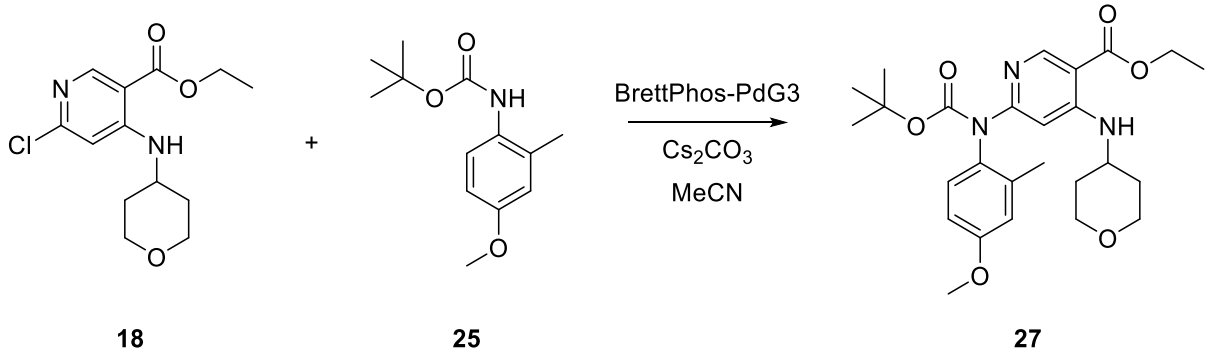

18 **25** **27**

Scheme 26: Buchwald-Hartwig coupling of chloride 18 and carbamate 25

The standard conditions and work-up were used and as with the other attempts at coupling carbamate **25** isolation challenges ensued. MS of the reaction mixture showed an ion at 485.6 *m/z* consistent with the expected $[M+H]^+$ of carbamate **27** (Scheme 26) albeit with the absence of any ion signifying Boc cleavage during ionisation. Despite observation of this ion, after the standard work-up, no product could be isolated. Fractions thought to contain carbamate **27**, had similar complex isotope patterns to those seen in the model coupling, tentatively attributed to the presence of palladium.

Throughout all attempted couplings with carbamate **25** we were unable to successfully isolate any of the expected Boc-protected coupling products despite MS implying their existence. We considered whether this was due to instability of the product on the silica. We had no evidence of this occurring for the unprotected variants however there is literature on the deprotection of N-Boc groups occurring on silica.[63] Further investigation of this is warranted. Regardless, we could not accurately judge if these couplings were successful or whether suppression of the dimerized structures had any improvement to the yield of the expected coupling product rendering the protected aniline studies inconclusive.

2.2.5 Reaction Feasibility

As a concluding effort the initially proposed novel coupling between chloride **18** and aniline **11** (Scheme 17) was attempted a final time. This exploration was done concurrently with the work described in *Section 2.1.5*, and so freshly prepared $Pd_2(dba)_3 \cdot CHCl_3$ was available. The standard conditions and work-up were employed however aniline **20** was isolated with minor contamination. The ^{1}H-NMR data from this crude isolation was consistent with the fully characterized clean material however additional signals in the aliphatic region verified its impurity. The crude yield was calculated to be 19.0% and the consideration that this is an overrepresentation likely placed the hypothetical pure yield in line with the other attempts. This represented the final variation we could test with the available resources. A successful coupling eluded us despite investigating the alternative catalytic options that were available to us (both palladium source and phosphine ligand), the choice of solvent and verifying that the base was an appropriate choice for the substrate. This leaves the findings from the substrate studies the only feasible possibilities as to why the reaction is consistently unsuccessful. The analysis of the quantum chemical calculations revealed a similarity between our substrate chloride **18** and the ACSRC's chloride **10** regarding the electronics of the aromatic ring and C-Cl bond. This renders the possibility of an unfavourable oxidative addition environment unlikely. We then endeavoured to explore if there was a relationship between chloride **18's** substituents and the consistently low coupling yields. Our findings from the resultant model study in conjunction with literature consultation suggests that chloride **18** lacks a balance to its functionality that allows aniline **11** to be coupled to functionalized 2-chloropyridines. Additionally, we attempted to establish whether the formation of the dimerized structure had any relationship to the reaction yield through our studies of the coupling using carbamate **25**. However, due to the challenge we experienced in isolating any pure material containing a Boc group we were unable to make any conclusions.

The only viable suggestion from the limited perspective of our substrate studies is that chloride **18** lacks the required balance in functionality to undergo a successful coupling with aniline **11**. Therefore, it is logical to compare the functionality of chloride **18** to chloride **10** (Figure 27).

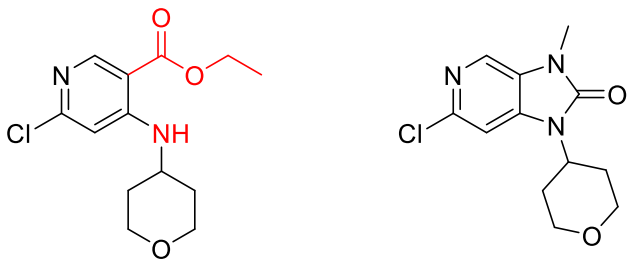

18 **10**

Figure 27: Key functional difference between chloride 18 and chloride 10

There are two notable differences in functionality that chloride **18** possesses. The ethyl ester and the NH of the THP (Figure 27). The ester is not typically considered a problematic functional group in Buchwald-Hartwig couplings outside of the restriction it places onto base selection. The literature suggests that if a base that is unable to facilitate a hydrolysis is used, this group is tolerated and compatible within a variety of coupling systems.[64,65] This leaves the THP-NH group as being the potentially problematic structural group. There are a variety of situations where the presence of this free amine may be negatively impacting the reaction system due to its probable basic and nucleophilic properties. We considered it a possibility that this amine could be competing with the aniline amine of **11** for nucleophilic addition onto the catalytic intermediate, however we saw no evidence of the products consistent with this. An alternative possibility is inhibition of the catalyst outside of the mechanism by coordinative means. It could be the case that the amine is sufficiently nucleophilic to occupy coordination sites around the palladium necessary for the coupling. This seems plausible when it is recognized that the substrate, chloride **18**, is present in a large excess compared to the 5 mol% of input catalyst; even if this coordination proceeds through an unfavourable equilibrium a small percentage of the substrate undesirably coordinating to the catalyst could significantly impact reaction performance. This coordination would be expected to inhibit the reaction even if all other aspects of the conditions were investigated which is consistent with the observations of our studies. However, this remains a theory and further evidence would be required to support this.

This could be investigated *via* protection of the THP-NH (e.g. as a Boc carbamate) on chloride **18** and whether there is an increase in yield of the expected coupling product. An additional investigation could be conducted by trialling LiHMDS as the base and establishing whether an increased yield of aniline **20** is observed. Literature examples suggest that Buchwald-Hartwig couplings using LiHMDS will typically allow for the tolerance of hydroxyl groups on the substrate.[66] This is not an exact match to the amine of chloride **18**, however there is a specific literature reporting concerning the coupling of unprotected benzyl-fused aminocyclic halides with a variety of primary amine coupling partners using LiHMDS as the base.[67]

Regarding the feasibility of the reaction, it is difficult to judge definitively whether it is possible to optimize the conditions further as our findings implicate the structure of the substrate itself to be the issue. However, due to the vast array of alternative reaction conditions, catalyst variants and phosphine ligands available to trial it is highly likely that there exist conditions to allow for the successful coupling, but it is rather a matter of tenacious trialling beyond what was investigated here to find the viable reaction conditions.

2.3 Evaluation

2.3.1 The Novel Route

In order to evaluate whether the novel route is superior to the ACSRC route for the synthesis of inhibitor **2** it is critical to consider the steps up to the convergence of the routes. The overall synthetic yield for the novel route to generate imidazopyridinone **9** is 53.3%. This is contrasted to the ACSRC's overall yield of 70.6% (not including the initial chlorination as Table 4 suggests it is more economical to avoid this reaction and start their route with dichloride **5**) to produce the same compound (Figure 28). This highlights that from a synthetic efficiency perspective the ACSRC's route is superior. The primary reason behind this is the diminished yield of the Curtius rearrangement compared to ACSRC's CDI coupling.

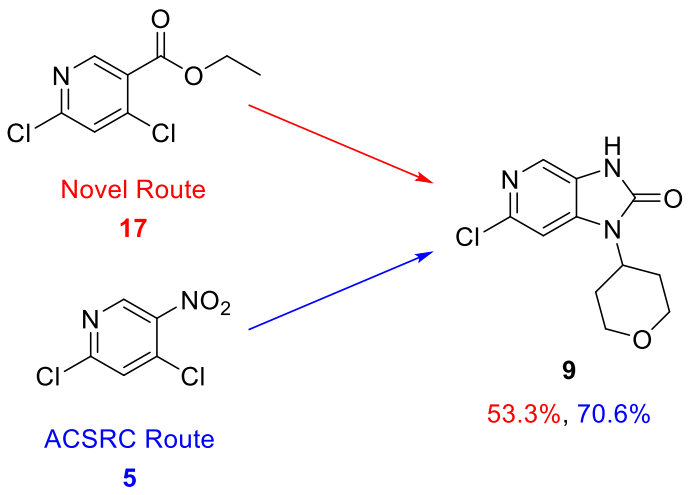

Figure 28: Overall yield of the novel route versus the ACSRC route to produce imidazopyridinone 9

Currently, we propose that the ACSRC route remains the superior option however this may be subject to change. Consideration should be given to the possibility of further Curtius rearrangement optimization and the cheaper starting material of the novel route. Further optimization of the Curtius rearrangement was unfeasible for us due to resource limitations however if accomplished this may align the yield with the CDI coupling rendering the novel route a competitive alternative with a lower-cost starting material for the synthesis of inhibitor **2**.

2.3.2 Attempted Rearrangement of the Novel Route

Due to the challenge in finding viable reaction conditions for the first novel step of the rearranged novel route we were unable to establish further whether this rearrangement was of any advantage. We had considered scaling up the Buchwald-Hartwig coupling despite the low yields to continue our investigation of the rearrangement however we thought this fruitless as the primary objective was to assess any differences in synthetic efficiency. Even if the remaining steps to produce inhibitor **2** were more efficient than the ACSRC route or trialled route an unviable Buchwald-Harwig coupling would automatically render the rearrangement an inferior alternative.

Additionally, through our studies of the coupling involving carbamate **25** we discovered future synthetic challenges relating to the rearrangement. Due to the unsuccessful isolation of any coupling product containing a Boc group we were unable to establish if protection of the aniline NH with a Boc group pre-installation was viable. The condemns the route to require even further study to determine a viable protection strategy for the aniline NH on chloride **20**. This may also be amplified if in future the THP-NH was confirmed to be the cause of the inhibited cross-coupling. This would require additional protection with an alternative protecting group. The prospective protection strategies that may be required greatly complicates this proposed rearrangement and is expected to certainly dimmish the synthetic efficiency of the route. This consideration in conjunction with the currently unviable Buchwald-Hartwig coupling is why we propose the rearranged novel route is unlikely to be useful as an alternative to the novel route or the ACSRC route for the synthesis of imidazopyridinones and hence inhibitor **2**.

2.3.3 Future Work

If the rearranged novel route becomes desirable for alternative reasons it would be reasonable that future work investigate potential alternative strategies to install aniline **11** onto chloride **18**. A commonly employed alternative to the Buchwald-Hartwig amination is the Goldberg reaction. This reaction is an Ullmann-type coupling which involves the coupling of an aniline to an aryl halide in the presence of a copper(I) catalyst and base.[68]

Another plausible alternative could be a Chan-Lam coupling where an aryl boronic acid can be coupled with an amine using a copper catalyst in the presence of base.[69,70] However, this would require substrate alteration and the efficiency of doing such would need to be evaluated. Both alternative couplings are through the use of a copper catalyst however it is difficult to predict whether either of them are likely to be high-yielding due to the less consistent nature of copper-mediated couplings compared to palladium-mediated couplings due to limitations in substrate scope and the requirement of more forcing reaction conditions. Additionally, it is critical to note that if the THP-NH of chloride **18** was

coordinatively deactivating the palladium catalyst (which could be discerned through the investigations proposed in *Section 2.2.5*), it remains a possibility that this may occur with a copper catalyst.

Although investigation into these alternative couplings would not address the required protection strategy for the rearranged route it may bring the rearrangement into the realm of plausibility. Once a viable strategy to install aniline **11** onto chloride **18** is established it would then be realistic to devise a suitable protection strategy ideally by the simple adjustment of substrates using the established cross-coupling conditions.

3 Experimental

3.1 General Details

All NMR spectra were acquired using a JEOL ECZR 600 MHz spectrometer equipped with a Royal HFX probe. NMR data was processed using Delta 6.0.0 software. MS was carried out using a Bruker micrOTOF instrument, using ESI and a TOF analyser (positive ion mode). The micrOTOF instrument was not calibrated during much of the course of this work and reached end-of-life prior to thesis writing. While nominally this instrument would produce high-resolution data it is being treated as low-resolution in this thesis aside from the data in relation to ethyl ester **18** and carboxylic acid **19** which were characterized early in the project. The MS data was analysed using Bruker's DataAnalysis software. Melting points were established using the Cole-Palmer MP-400D Digital Melting Point Apparatus (0.1 °C resolution).

3.2 Quantum Chemical Calculations

Geometry optimisation and single point calculations were conducted using the 'Q-Chem 6.0' software at the ωB97XD level of theory using the cc-pVTZ basis set.[53] Frequency calculations were used to confirm that a global minimum was found. The wavefunctions derived from single point calculations were used with 'Multiwfn 3.8' to calculate electron density maps at the 0.01 isolevel.[54–57] Electrostatic potential was mapped on to the electron density map. Images were produced in 'Visual Molecular Dynamics'[58] and colour scaling was conserved between images allowing direct comparison.

3.3 Catalytic Material

Recrystallisation of $Pd_2(dba)_3$

$Pd_2(dba)_3$ (0.50 g, 0.55 mmol) was dissolved in an excess of $CHCl_3$, and the precipitate was removed without further work-up. The remaining solution was dried under reduced pressure. The solid that remained was redissolved in a minimum amount of $CHCl_3$ (5 mL), to which a 4-fold excess of acetone (40 mL) was added. This was left to recrystallize under refrigeration overnight. The crystals were filtered off and washed with cold acetone (5 °C, 2 × 5 mL). This was dried *in vacuo* furnishing $Pd_2(dba)_3 \cdot CHCl_3$ as purple crystals (0.198 g, 34.7%).

Synthesis of $Pd_2(dba)_3$

To a flask of MeOH (10 mL), $Pd(OAc)_2$ (0.1 g, 0.45 mmol) and NaOAc (0.365 g, 4.45 mmol) dba (0.209 g, 0.89 mmol) was added. This was stirred at 40 °C for 3 hours. The solid formed was collected by filtration and washed (2 × 3 mL MeOH, 3 × 3 mL of H_2O). The solid was redissolved in $CHCl_3$ and dried *in vacuo* then redissolved in a minimum amount of $CHCl_3$ (5 mL). A 4-fold excess of acetone (20 mL) was added and the solution was left overnight under refrigeration. The crystals were collected by filtration and washed with cold acetone (5 °C, 2 × 5 mL). Drying under reduced pressure afforded $Pd_2(dba)_3 \cdot CHCl_3$ as purple crystals (0.096 g, 41.7%).

3.4 Synthetic Compounds

Ethyl 6-chloro-4-((tetrahydro-2*H*-pyran-4-yl)amino)nicotinate (**18**)

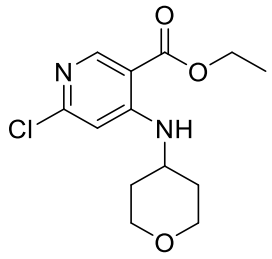

18

To a solution of dichloride **17** (1.00 g, 4.54 mmol) in MeCN (20 mL), was added amine **6** (0.69 g, 6.8 mmol) and Cs_2CO_3 (3.7 g, 11 mmol). The reaction mixture was stirred for 40 hours with heating (75 °C), then cooled to room temperature and filtered. The precipitate was discarded, and the mother liquor was concentrated *in vacuo* to yield the crude product. Column chromatography (10-20% EtOAc in hexanes) gave the purified product chloride **18** as a colourless crystalline solid (1.10 g, 85.3%): mp 72-74 °C; ^{1}H NMR (600 MHz, $CDCl_3$) δ 8.69 (s, 1H, H-2), 8.28 (br d, J = 7.1 Hz, 1H, 4-NH), 6.55 (s, 1H, H-5), 4.34 (q, J = 7.1 Hz, 2H, H-1″), 3.98-4.03 (m, 2H, H-2′a, H-6′a), 3.53-3.63 (m, 3H, H-2′b, H-4′, H-6′b), 1.98-2.04 (m, 2H, H-3′a, H-5′a), 1.60-1.67 (m, 2H, H-3′b, H-5′b), 1.39 (t, J = 7.1 Hz, 3H, H-2″); ^{13}C NMR (150 MHz, $CDCl_3$) δ 167.8 (C=O), 155.9 (4-C, 6-C), 154.9 (4-C, 6-C), 153.5 (2-CH), 107.1 (3-C), 104.8 (5-CH), 66.3 (2′-CH_2, 6′-CH_2), 61.2 (1″-CH_2), 48.1 (4′-CH), 32.5 (3′-CH_2, 5′-CH_2), 14.4 (2″-CH_3); HRMS calculated for $C_{13}H_{18}{}^{35}ClN_2O_3$ $[M+H]^+$ *m/z* 285.10005, found 285.10005 (0.0 ppm).

6-Chloro-4-((tetrahydro-2*H*-pyran-4-yl)amino)nicotinic acid (**19**)

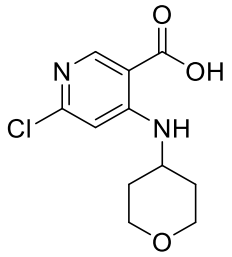

19

To a solution of ethyl ester **18** (0.908 g, 3.19 mmol) in THF (12 mL), LiOH (0.15 g, 6.4 mmol) solvated in 12 mL of H_2O was added. The reaction mixture was stirred for 16 hours at room temperature. The THF was subsequently removed from the mother liquor *in vacuo*, and the remaining mixture was acidified (pH = 3) with 2M HCl. This gave the product as a white solid which was collected *via* filtration. Drying yielded carboxylic acid **19** as a white powder (0.737 g, 89.9%): mp 256-258 °C; ^{1}H NMR (600 MHz, $CDCl_3$) δ 8.51 (s, 1H, H-2), 8.31 (br d, J = 7.8 Hz, 1H, 4-NH), 6.94 (s, 1H, H-5), 3.74-3.89 (m, 3H, H-2′a, H-4′, H-6′a), 3.43-3.52 (m, 2H, H-2′b, H-6′b), 1.86-1.94 (m, 2H, H-3′a, H-5′a), 1.38-1.49 (m, 2H, H-3′b, H-5′b); ^{13}C NMR (150 MHz, $CDCl_3$) δ 169.0 (C=O), 154.8 (4-C, 6-C), 154.7 (4-C, 6-C), 152.9 (2-CH), 107.1 (3-C), 105.0 (5-CH), 65.5 (2′-CH_2, 6′-CH_2), 47.1 (4′-CH), 32.2 (3′-CH_2, 5′-CH_2); HRMS calculated for $C_{11}H_{14}{}^{35}ClN_2O_3$ $[M+H]^+$ *m/z* 257.06875, found 257.06875 (0.0 ppm).

6-Chloro-1-(tetrahydro-2*H*-pyran-4-yl)-1,3-dihydro-2*H*-imidazo[4,5-*c*]pyridin-2-one (**9**)

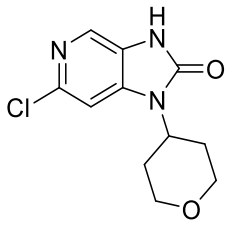

9

To a solution of carboxylic acid **19** (0.400 g, 1.55 mmol) in DMA (6 mL), was added NEt_3 (0.22 mL, 1.6 mmol) and DPPA (0.33 mL, 1.6 mmol). Under N_2 the reaction was left to stir at room temperature for 6 hours then at 120 °C for 16 hours. The reaction was quenched with ice, and the product was extracted with EtOAc (3 × 12 mL). The organic layers were washed with H_2O (2 × 40 mL), brine (1 × 40 mL) and dried with $NaSO_4$. The solvent was removed *in vacuo*, giving the crude product. This was purified with column chromatography (50-100% EtOAc in hexanes) followed by trituration with 1:1 EtOAc/hexanes affording imidazopyridinone **9** as a white powder (0.271 g, 69.5%): mp 278-281 °C (lit.[22] mp 281-283 °C); ^{1}H NMR (600 MHz, $CDCl_3$) δ_H 9.35 (br s, 1H), 8.13 (s, 1H), 7.19 (s, 1H), 4.54 (tt, J = 12.5, 4.4 Hz, 1H), 4.17 (dd, J = 11.8, 4.6 Hz, 2H), 3.53-3.60 (m, 2H), 2.36-2.46 (m, 2H), 1.78-1.83 (m, 2H).

6-Chloro-3-methyl-1-(tetrahydro-2*H*-pyran-4-yl)-1,3-dihydro-2*H*-imidazo[4,5-*c*]pyridin-2-one (**10**)

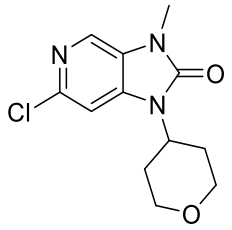

10

Imidazopyridinone **9** (0.785 g, 3.09 mmol) was added to 5 mL of DMF with subsequent addition of NaH (0.082 g, 3.4 mmol). This was stirred at 5 °C for 3 minutes after which MeI (0.25 mL, 4.0 mmol) was added. The mixture was left for a further 5 minutes at 5 °C, then stirred at room temperature for 16 hours. The reaction was quenched with ice and the product extracted with EtOAc (3 × 10 mL). The organic phases were washed with H_2O (2 × 30 mL) and dried with $NaSO_4$. The remaining solvent was removed *in vacuo* yielding the crude product. This was purified using column chromatography (80% EtOAc in hexanes) affording chloride **10** as white crystals (0.551 g, 66.4%): mp 190-192 °C (lit.[22] mp 190-192 °C); ^{1}H NMR (600 MHz, $CDCl_3$) δ_H 7.99 (s, 1H), 7.15 (d, J = 0.6 Hz, 1H), 4.55 (tt, J = 12.5, 4.4 Hz, 1H), 4.15 (dd, J = 11.8, 4.7 Hz, 2H), 3.51-3.58 (m, 2 H), 3.45 (s, 3H), 2.33-2.43 (m, 2H), 1.74-1.80 (m, 2H).

6-((4-Methoxy-2-methylphenyl)amino)-3-methyl-1-(tetrahydro-2*H*-pyran-4-yl)-1,3-dihydro-2*H*-imidazo[4,5-*c*]pyridin-2-one (**2**)

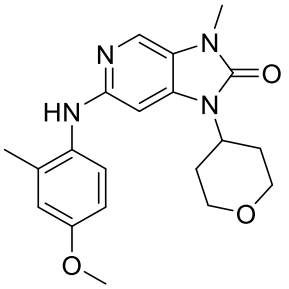

2

To a degassed mixture of chloride **10** (0.200 g, 0.750 mmol), aniline **11** (0.123 g, 0.900 mmol), Cs_2CO_3 (0.54 g, 1.7 mmol) and XPhos (0.07 g, 0.2 mmol) in MeCN (10 mL), $Pd_2(dba)_3 \cdot CHCl_3$ (0.04 g, 0.04 mmol) was added. This was stirred at 120 °C for 16 hours under N_2. The mixture was cooled to room temperature, diluted with EtOAc and filtered through diatomaceous earth. The solvent from the filtrate was removed *in vacuo* yielding the crude product. Subsequent purification with column chromatography (80-100% EtOAc in hexanes) yielded inhibitor **2** as a brown amorphous solid (0.242 g, 86.4%): mp 169-171 °C (lit.[22] mp 176-178 °C); ^{1}H NMR (600 MHz, $CDCl_3$) δ_H 7.69 (s, 1H), 7.21 (d, J = 8.7 Hz, 1H), 6.84 (d, J = 2.9 Hz, 1H), 6.77 (dd, J = 8.6, 2.9 Hz, 1H), 6.20 (d, J = 0.6 Hz, 1H), 4.37 (tt, J = 12.5, 4.2 Hz, 1H), 4.06 (dd, J = 11.6, 4.5 Hz, 2H), 3.83 (s, 3H), 3.44-3.52 (m, 2H), 3.37 (s, 3H), 2.19-2.30 (m, 5H), 1.65-1.71 (m, 2H).

Ethyl 6-((4-methoxy-2-methylphenyl)amino)-4-((tetrahydro-2*H*-pyran-4-yl)amino)nicotinate (**20**)

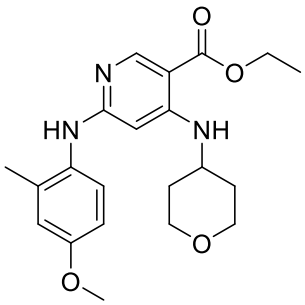

20

To a degassed mixture of chloride **18** (0.200 g, 0.700 mmol), aniline **11** (0.115 g, 0.840 mmol), Cs_2CO_3 (0.50 g, 1.5 mmol) and XPhos (0.07 g, 0.1 mmol) in MeCN (10 mL), $Pd_2(dba)_3 \cdot CHCl_3$ (0.04 g, 0.04 mmol) was added. After stirring at 90 °C for 16 hours under N_2, the mixture was cooled to room temperature, diluted with EtOAc and filtered through diatomaceous earth. The filtrate was dried *in vacuo* and purified with column chromatography (20-40% EtOAc in hexanes) giving aniline **20** as a brown powder (0.0514 g, 19.0%): mp 187-189 °C; ^{1}H NMR (600 MHz, $CDCl_3$) δ 8.62 (s, 1H, H-2), 8.08 (br d, 1H, *J* = 7.1 Hz, 4-NH), 7.20 (d, 1H, *J* = 8.7 Hz, H-6″), 6.83 (d, *J* = 2.8 Hz, 1H, H-3″), 6.77 (dd, *J* = 8.6, 2.9 Hz, 1H, H-5″), 6.28 (br s, 1H, 6-NH) 5.40 (s, 1H, H-5), 4.29 (q, *J* = 7.1 Hz, 2H, H-1‴), 3.88-3.94 (m, 2H, H-2′a, H-6′a), 3.82 (s, 3H, O-CH_3), 3.41-3.48 (m, 2H, H-2′b, H-6′b), 3.31-3.38 (m, 1H, H-4’), 2.24 (s, 3H, CCH_3-2″), 1.84-1.91 (m, 2H, H-3′a, H-5′a), 1.50-1.59 (m, 2H, H-3′b, H-5′b), 1.37 (t, *J* = 7.1 Hz, 3H, H-2‴); ^{13}C NMR (150 MHz, $CDCl_3$) δ 168.4 (C=O), 160.9 (4-C, 6-C), 157.9 (4″-C), 155.0 (4-C, 6-C), 154.1 (2-CH), 136.0 (1″-C), 130.4 (2″-C), 127.6 (6″-CH), 116.3 (3″-CH), 112.2 (5″-CH), 101.2 (3-C), 84.2 (5-CH), 66.1 (2′-CH_2, 6′-CH_2), 60.1 (1‴-CH_2), 55.6 (O-CH_3), 47.3 (4′-CH), 32.5 (3′-CH_2, 5′-CH_2), 18.4 (2″-CH_3), 14.6 (2‴-CH_3); MS calculated for $C_{21}H_{27}N_3O_4$ $[M+H]^+$ *m/z* 386.2, found 386.2.

N-(4-Methoxy-2-methylphenyl)pyridin-2-amine (**23**)

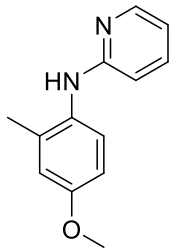

23

To a degassed mixture of chloride **22** (0.200 g, 1.76 mmol), aniline **11** (0.290 g, 2.11 mol), Cs_2CO_3 (1.3 g, 3.9 mol) and XPhos (0.17 g, 0.35 mmol) in MeCN (10 mL), $Pd_2(dba)_3 \cdot CHCl_3$ (0.09 g, 0.09 mmol) was added. This was stirred at 120 °C for 16 hours under N_2. The mixture was then cooled to room temperature, diluted with EtOAc and filtered through diatomaceous earth. The solvent was removed *in vacuo* and column chromatography (50% EtOAc in hexanes) afforded aniline **23** as a brown viscous gum (0.0041 g, 1.1%): ^{1}H NMR (600 MHz, $CDCl_3$) δ 8.13 (ddd, *J* = 5.0, 1.9, 0.9 Hz, 1H, H-6), 7.38-7.42 (m, 1H, H-4), 7.22 (d, *J* = 8.6 Hz, 1H, H-6′), 6.81 (d, *J* = 2.9 Hz, 1H, H-3′), 6.76 (dd, *J* = 8.6, 2.9 Hz, 1H, H-5′), 6.64 (ddd, *J* = 7.41, 5.0, 1.0 Hz, 1H, H-5), 6.36-6.39 (m, 1H, H-3), 3.80 (s, 3H, O-CH_3), 2.22 (s, 3H, CCH_3-2′); ^{13}C NMR (150 MHz, $CDCl_3$) δ 158.0 (2-C), 157.6 (4-C′), 147.8 (6-CH), 138.0 (4-CH), 135.9 (1′-C), 130.6 (2′-C), 127.3 (6′-CH), 116.4 (3′-CH), 113.9 (5-CH), 112.2 (5′-CH), 106.9 (3-CH), 55.6 (O-CH_3), 18.4 (2′-CH_3); MS calculated for $C_{13}H_{14}N_2O$ $[M+H]^+$ *m/z* 215.1, found 215.1.

1,1-Dimethylethyl *N*-(4-methoxy-2-methylphenyl)carbamate (**25**)

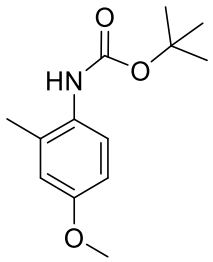

25

To a flask containing THF (25 mL) and aniline **11** (0.60 g, 4.4 mmol), Boc_2O (1.14 g, 5.24 mmol) was added. This was heated at reflux for 16 hours under N_2. Solvent was then removed *in vacuo* followed by purification *via* column chromatography (15% EtOAc in hexanes) yielding carbamate **25** as an orange crystalline solid (1.12 g, quant.): mp 79-81 °C; ^{1}H NMR (600 MHz, $CDCl_3$) δ_H 7.50 (br s, 1H), 6.70-6.74 (m ,2H), 6.05 (br s, 1H), 3.77 (s, 3H), 2.23 (s, 3H), 1.51 (s, 9H).

4 References

(1) Hanahan, D.; Weinberg, R. A. The Hallmarks of Cancer. *Cell* **2000**, *100* (1), 57–70. https://doi.org/10.1016/S0092-8674(00)81683-9.

(2) Patel, A. Benign vs Malignant Tumors. *JAMA Oncol.* **2020**, *6* (9), 1488. https://doi.org/10.1001/jamaoncol.2020.2592.

(3) Franks, L. M.; Teich, N. M. *Introduction to the Cellular and Molecular Biology of Cancer*; Oxford University Press, 1997.

(4) *Cancer data web tool*. https://tewhatuora.shinyapps.io/cancer-web-tool/ (accessed 2024-12-05).

(5) Gianfaldoni, S.; Gianfaldoni, R.; Wollina, U.; Lotti, J.; Tchernev, G.; Lotti, T. An Overview on Radiotherapy: From Its History to Its Current Applications in Dermatology. *Open Access Maced. J. Med. Sci.* **2017**, *5* (4), 521–525. https://doi.org/10.3889/oamjms.2017.122.

(6) Baskar, R.; Lee, K. A.; Yeo, R.; Yeoh, K.-W. Cancer and Radiation Therapy: Current Advances and Future Directions. *Int. J. Med. Sci.* **2012**, *9* (3), 193–199. https://doi.org/10.7150/ijms.3635.

(7) Johnson, D. E.; Burtness, B.; Leemans, C. R.; Lui, V. W. Y.; Bauman, J. E.; Grandis, J. R. Head and Neck Squamous Cell Carcinoma. *Nat. Rev. Dis. Primer* **2020**, *6* (1), 1–22. https://doi.org/10.1038/s41572-020-00224-3.

(8) *Cancer Society pleased to publish NZ head and neck cancer booklet*. Cancer Society NZ. https://www.cancer.org.nz/about-us/cancer-society-media-releases/cancer-society-pleased-to-publish-nz-head-and-neck-cancer-booklet/ (accessed 2024-12-10).

(9) *Head and neck cancer*. Cancer Society NZ. https://www.cancer.org.nz/cancer/types-of-cancer/head-and-neck-cancer/ (accessed 2024-12-10).

(10) Hutchinson, M.-K. N. D.; Mierzwa, M.; D'Silva, N. J. Radiation Resistance in Head and Neck Squamous Cell Carcinoma: Dire Need for an Appropriate Sensitizer. *Oncogene* **2020**, *39* (18), 3638–3649. https://doi.org/10.1038/s41388-020-1250-3.

(11) Baskar, R.; Dai, J.; Wenlong, N.; Yeo, R.; Yeoh, K.-W. Biological Response of Cancer Cells to Radiation Treatment. *Front. Mol. Biosci.* **2014**, *1*, 24. https://doi.org/10.3389/fmolb.2014.00024.

(12) Brown, J. M. Exploiting the Hypoxic Cancer Cell: Mechanisms and Therapeutic Strategies. *Mol. Med. Today* **2000**, *6* (4), 157–162. https://doi.org/10.1016/S1357-4310(00)01677-4.

(13) Marcu, L. G. Altered Fractionation in Radiotherapy: From Radiobiological Rationale to Therapeutic Gain. *Cancer Treat. Rev.* **2010**, *36* (8), 606–614. https://doi.org/10.1016/j.ctrv.2010.04.004.

(14) Burma, S.; Chen, D. J. Role of DNA–PK in the Cellular Response to DNA Double-Strand Breaks. *DNA Repair* **2004**, *3* (8), 909–918. https://doi.org/10.1016/j.dnarep.2004.03.021.

(15) Scully, R.; Panday, A.; Elango, R.; Willis, N. A. DNA Double-Strand Break Repair-Pathway Choice in Somatic Mammalian Cells. *Nat. Rev. Mol. Cell Biol.* **2019**, *20* (11), 698–714. https://doi.org/10.1038/s41580-019-0152-0.

(16) Mao, Z.; Bozzella, M.; Seluanov, A.; Gorbunova, V. DNA Repair by Nonhomologous End Joining and Homologous Recombination during Cell Cycle in Human Cells. *Cell Cycle Georget. Tex* **2008**, *7* (18), 2902–2906.

(17) Chang, H. H. Y.; Pannunzio, N. R.; Adachi, N.; Lieber, M. R. Non-Homologous DNA End Joining and Alternative Pathways to Double-Strand Break Repair. *Nat. Rev. Mol. Cell Biol.* **2017**, *18* (8), 495–506. https://doi.org/10.1038/nrm.2017.48.

(18) Lee, T. W.; Wong, W. W.; Dickson, B. D.; Lipert, B.; Cheng, G. J.; Hunter, F. W.; Hay, M. P.; Wilson, W. R. Radiosensitization of Head and Neck Squamous Cell Carcinoma Lines by DNA-PK Inhibitors Is More Effective than PARP-1 Inhibition and Is Enhanced by SLFN11 and Hypoxia. *Int. J. Radiat. Biol.* **2019**, *95* (12), 1597–1612. https://doi.org/10.1080/09553002.2019.1664787.

(19) Yin, X.; Liu, M.; Tian, Y.; Wang, J.; Xu, Y. Cryo-EM Structure of Human DNA-PK Holoenzyme. *Cell Res.* **2017**, *27* (11), 1341–1350. https://doi.org/10.1038/cr.2017.110.

(20) Lempiäinen, H.; Halazonetis, T. D. Emerging Common Themes in Regulation of PIKKs and PI3Ks. *EMBO J.* **2009**, *28* (20), 3067–3073. https://doi.org/10.1038/emboj.2009.281.

(21) Olivieri, C.; Li, G. C.; Wang, Y.; V.S., M.; Walker, C.; Kim, J.; Camilloni, C.; De Simone, A.; Vendruscolo, M.; Bernlohr, D. A.; Taylor, S. S.; Veglia, G. ATP-Competitive Inhibitors Modulate

the Substrate Binding Cooperativity of a Kinase by Altering Its Conformational Entropy. *Sci. Adv.* *8* (30), eabo0696. https://doi.org/10.1126/sciadv.abo0696.
(22) Hong, C. R.; Liew, L. P.; Wong, W. W.; Dickson, B. D.; Cheng, G.; Shome, A.; Airey, R.; Jaiswal, J.; Lipert, B.; Jamieson, S. M. F.; Wilson, W. R.; Hay, M. P. Identification of 6-Anilino Imidazo[4,5-c]Pyridin-2-Ones as Selective DNA-Dependent Protein Kinase Inhibitors and Their Application as Radiosensitizers. *J. Med. Chem.* **2024**, *67* (14), 12366–12385. https://doi.org/10.1021/acs.jmedchem.4c01120.
(23) Maira, S.-M.; Stauffer, F.; Brueggen, J.; Furet, P.; Schnell, C.; Fritsch, C.; Brachmann, S.; Chène, P.; De Pover, A.; Schoemaker, K.; Fabbro, D.; Gabriel, D.; Simonen, M.; Murphy, L.; Finan, P.; Sellers, W.; García-Echeverría, C. Identification and Characterization of NVP-BEZ235, a New Orally Available Dual Phosphatidylinositol 3-Kinase/Mammalian Target of Rapamycin Inhibitor with Potent in Vivo Antitumor Activity. *Mol. Cancer Ther.* **2008**, *7* (7), 1851–1863. https://doi.org/10.1158/1535-7163.MCT-08-0017.
(24) Kong, D.; Yaguchi, S.; Yamori, T. Effect of ZSTK474, a Novel Phosphatidylinositol 3-Kinase Inhibitor, on DNA-Dependent Protein Kinase. *Biol. Pharm. Bull.* **2009**, *32* (2), 297–300. https://doi.org/10.1248/bpb.32.297.
(25) Goldberg, F. W.; Finlay, M. R. V.; Ting, A. K. T.; Beattie, D.; Lamont, G. M.; Fallan, C.; Wrigley, G. L.; Schimpl, M.; Howard, M. R.; Williamson, B.; Vazquez-Chantada, M.; Barratt, D. G.; Davies, B. R.; Cadogan, E. B.; Ramos-Montoya, A.; Dean, E. The Discovery of 7-Methyl-2-[(7-Methyl[1,2,4]Triazolo[1,5-a]Pyridin-6-Yl)Amino]-9-(Tetrahydro-2H-Pyran-4-Yl)-7,9-Dihydro-8H-Purin-8-One (AZD7648), a Potent and Selective DNA-Dependent Protein Kinase (DNA-PK) Inhibitor. *J. Med. Chem.* **2020**, *63* (7), 3461–3471. https://doi.org/10.1021/acs.jmedchem.9b01684.
(26) Nageswara Rao, R.; Kumar Talluri, M. V. N. An Overview of Recent Applications of Inductively Coupled Plasma-Mass Spectrometry (ICP-MS) in Determination of Inorganic Impurities in Drugs and Pharmaceuticals. *J. Pharm. Biomed. Anal.* **2007**, *43* (1), 1–13. https://doi.org/10.1016/j.jpba.2006.07.004.
(27) Purohit, V.; Basu, A. K. Mutagenicity of Nitroaromatic Compounds. *Chem. Res. Toxicol.* **2000**, *13* (8), 673–692. https://doi.org/10.1021/tx000002x.
(28) Curtius, Th. Ueber Stickstoffwasserstoffsäure (Azoimid) N3H. *Berichte Dtsch. Chem. Ges.* **1890**, *23* (2), 3023–3033. https://doi.org/10.1002/cber.189002302232.
(29) Curtius, Th. 20. Hydrazide Und Azide Organischer Säuren I. Abhandlung. *J. Für Prakt. Chem.* **1894**, *50* (1), 275–294. https://doi.org/10.1002/prac.18940500125.
(30) Ghosh, A. K.; Sarkar, A.; Brindisi, M. The Curtius Rearrangement: Mechanistic Insight and Recent Applications in Natural Product Syntheses. *Org. Biomol. Chem.* **2018**, *16* (12), 2006–2027. https://doi.org/10.1039/c8ob00138c.
(31) Choudhary, G.; Hansen, H. Human Health Perspective on Environmental Exposure to Hydrazines: A Review. *Chemosphere* **1998**, *37* (5), 801–843. https://doi.org/10.1016/s0045-6535(98)00088-5.
(32) *Organic Azides*, 1st ed.; John Wiley & Sons, Ltd, 2009. https://doi.org/10.1002/9780470682517.
(33) Gray, P.; Lee, J. C. Explosive Decomposition and Combustion of Hydrazine. *Symp. Int. Combust.* **1955**, *5* (1), 692–700. https://doi.org/10.1016/S0082-0784(55)80095-1.
(34) Shioiri, T.; Ninomiya, K.; Yamada, S. Diphenylphosphoryl Azide. New Convenient Reagent for a Modified Curtius Reaction and for Peptide Synthesis. *J. Am. Chem. Soc.* **1972**, *94* (17), 6203–6205. https://doi.org/10.1021/ja00772a052.
(35) Ingoglia, B. T.; Wagen, C. C.; Buchwald, S. L. Biaryl Monophosphine Ligands in Palladium-Catalyzed C–N Coupling: An Updated User's Guide. *Tetrahedron* **2019**, *75* (32), 4199–4211. https://doi.org/10.1016/j.tet.2019.05.003.
(36) Galli, C. "CESIUM ION EFFECT" AND MACROCYCLIZATION. A CRITICAL REVIEW. *Org. Prep. Proced. Int.* **1992**. https://doi.org/10.1080/00304949209355891.
(37) Dickson, B. D.; Hay, M. P.; Hong, C. R.; Wong, W. W.; Wilson, W. R.; Liew, L. P.; Jamieson, S. M. F. NOVEL AMINOPYRIDINES AND THEIR USE IN TREATING CANCER. WO/2022/064430 A1, 2022.
(38) Reif, B.; Köck, M.; Kerssebaum, R.; Kang, H.; Fenical, W.; Griesinger, C. ADEQUATE, a New Set of Experiments to Determine the Constitution of Small Molecules at Natural Abundance. *J. Magn. Reson. A* **1996**, *118* (2), 282–285. https://doi.org/10.1006/jmra.1996.0038.

(39) Mallia, C. J.; McCreanor, N. G.; Legg, D. H.; Stewart, C. R.; Coppock, S.; Ashworth, I. W.; Le Bars, J.; Clarke, A.; Clemens, G.; Fisk, H.; Benson, H.; Oke, S.; Churchill, T.; Hoyle, M.; Timms, L.; Vare, K.; Sims, M.; Knight, S. Development and Manufacture of a Curtius Rearrangement Using Continuous Flow towards the Large-Scale Manufacture of AZD7648. *Org. Process Res. Dev.* **2022**, *26* (12), 3312–3322. https://doi.org/10.1021/acs.oprd.2c00316.
(40) Zalesskiy, S. S.; Ananikov, V. P. Pd2(Dba)3 as a Precursor of Soluble Metal Complexes and Nanoparticles: Determination of Palladium Active Species for Catalysis and Synthesis. *Organometallics* **2012**, *31* (6), 2302–2309. https://doi.org/10.1021/om201217r.
(41) Gustin, J.-L. Runaway Reaction Hazards in Processing Organic Nitro Compounds. *Org. Process Res. Dev.* **1998**, *2* (1), 27–33. https://doi.org/10.1021/op970035s.
(42) Zanger, M. The Determination of Aromatic Substitution Patterns by Nuclear Magnetic Resonance. *Org. Magn. Reson.* **1972**, *4* (1), 1–25. https://doi.org/10.1002/mrc.1270040102.
(43) Whitcombe, N. J.; Hii, K. K. (Mimi); Gibson, S. E. Advances in the Heck Chemistry of Aryl Bromides and Chlorides. *Tetrahedron* **2001**, *57* (35), 7449–7476. https://doi.org/10.1016/S0040-4020(01)00665-2.
(44) Barnard, B. C. Palladium-Catalysed C–C Coupling: Then and Now. *Platin. Met. Rev.* **2008**, *52* (1), 38–45. https://doi.org/10.1595/147106708X256634.
(45) Shaughnessy, K. H. Development of Palladium Precatalysts That Efficiently Generate LPd(0) Active Species. *Isr. J. Chem.* **2020**, *60* (3–4), 180–194. https://doi.org/10.1002/ijch.201900067.
(46) Amatore, C.; Jutand, A.; Khalil, F.; M'Barki, M. A.; Mottier, L. Rates and Mechanisms of Oxidative Addition to Zerovalent Palladium Complexes Generated in Situ from Mixtures of Pd0(Dba)2 and Triphenylphosphine. *Organometallics* **1993**, *12* (8), 3168–3178. https://doi.org/10.1021/om00032a045.
(47) Fors, B. P.; Watson, D. A.; Biscoe, M. R.; Buchwald, S. L. A Highly Active Catalyst for Pd-Catalyzed Amination Reactions: Cross-Coupling Reactions Using Aryl Mesylates and the Highly Selective Monoarylation of Primary Amines Using Aryl Chlorides. *J. Am. Chem. Soc.* **2008**, *130* (41), 13552–13554. https://doi.org/10.1021/ja8055358.
(48) Lee, H. G.; Milner, P. J.; Buchwald, S. L. An Improved Catalyst System for the Pd-Catalyzed Fluorination of (Hetero)Aryl Triflates. *Org. Lett.* **2013**, *15* (21), 5602–5605. https://doi.org/10.1021/ol402859k.
(49) Sherwood, J.; Clark, J. H.; Fairlamb, I. J. S.; Slattery, J. M. Solvent Effects in Palladium Catalysed Cross-Coupling Reactions. *Green Chem.* **2019**, *21* (9), 2164–2213. https://doi.org/10.1039/C9GC00617F.
(50) Elias, E. K.; Rehbein, S. M.; Neufeldt, S. R. Solvent Coordination to Palladium Can Invert the Selectivity of Oxidative Addition. *Chem. Sci.* **2022**, *13* (6), 1618–1628. https://doi.org/10.1039/D1SC05862B.
(51) Kaestle, K. L.; Anwer, M. K.; Audhya, T. K.; Goldstein, G. Cleavage of Esters Using Carbonates and Bicarbonates of Alkali Metals: Synthesis of Thymopentin. *Tetrahedron Lett.* **1991**, *32* (3), 327–330. https://doi.org/10.1016/S0040-4039(00)92619-4.
(52) González-Fernández, E.; Marinus, N.; Dhankhar, J.; Linden, A.; Čorić, I. Control over Anion Coordination on Pd(II), Cu(I), and Ag(I) with Regioisomeric Phosphine-Carboxylate Ligands. *Chem. – Eur. J.* **2024**, *30* (37), e202401215. https://doi.org/10.1002/chem.202401215.
(53) Epifanovsky, E.; Gilbert, A. T. B.; Feng, X.; Lee, J.; Mao, Y.; Mardirossian, N.; Pokhilko, P.; White, A. F.; Coons, M. P.; Dempwolff, A. L. *et al*. Software for the Frontiers of Quantum Chemistry: An Overview of Developments in the Q-Chem 5 Package. *J. Chem. Phys.* **2021**, *155* (8), 084801. https://doi.org/10.1063/5.0055522.
(54) Lu, T.; Chen, F. Multiwfn: A Multifunctional Wavefunction Analyzer. *J. Comput. Chem.* **2012**, *33* (5), 580–592. https://doi.org/10.1002/jcc.22885.
(55) Lu, T.; Chen, F. Quantitative Analysis of Molecular Surface Based on Improved Marching Tetrahedra Algorithm. *J. Mol. Graph. Model.* **2012**, *38*, 314–323. https://doi.org/10.1016/j.jmgm.2012.07.004.
(56) Zhang, J.; Lu, T. Efficient Evaluation of Electrostatic Potential with Computerized Optimized Code. *Phys. Chem. Chem. Phys.* **2021**, *23* (36), 20323–20328. https://doi.org/10.1039/D1CP02805G.

(57) Lu, T. A Comprehensive Electron Wavefunction Analysis Toolbox for Chemists, Multiwfn. *J. Chem. Phys.* **2024**, *161* (8), 082503. https://doi.org/10.1063/5.0216272.
(58) Humphrey, W.; Dalke, A.; Schulten, K. VMD: Visual Molecular Dynamics. *J. Mol. Graph.* **1996**, *14* (1), 33–38. https://doi.org/10.1016/0263-7855(96)00018-5.
(59) Gentile, G.; Di Fabio, R.; Pavone, F.; Sabbatini, F. M.; St-Denis, Y.; Zampori, M. G.; Vitulli, G.; Worby, A. Novel Substituted Tetrahydrotriazaacenaphthylene Derivatives as Potent CRF1 Receptor Antagonists. *Bioorg. Med. Chem. Lett.* **2007**, *17* (18), 5218–5221. https://doi.org/10.1016/j.bmcl.2007.06.077.
(60) Di Fabio, R.; Arban, R.; Bernasconi, G.; Braggio, S.; Blaney, F. E.; Capelli, A. M.; Castiglioni, E.; Donati, D.; Fazzolari, E.; Ratti, E.; Feriani, A.; Contini, S.; Gentile, G.; Ghirlanda, D.; Sabbatini, F. M.; Andreotti, D.; Spada, S.; Marchioro, C.; Worby, A.; St-Denis, Y. Dihydropyrrole[2,3-d]Pyridine Derivatives as Novel Corticotropin-Releasing Factor-1 Antagonists: Mapping of the Receptor Binding Pocket by in Silico Docking Studies. *J. Med. Chem.* **2008**, *51* (22), 7273–7286. https://doi.org/10.1021/jm800743q.
(61) Vitaku, E.; Smith, D. T.; Njardarson, J. T. Metal-Free Synthesis of Fluorinated Indoles Enabled by Oxidative Dearomatization. *Angew. Chem.* **2016**, *128* (6), 2283–2287. https://doi.org/10.1002/ange.201511149.
(62) Hicks, J. D.; Hyde, A. M.; Cuezva, A. M.; Buchwald, S. L. Pd-Catalyzed N-Arylation of Secondary Acyclic Amides: Catalyst Development, Scope, and Computational Study. *J. Am. Chem. Soc.* **2009**, *131* (46), 16720–16734. https://doi.org/10.1021/ja9044357.
(63) Apelqvist, T.; Wensbo, D. Selective Removal of the *N*-BOC Protective Group Using Silica Gel at Low Pressure. *Tetrahedron Lett.* **1996**, *37* (9), 1471–1472. https://doi.org/10.1016/0040-4039(95)02398-4.
(64) Osborne, J. D.; Matthews, T. P.; McHardy, T.; Proisy, N.; Cheung, K.-M. J.; Lainchbury, M.; Brown, N.; Walton, M. I.; Eve, P. D.; Boxall, K. J.; Hayes, A.; Henley, A. T.; Valenti, M. R.; De Haven Brandon, A. K.; Box, G.; Jamin, Y.; Robinson, S. P.; Westwood, I. M.; van Montfort, R. L. M.; Leonard, P. M.; Lamers, M. B. A. C.; Reader, J. C.; Aherne, G. W.; Raynaud, F. I.; Eccles, S. A.; Garrett, M. D.; Collins, I. Multiparameter Lead Optimization to Give an Oral Checkpoint Kinase 1 (CHK1) Inhibitor Clinical Candidate: (R)-5-((4-((Morpholin-2-Ylmethyl)Amino)-5-(Trifluoromethyl)Pyridin-2-Yl)Amino)Pyrazine-2-Carbonitrile (CCT245737). *J. Med. Chem.* **2016**, *59* (11), 5221–5237. https://doi.org/10.1021/acs.jmedchem.5b01938.
(65) Carcache, D.; Vranesic, I.; Blanz, J.; Desrayaud, S.; Fendt, M.; Glatthar, R. Benzimidazoles as Potent and Orally Active mGlu5 Receptor Antagonists with an Improved PK Profile. *ACS Med. Chem. Lett.* **2011**, *2* (1), 58–62. https://doi.org/10.1021/ml100215b.
(66) Harris, M. C.; Huang, X.; Buchwald, S. L. Improved Functional Group Compatibility in the Palladium-Catalyzed Synthesis of Aryl Amines. *Org. Lett.* **2002**, *4* (17), 2885–2888. https://doi.org/10.1021/ol0262688.
(67) Henderson, J. L.; Buchwald, S. L. Efficient Pd-Catalyzed Amination Reactions for Heterocycle Functionalization. *Org. Lett.* **2010**, *12* (20), 4442–4445. https://doi.org/10.1021/ol101929v.
(68) Goldberg, I. Ueber Phenylirungen Bei Gegenwart von Kupfer Als Katalysator. *Berichte Dtsch. Chem. Ges.* **1906**, *39* (2), 1691–1692. https://doi.org/10.1002/cber.19060390298.
(69) Chan, D. M. T.; Monaco, K. L.; Wang, R.-P.; Winters, M. P. New N- and O-Arylations with Phenylboronic Acids and Cupric Acetate. *Tetrahedron Lett.* **1998**, *39* (19), 2933–2936. https://doi.org/10.1016/S0040-4039(98)00503-6.
(70) Lam, P. Y. S.; Clark, C. G.; Saubern, S.; Adams, J.; Winters, M. P.; Chan, D. M. T.; Combs, A. New Aryl/Heteroaryl C□N Bond Cross-Coupling Reactions via Arylboronic Acid/Cupric Acetate Arylation. *Tetrahedron Lett.* **1998**, *39* (19), 2941–2944. https://doi.org/10.1016/S0040-4039(98)00504-8.